Queensland University of Technology
School of Physical and Chemical Sciences

The Effect of Red Blood Cell Orientation on the Electrical Impedance of Pulsatile Blood with Implications for Impedance Cardiography

Richelle Leanne Gaw
B.Eng (Aerospace Avionics) (Hons)

A thesis submitted at the Queensland University of Technology, in the School of Physical and Chemical Sciences in partial fulfilment of the requirements for the degree of Doctor of Philosophy

2010

Statement of Original Authorship

The work contained in this thesis has not been previously submitted to meet requirements for an award at this or any other higher education institution. To the best of my knowledge and belief, the thesis contains no material previously published or written by another person except where due reference is made.

Richelle Leanne Gaw

Acknowledgements

My supervisors, Assoc Prof Bruce Cornish and Assoc Prof Brian Thomas, have been a never ending source of inspiration, support and encouragement. The faith that they have shown in my work has given me the confidence and determination to achieve my goals. I hold both in the highest regard, both scientifically and personally, and am proud to name them both as my supervisors. Perhaps one day I will be consistent with my written tenses and be able to spell dependent!

To my husband Andrew. Your talent for making me laugh has elevated me through some of the lower moments of my PhD and I am forever grateful. Thanks must also go to my family. The familiar question of 'How is your PhD going?' kept me striving to be able to answer 'It's finished!'. The love and support that I received from my family, along with their never ending belief in my abilities, has inspired me to work hard and achieve the best that I can in all facets of life.

There are a number of other people who deserve thanks for their contributions during the completion of my PhD. To Jye Smith, Sean McConnell and the numerous students who inhabited the body composition lab with me. Thank you for making my working environment a pleasant and cheery place to be. To Glen Fulford, I must thank for his advice during the initial stages of theoretical modelling. The staff of mechanical engineering at QUT, Melissa Johnston, Mark Hayne, Kimble Dunster and Greg Tevelen have also been most accommodating in allowing me to use their facilities and it is very much appreciated.

Dr Wayne Stafford and Rohan Swann have provided great support and encouragement while completing the clinical trial, especially during those times

when things did not quite go as planned. The echocardiography technicians at Queensland Cardiovascular Group must also be thanked for their contributions to collecting echocardiography data. Scott Chetham and Catherine Kingsford have also been pivitol in bringing the clinical trial to fruition and I thank them greatly for their support and interest.

And finally perhaps the greatest thanks of all must go to God. I am truly blessed in your love.

Keywords

Bioimpedance, Impedance Cardiography, Red Blood Cells, Erythrocytes, Cell Orientation, Impedance, Blood Flow, Mock Circulatory System, Analytical Model, Lattice Boltzmann

Abstract

Impedance cardiography is an application of bioimpedance analysis primarily used in a research setting to determine cardiac output. It is a non invasive technique that measures the change in the impedance of the thorax which is attributed to the ejection of a volume of blood from the heart. The cardiac output is calculated from the measured impedance using the parallel conductor theory and a constant value for the resistivity of blood. However, the resistivity of blood has been shown to be velocity dependent due to changes in the orientation of red blood cells induced by changing shear forces during flow. The overall goal of this thesis was to study the effect that flow deviations have on the electrical impedance of blood, both experimentally and theoretically, and to apply the results to a clinical setting.

The resistivity of stationary blood is isotropic as the red blood cells are randomly orientated due to Brownian motion. In the case of blood flowing through rigid tubes, the resistivity is anisotropic due to the biconcave discoidal shape and orientation of the cells. The generation of shear forces across the width of the tube during flow causes the cells to align with the minimal cross sectional area facing the direction of flow. This is in order to minimise the shear stress experienced by the cells. This in turn results in a

larger cross sectional area of plasma and a reduction in the resistivity of the blood as the flow increases. Understanding the contribution of this effect on the thoracic impedance change is a vital step in achieving clinical acceptance of impedance cardiography.

Published literature investigates the resistivity variations for constant blood flow. In this case, the shear forces are constant and the impedance remains constant during flow at a magnitude which is less than that for stationary blood. The research presented in this thesis, however, investigates the variations in resistivity of blood during pulsataile flow through rigid tubes and the relationship between impedance, velocity and acceleration. Using rigid tubes isolates the impedance change to variations associated with changes in cell orientation only. The implications of red blood cell orientation changes for clinical impedance cardiography were also explored. This was achieved through measurement and analysis of the experimental impedance of pulsatile blood flowing through rigid tubes in a mock circulatory system.

A novel theoretical model including cell orientation dynamics was developed for the impedance of pulsatile blood through rigid tubes. The impedance of flowing blood was theoretically calculated using analytical methods for flow through straight tubes and the numerical Lattice Boltzmann method for flow through complex geometries such as aortic valve stenosis. The result of the analytical theoretical model was compared to the experimental impedance measurements through rigid tubes. The impedance calculated for flow through a stenosis using the Lattice Boltzmann method provides results for comparison with impedance cardiography measurements collected as part of a pilot clinical trial to assess the suitability of using

bioimpedance techniques to assess the presence of aortic stenosis.

The experimental and theoretical impedance of blood was shown to inversely follow the blood velocity during pulsatile flow with a correlation of -0.72 and -0.74 respectively. The results for both the experimental and theoretical investigations demonstrate that the acceleration of the blood is an important factor in determining the impedance, in addition to the velocity. During acceleration, the relationship between impedance and velocity is linear ($r^2 = 0.98$, experimental and $r^2 = 0.94$, theoretical). The relationship between the impedance and velocity during the deceleration phase is characterised by a time decay constant, τ, ranging from 10 to 50 s. The high level of agreement between the experimental and theoretically modelled impedance demonstrates the accuracy of the model developed here.

An increase in the haematocrit of the blood resulted in an increase in the magnitude of the impedance change due to changes in the orientation of red blood cells. The time decay constant was shown to decrease linearly with the haematocrit for both experimental and theoretical results, although the slope of this decrease was larger in the experimental case. The radius of the tube influences the experimental and theoretical impedance given the same velocity of flow. However, when the velocity was divided by the radius of the tube (labelled the reduced average velocity) the impedance response was the same for two experimental tubes with equivalent reduced average velocity but with different radii. The temperature of the blood was also shown to affect the impedance with the impedance decreasing as the temperature increased. These results are the first published for the impedance of pulsatile blood.

The experimental impedance change measured orthogonal to the direc-

tion of flow is in the opposite direction to that measured in the direction of flow. These results indicate that the impedance of blood flowing through rigid cylindrical tubes is axisymmetric along the radius. This has not previously been verified experimentally. Time frequency analysis of the experimental results demonstrated that the measured impedance contains the same frequency components occuring at the same time point in the cycle as the velocity signal contains. This suggests that the impedance contains many of the fluctuations of the velocity signal.

Application of a theoretical steady flow model to pulsatile flow presented here has verified that the steady flow model is not adequate in calculating the impedance of pulsatile blood flow. The success of the new theoretical model over the steady flow model demonstrates that the velocity profile is important in determining the impedance of pulsatile blood.

The clinical application of the impedance of blood flow through a stenosis was theoretically modelled using the Lattice Boltzman method (LBM) for fluid flow through complex geometeries. The impedance of blood exiting a narrow orifice was calculated for varying degrees of stenosis. Clincial impedance cardiography measurements were also recorded for both aortic valvular stenosis patients ($n = 4$) and control subjects ($n = 4$) with structurally normal hearts. This pilot trial was used to corroborate the results of the LBM.

Results from both investigations showed that the decay time constant for impedance has potential in the assessment of aortic valve stenosis. In the theoretically modelled case (LBM results), the decay time constant increased with an increase in the degree of stenosis. The clinical results also showed

a statistically significant difference in time decay constant between control and test subjects ($P = 0.03$). The time decay constant calculated for test subjects (τ = 180 - 250 s) is consistently larger than that determined for control subjects (τ = 50 - 130 s). This difference is thought to be due to difference in the orientation response of the cells as blood flows through the stenosis.

Such a non-invasive technique using the time decay constant for screening of aortic stenosis provides additional information to that currently given by impedance cardiography techniques and improves the value of the device to practitioners. However, the results still need to be verified in a larger study. While impedance cardiography has not been widely adopted clinically, it is research such as this that will enable future acceptance of the method.

Contents

List of Publications

1. Gaw R.L., Cornish B.H. and Thomas B.J. (2007) Comparison of a theoretical impedance model with experimental measurements of pulsatile blood flow. Proceedings of 13th International Conference on Electrical Bioimpedance, pp 32-5

2. Gaw R.L., Cornish B.H. and Thomas B.J. (2007) The electrical impedance of pulsatile blood flowing through rigid tubes: an experimental investigation. Proceedings of 13th International Conference on Electrical Bioimpedance, pp 73-6

3. Gaw R.L., Cornish B.H. and Thomas B.J. (2008) The electrical impedance of pulsatile blood flowing through rigid tubes: a theoretical investigation. IEEE Trans Biomed Eng 55:721-7

4. Gaw R.L., Cornish B.H. and Thomas B.J. (2009) Time frequency analysis of the experimental electrical impedance of pulsatile blood flowing through rigid tubes. Proceedings of 11th Medical Physics and Biomedical Engineering World Congress, 25/VII, pp 255-8

5. Gaw R.L., Cornish B.H. and Thomas B.J. (2009) Decay properties of the experimental electrical impedance of pulsatile blood flowing through rigid tubes. Proceedings of 11th Medical Physics and Biomedical Engineering World Congress, 25/VII, pp 259-62

List of Figures

List of Tables

List of Abbreviations

A	Area
AC	Alternating Current
AS	Aortic Stenosis
AV	Aortic Valve
AVA	Aortic Valve Area
BIA	Bioelectrical Impedance Analysis
bpm	Beats Per Minute
CI	Cardiac Index
Cm	Membrane Capacitance
CO	Cardiac Output
CV	Coefficient of Variation
CWT	Continuous Wavelet Transform
D, d	Diameter
DC	Direct Current
ECG	Electrocardiogram
ELVET	Effective Left Ventricular Ejection Time
f_c	Characteristic Frequency
H, h	Haematocrit
IC	Impedance Cardiography
ICG	Impedance Cardiogram
kHz	kilohertz
l, L	Length
LBM	Lattice Boltzmann Method
LVOT	Left Ventricular Outflow Tract
MRI	Magnetic Resonance Imaging
PCG	Phonocardiogram
QCG	Queensland Cardiovascular Group
QUT	Queensland University of Technology
R	Resistance, Radius
R, r	Radius
R_E	Resistance of Extra-cellular fluid

R_I	Resistance of Intra-cellular fluid
R_0	Resistance at DC (or 0 kHz)
R_∞	Resistance at Infinite Frequency
RBC	Red Blood Cells
RMS	Root Mean Square
ρ	Resistivity, Density
SNR	Signal to Noise Ratio
SV	Stroke Volume
T	Temperature
τ	Time Constant
VET	Ventricular Ejection Time
ω	Angular Frequency
X	Reactance
Z	Impedance

Chapter 1

Introduction

1.1 The Challenge

Impedance Cardiography, developed by Kubicek, Karnegis, Patterson, Witsoe & Mattson (1966) is an inexpensive and non-invasive method of determining cardiac output based on the measurement of impedance changes of the thorax. These impedance changes are reported to be due to changes in blood volume being pumped through the thorax. Despite the many advantages over other cardiac monitoring techniques, Impedance Cardiography has not been widely adopted in clinical settings (Newman & Callister 1999, Bour & Kellett 2008). This may be because the origin of the thoracic impedance change is controversial and not well understood. The assumption that impedance changes are due to changes in blood volume is questionable because many other factors may affect the impedance. One possible factor is that changes in velocity alter the orientation of the red blood cells which in turn alters the impedance of the blood flowing through the thorax. Further understanding of this phenomenon is important to better understand and provide additional information from Impedance Cardiography waveforms (ICG).

1.2 Background

Diseases of the heart and blood vessels cause up to 50% of deaths in modern western society (Pedley 2003) which projects a significant financial burden on the health care system. Stroke volume (SV) and cardiac output (CO) are important indicators of overall cardiovascular function (Moshkovitz, Kaluski, Milo, Vered & Cotter 2004). Increasing evidence shows that the measurement of these indicators plays a significant role in the diagnosis and monitoring of patients with heart failure. Thus early detection of heart disease may be achieved by monitoring the cardiac output and therefore reduce the financial burden caused by heart disease.

There are many techniques for the measurement of cardiac output with various advantages and disadvantages. The Fick method is considered the gold standard for measuring cardiac output due to its accuracy and reliability. The Fick method uses the principle that if the blood flow to the organ and the arterial and venous concentrations of the marker substance are known, then the consumption of the substance by the organ can be calculated (Mohapatra 1981). Cardiac output is equal to the uptake of oxygen by the heart divided by the difference in oxygen concentration of aortic blood and venous blood. However, the procedure is complicated to perform and invasive.

Other techniques such as indicator-dilution and thermo-dilution are easier to perform, although these techniques are still moderately invasive. Echocardiography techniques are non invasive; however, they require expert operators and expensive equipment to ensure accurate results. In addition, these present techniques also come with an associated high cost. Extensive research has been conducted in determining correlations between impedance cardiography and other cardiac monitoring techniques and results have shown that potential applications arise in both clinical and research settings.

ICG waveforms appear to contain much more information than the detail used to calculate the stroke volume alone. Previous research conducted by Chetham (2003) has shown that the waveforms, along with all the notches and peaks, are consistently reproducible and synchronous with each heart beat, indicating that these variations are real and not a result of noise. It is believed that these variations in impedance are related to heart function and changes in red blood cell orientation as the blood flows.

Many previous studies have investigated the phenomenon using blood flowing at constant velocities. However, blood flow through the body is pulsatile in nature. Therefore, there exists an opportunity to explore the effect of velocity changes on the impedance of blood during pulsatile flow. The information able to be derived from these variations will provide insight into the relationship between the velocity and the impedance of blood. This may lead to further understanding of physiological events such as valves opening and closing or changes in blood flow speeds as a result of various arrhythmias. This type of diagnostic information, obtained by a completely non invasive technique, would prove invaluable in monitoring cardiac function.

1.3 Objectives and Aims

The objective of the research project is to investigate the electrical characteristics of blood caused by flow induced changes in cell orientation and the potential implications for Impedance Cardiography waveforms.

The specific aims of the project are to:

1. Simulate the physiological flow of blood through the human aorta using rigid tubes in a mock circulatory system.

2. Measure the variations in blood impedance as a function of flow over a

range of physical and flow parameters.

3. Investigate the experimental relationship between impedance variations and flow variations for various physical and flow parameters.

4. Theoretically model the impedance of blood as it flows in a pulsatile nature through rigid tubes.

5. Compare the modelled results to those collected experimentally.

6. Collect Impedance Cardiography waveforms in control and abnormal subjects in a clinical trial.

7. Analyse the collected clinical data for obvious differences and evidence of red blood cell orientation changes.

1.4 Methodology

The research was separated into three distinct topics and a number of stages. The three topics were experimental measurements, theoretical modelling and the clinical trial. Figure 1.1 shows the relationship between the stages within each topic.

Experimental Set-up

The mock circulatory system was designed to simulate blood flow through the aorta. Rigid tubes were used in order to eliminate the impedance change due to cross sectional area changes and isolate the red blood cell orientation effect. Trade studies were performed and equipment was chosen to meet physiological blood flow specifications as well as adequate acquisition and data storage requirements. The system was tested using physiological saline.

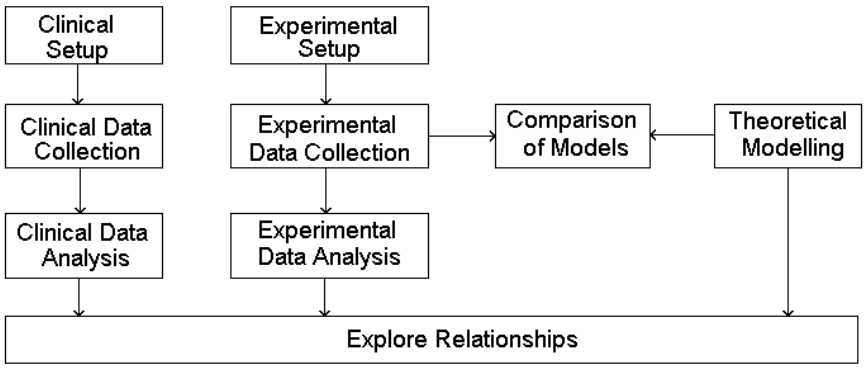

Figure 1.1: Research Methodology

Experimental Data Collection

The impedance and velocity of bovine blood was measured and recorded as it was pumped through the mock circulatory system. Frequency of measurement, pulse rate, stroke volume, haematocrit of the blood, temperature of the blood and the radius of the tube were all varied and measurements recorded.

Experimental Data Analysis

Various signal processing and waveform analysis techniques have been investigated during the analysis of the experimental data. The relationship between impedance and velocity, and impedance and acceleration, and the time decay properties and time frequency properties have been explored.

Theoretical Modelling

A theoretical model has been developed to simulate the impedance change of pulsatile blood flowing through rigid tubes. This model has been expanded from previous constant flow models and models the orientation of the cells from the velocity profile of the blood. Impedance is then calculated based on the orientation of the cells. Input parameters of the model are pulse rate, haematocrit, temperature and radius.

Comparison of Models

Verification of the theoretical model was achieved by comparison of the modelled results to experimentally collected data. Features of the waveforms were compared as well as the variation of parameters.

Clinical Setup

A test plan was developed in order to explore the clinical implications of red blood cell orientation on the Impedance Cardiogram in patients with a narrowing of the aortic valve (aortic stenosis (AS)). Ethics approval was sought and granted to conduct a clinical trial in collaboration with Queensland Cardiovascular Group (QCG) at St Andrew's Place, Spring Hill.

Clinical Data Collection

Data was collected from two sets of subjects: healthy control patients with normal heart function and test subjects previously diagnosed with aortic stenosis. Subjects underwent a routine echocardiography exam. In addition, the impedance of the thorax was measured.

Clinical Data Analysis

Parameters derived from the impedance cardiogram were compared for differences between the test and control subject groups. These results were compared to theoretical modelling of blood flow through a stenosis.

Chapter 2

Literature Review

2.1 Bioelectrical Impedance

Impedance cardiography is an application of Bioelectrical Impedance Analysis (BIA). BIA is the measurement of the electrical impedance of biological tissue in response to an applied current. According to Kirchhoff's law, electric current will flow through different materials dependent upon their electrical impedance to flow. Electrical currents applied to the body are primarily distributed in fluids and blood, as these tissues exhibit low resistivity compared to other tissues such as cardiac muscle, lungs and fat (150 $\Omega.\text{cm}^{-1}$ for blood and 750, 1275 and 2500 $\Omega.\text{cm}^{-1}$ for cardiac muscle, lungs and fat respectively) (Moshkovitz et al. 2004). This principle is utilised in impedance cardiography techniques as an alternating electrical current passing through the thorax will be conducted mainly through the blood and thus the resulting impedance variations will give an indication of the amount of blood pumped by the heart.

2.1.1 Principles of Bioelectrical Impedance

Bioelectrical impedance is measured by passing a constant amplitude alternating current (AC) through biological tissue, either in-vivo or in-vitro. Living tissue is predominately an electrolytic conductor in which ions are the charge carriers. The flow of ionic current gives rise to an induced voltage difference which can then be measured. The fundamental basis of the technique is Ohms Law in which the ratio of the measured voltage signal to the applied current yields the electrical impedance. In AC, the impedance is a function of both the magnitude and the phase relationship between the measured voltage and the applied current. Thus the impedance of biological material is a vector composed of two elements: the magnitude (impedance, Z) and the direction (phase, ϕ). Cartesian coordinates of these parameters are: resistance (R) and reactance (X).

$$Z = |Z| \angle \phi = R + jX \tag{2.1}$$

$$|Z| = \sqrt{R^2 + X^2} \tag{2.2}$$

$$\tan \phi = \frac{X}{R} \tag{2.3}$$

Biological tissue consists of intra-cellular fluid enveloped by a cell membrane and surrounded by extra-cellular fluid. When current is applied to the tissue, the extra- and intra- cellular fluids behave as resistive components while the cell membrane behaves as a reactive component.

Skin acts primarily as a dielectric with a low conductance that allows current to flow. Because of this, polarisation occurs when current flows through

the electrode/skin interface. Polarisation is the disturbance of the charge distribution in a region induced by the introduction of an electric field. To minimise the error resulting from the polarisation effects of the electrode/skin interface, the current supply and voltage measurement electrodes are separated in a tetra-polar arrangement (Patterson 1989).

2.1.2 Equivalent Circuits for Biological Tissue

The electrical properties of tissue can be described by an electrically equivalent circuit. A number of models have been suggested in the literature. These circuits contain a combination of ideal electrical components that mimic the electrical behaviour of biological tissue. Example of four equivalent circuits are shown in Figure 2.1.

Of these, the first three models can be realised by ideal electrical components. The analogue Cole model of Figure 2.1a) models the extra-cellular and intra-cellular fluid as resistances (R_e and R_i respectively) and the cell membranes as a capacitance (Cm). Figure 2.1b) shows the double shell model which models cells with large cytoplasmic organelles. Figure 2.1c) includes an inductor in the analogue Cole circuit to model the blood and plasma volumes. Figure 2.1d) consists of a non-ideal frequency dependent component (Zcpa) in which the resulting phase remains independent of frequency. This circuit is not physically realisable. Of these, the Cole model is the simplest and most widely used.

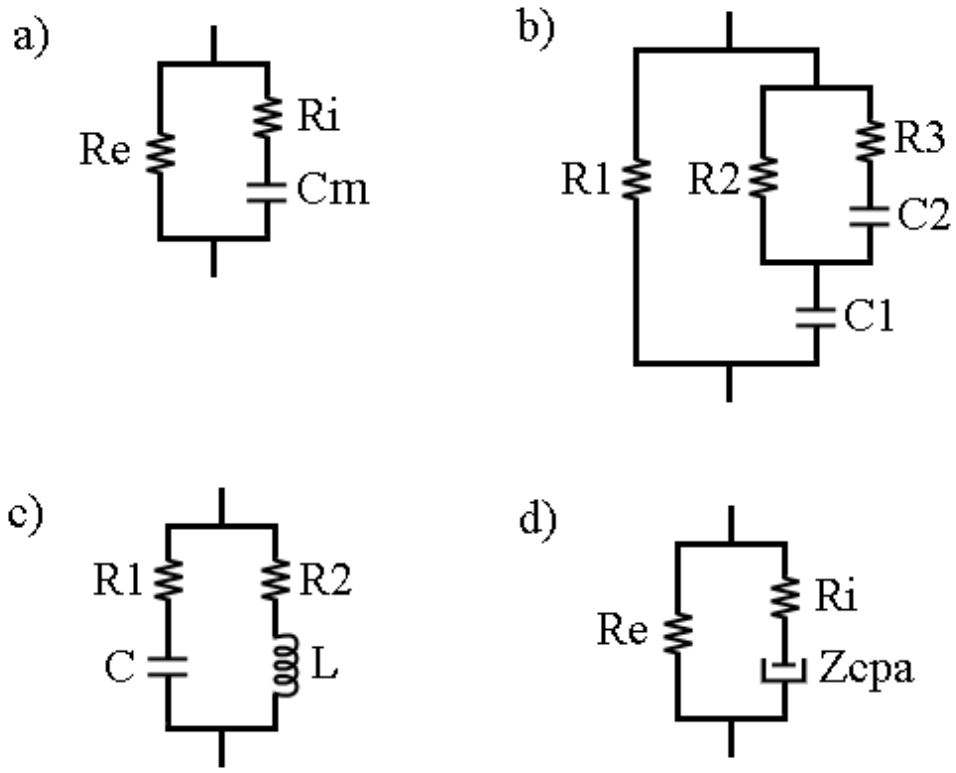

Figure 2.1: Equivalent Electrical Circuits for Biological Tissue a) analogue Cole model (Cole 1968), b) double shell model (Zhang & Willison 1991), c) inductor model (Siconolfi et al. 1997), and d) constant phase element model (Grimnes & Martinsen 2000)

2.1.3 Frequency Response

Traditionally, a single frequency current at (typically) 100 kHz and 4 mA RMS is used in impedance cardiography. However, as suggested by the frequency dependent components of the equivalent circuits, the impedance of tissue is also frequency dependent. Some studies have investigated the effects of measuring impedance cardiography waveforms at a number of frequencies (Palko, Bialokoz & Weglarz 1995, Wtorek & Polinski 1996, Goovaerts, Faes, Raaijmakers & Heethaar 1998). Chetham (2003) has highlighted the advan-

tages of using a simultaneous or swept frequency approach based on the Cole equation known as Bioimpedance Spectroscopy (BIS).

As AC passes through biological tissue, it conducts in both the extra-cellular and intra-cellular fluid in a ratio that is dependent on the applied current frequency. This is because the reactive component of the cell membrane behaves as a capacitor and reacts differently to variations in electrical current frequency. Under direct current (DC) the cell membrane acts as an insulator (open circuit) and all current flows through the extra-cellular fluid. As the frequency increases, the membrane becomes a conductor (approaching a short circuit at infinite frequency) and current passes through both the intra- and extra-cellular fluid with the proportion of the current in each being dependent on the frequency.

This is most simply explained by the analogue circuit of the Cole model (Figure 2.1a) in which the extra-cellular fluid and intra-cellular fluid surrounded by the cell membranes are modelled as parallel branches of an electrical circuit. The impedance at DC (labelled R_0) is that of the extra-cellular fluid only (R_E). At infinite frequency (R_∞) the impedance is a parallel combination of the extra-cellular and intra-cellular resistance.

$$R_\infty = \frac{R_E R_I}{R_E + R_I} \tag{2.4}$$

The resulting impedance of this circuit can be calculated by Equation 2.5. R_0 in particular is an important parameter as it represents the resistance of the extra-cellular fluid only and can be used in many clinical applications. Due to practical limitations, R_0 and R_∞ can not be measured directly; however, knowledge of the frequency response of biological material allows finite frequency data to be extrapolated in order to derive these values. Using least squares regression, R_0 and R_∞ can be extrapolated from the known

impedance/frequency data. The electrical time constant of the system is τ.

$$\begin{aligned} Z &= R_\infty + \frac{R_0 - R_\infty}{1 + j\omega\tau} \\ R_0 &= R_E \\ R_\infty &= \frac{R_E R_I}{R_E + R_I} \\ \tau &= C_m(R_E + R_I) \end{aligned} \tag{2.5}$$

The behaviour of biological tissue impedance can be shown over the frequency range by means of an impedance locus known as a Cole plot. This is a complex plot of reactance and resistance as a function of frequency. Equation 2.6 and 2.7 shows the resistance and reactance.

$$R = R_\infty + \frac{R_0 - R_\infty}{1 + \omega^2\tau^2} \tag{2.6}$$

$$X = -\omega\tau\frac{R_0 - R_\infty}{1 + \omega^2\tau^2} \tag{2.7}$$

For ideal components, a plot of resistance (R) and reactance (X) from Equation 2.6 and 2.7 will be a circular arc with the centre on the R axis at $\frac{1}{2}(R_0 + R_\infty)$ and with a radius of $\frac{1}{2}(R_0 - R_\infty)$. This is shown in Figure 2.2a). In practice, measurements of biological tissue generate a circular locus with the centre depressed due to the non ideal capacitive nature of the physical cell membrane (see Figure 2.2b), where f_c is the frequency at which the maximum reactance occurs.

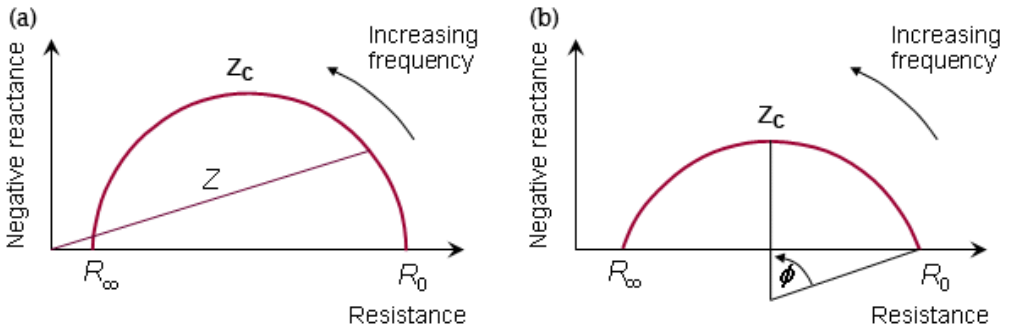

Figure 2.2: (a) Impedance locus for ideal components, (b) Impedance locus for a biological system where $\phi = \frac{\pi\alpha}{2}$ (Malmivuo & Plonsey 1995)

Cole (1940) introduced the first mathematical expression able to describe tissue impedance and the depressed semicircles found experimentally, by including a fourth parameter, α.

$$Z = R_\infty + \frac{R_0 - R_\infty}{1 + j\omega\tau^{(\alpha)}} \tag{2.8}$$

The physical meaning of α is not well understood. It has been considered a measure of the distribution of relaxation times (due to different degrees of cellular interactions, cell size and anisotropy), a measure of the deviation from ideal components or an effect of many body interactions in the material (Grimnes & Martinsen 2000). The characteristic time constant, τ, of Equation 2.8 can be considered the mean time constant of the distribution of relaxation time constants. As α deviates from 1, the distribution of time constants spreads.

2.2 Impedance Cardiography

Impedance cardiography is a non-invasive bioimpedance technique used to measure the stroke volume (SV) and resulting cardiac output of the heart.

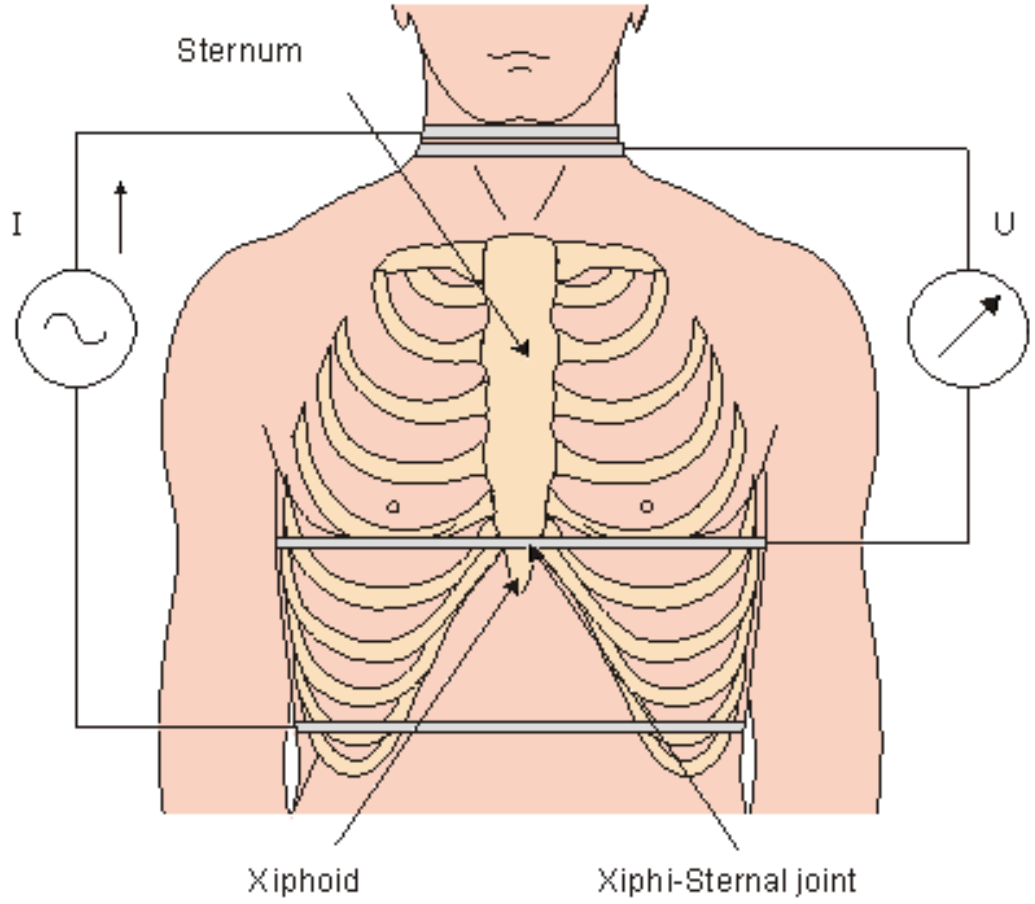

Figure 2.3: Band electrode configuration for impedance cardiography measurements (Malmivuo & Plonsey 1995)

This is achieved by measuring the electrical impedance of the thorax. The normal thoracic impedance range for an adult is 20 - 48 Ω at a frequency of 50 - 100 kHz (Critchley 1998). Figure 2.3 shows a common band electrode configuration. The outer electrodes supply the alternating current while the inner electrodes measure the induced voltage.

Changes in thoracic impedance are assumed to be related to the ejection of blood into the ascending aorta. This is because blood provides the path of least resistance over other muscle and tissue. Any increase in the

amount of blood volume (electrically participating tissue) will cause the electrical conductance of the thorax to increase and consequently a decrease in the thoracic impedance. From the absolute value of the heart synchronous variations (ΔZ) the stroke volume can be calculated (Visser, Lamberts & Zijlstra 1988, Newman & Callister 1999).

Figure 2.4 represents a typical thoracic impedance curve (Z) measured using a single AC frequency. The first time derivative ($\frac{dZ}{dt}$) and the simultaneous electrocardiogram (ECG) and phonocardiogram (PCG) are also shown. A decrease in impedance is shown as an upward inflection on the impedance cardiogram (ICG). The $\frac{dZ}{dt}$ waveform is the most important in the calculation of stroke volume as it contains clearly defined features. Each point labelled in Figure 2.4 and can be related to a certain event in the heart cycle as detailed in Table 2.1.

2.2.1 Cardiac Timing of the Impedance Signal

The $\frac{dZ}{dt}$ signal has many distinct peaks and notches that may be related to events in the cardiac cycle, such as the opening and closing of the aortic valve (Visser, Mook, van der Wall & Zijlstra 1993). Table 2.1 details the important points of the impedance waveform shown in Figure 2.4 that correlate most closely to the physiological events.

The baseline impedance is approximated by the B point which is the opening of the aortic valve. The C point occurs at the point of maximum acceleration of the blood and the slope between the B and C point is associated with cardiac contractility (Bour & Kellett 2008). Ventricular ejection time (VET) is the time period between the opening and closing of the heart valves during the systole-diastole cycle of the heart and is equal to the duration of blood flow in the aorta. Its determination plays an important role in

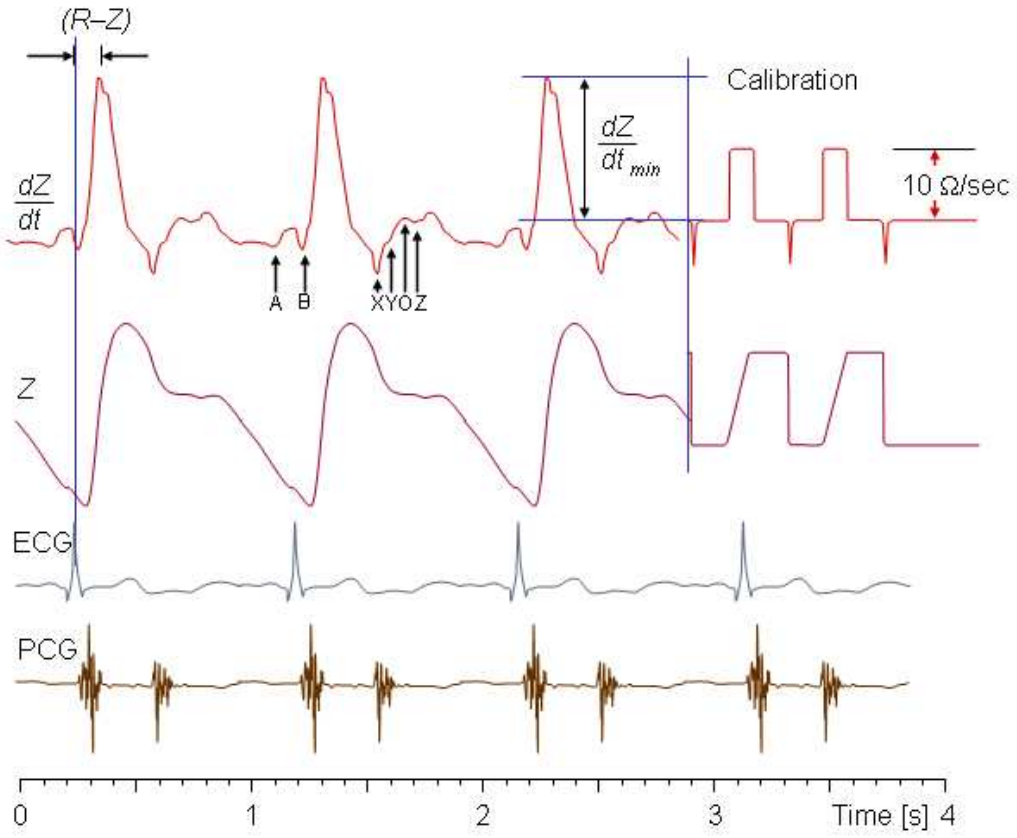

Figure 2.4: Impedance Cardiography Waveform (dZ/dt) with corresponding thoracic impedance (Z), Electrocardiogram (ECG) and Phonocardiogram (PCG) (Malmivuo & Plonsey 1995)

Point	Description
A	*Atrial contraction (systole)*
B	*Closure of tricuspid valve (seen after opening of aortic valve)*
C	*Rate of ventricular ejection into the ascending aorta* ($\frac{dZ}{dt_{max}}$)
X	*Closing of aortic valve*
Y	*Closing of pulmonary valve*
O	*Opening snap of mitral valve (rapid ventricular filling - diastole)*
Z	*Third heart sound*

Table 2.1: Cardiac timing descriptions

impedance cardiography and it is usually denoted as the time between the B and X points of the $\frac{dZ}{dt}$ signal as these points most closely correlate with the heart sounds in the ECG. Unfortunately, they often disappear under noise especially for critically ill patients with irregular or weak signals (Hu, Sun & Wang 1997, Critchley 1998). The O wave represents the impedance during diastole.

Although the timing of the various notches of the $\frac{dZ}{dt}$ waveform is well known, the origins of the main deflections are not well understood (Malmivuo & Plonsey 1995). Data collected by Chetham (2003) for multi-frequency impedance cardiography shows that there are many inflections in the $\frac{dZ}{dt}$ signal that are repeated for each heartbeat. This indicates that ICG waveforms may contain more information on cardiac function than cardiac output determination alone.

2.2.2 Theoretical Basis

The thoracic impedance can be modelled using the parallel conductor model as shown in Figure 2.5. This model consists of a parallel connection of constant tissue impedance Z_t and a time varying impedance Z_b associated with cyclic blood volume variations within the cardiac cycle. These changes are small compared to the total impedance (about 0.5%) which results in weak signals with low signal to noise ratios (SNR).

To relate blood volume changes to impedance changes using the parallel model, the total thoracic impedance is given by the parallel combination of the tissue and blood volume impedance:

$$Z = \frac{Z_b Z_t}{Z_b + Z_t} \tag{2.9}$$

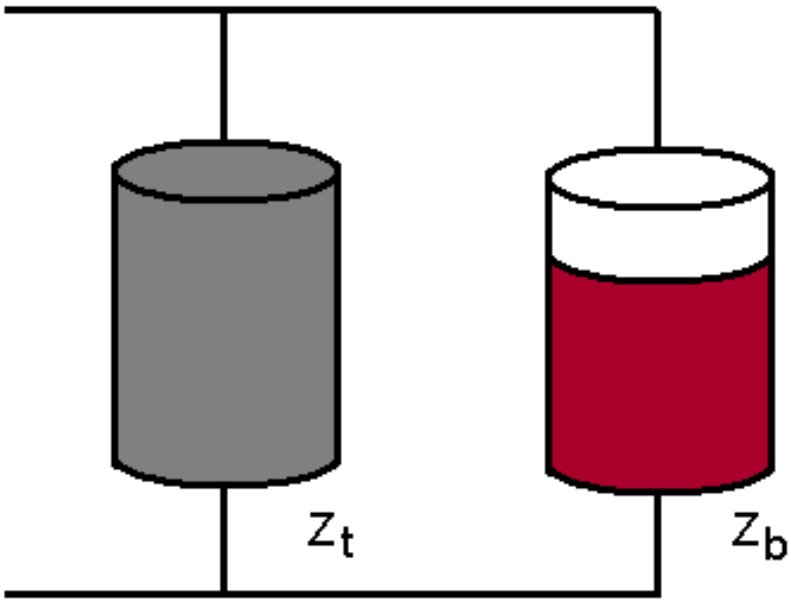

Figure 2.5: Parallel conductor model (Patterson 1989)

where Z = total impedance, Z_b = impedance of blood volume and Z_t = impedance of tissue volume.

Differentiating the above equation with respect to the blood volume impedance, Z_b, gives the relationship between the impedance change of the thorax and the impedance change of blood volume.

$$dZ = \frac{Z^2}{{Z_b}^2} dZ_b \tag{2.10}$$

By assuming that the thorax is a cylinder, the impedance of the blood volume can be derived from the resistivity of blood (ρ_b), the cross sectional area (A_b) and length of the thorax (l).

$$Z_b = \frac{\rho_b l}{A_b} \tag{2.11}$$

Assuming that changes in blood volume (dv_b) are caused only by a change in cross sectional area, the change in blood volume as a function of change in impedance (dZ_b) can be found.

$$dv_b = d(lA_b) = -\frac{\rho_b l^2}{{Z_b}^2} dZ_b \tag{2.12}$$

Therefore the change in blood volume can be found as a function of total thoracic impedance change by solving for dZ_b in Equation 2.10 and substituting into the above equation.

$$dv_b = -\frac{\rho_b l^2}{Z^2} dZ \tag{2.13}$$

The value of dZ can be determined by:

$$dZ = \frac{dZ}{dt} dt \tag{2.14}$$

Where dt is the time interval of ejection.

The stroke volume is determined using three variables measured from the impedance cardiography waveform shown in Figure 2.4. These are: the baseline impedance of the thorax (Z); the maximum gradient of the impedance waveform at the beginning of systole ($\frac{dZ}{dt}_{max}$); and the ventricular ejection time (VET), determined as the time between when the $\frac{dZ}{dt}_{max}$ curve crosses the zero line after the B point, and the X point in Figure 2.4. The conventional equation based on these and the distance between measurement electrodes (l) is known as the Kubicek Equation.

$$SV = \rho_b \frac{l^2}{Z^2} \Delta Z \tag{2.15}$$

$$\Delta Z = VET \left.\frac{dZ}{dt}\right|_{max} \tag{2.16}$$

Kubicek's equation relies on a number of assumptions (Malmivuo & Plonsey 1995, Chetham 2003). These are:

1. the thorax is cylindrical,
2. this cylinder is homogeneously perfused,
3. the perfusing blood has a specific resistivity which only varies with haematocrit,
4. the cylindrical uniform volume conductor has a constant mean thoracic impedance, Z_0,
5. the peak value of $\frac{dZ}{dt}$ is proportional to peak ascending aortic blood flow.

Perhaps the most important of these assumptions is that resistivity of blood remains constant for a specific haematocrit and that heart synchronous transthoracic impedance changes are only caused by volume variations of the large blood vessels.

Several authors have explored refinements to the Kubicek equation, the most notable of which are Sramek and Bernstein. Sramek (Sramek 1982) represented the thorax as a truncated cone as well as taking into account the morphology of the subject. The variable for resistivity was eliminated based on the assumption that this remains constant (which has later been shown to be incorrect). Bernstein (Bernstein 1986) proposed a modification to Sramek's equation by incorporating a scaling factor (δ) to incorporate body weight. The resulting equation is known as the Sramek-Bernstein equation.

$$SV = \delta \left[\frac{(0.17H)^3}{4.2} \right] \frac{dZ}{dt} \frac{t}{Z} \tag{2.17}$$

Chetham (2003) has shown success in using multiple frequencies to generate the circular impedance locus and estimation of DC impedance, R_0. In impedance cardiography, the value of R_0 primarily represents the resistance of plasma, as red blood cells (red blood cells) will act as insulators at zero frequency. Stroke volumes calculated from R_0 have shown good correlation to traditional methods such as echocardiography and thermodilution techniques in both normal (r = 0.79 with echocardiography) and abnormal patients (r = 0.99 with thermodilution and r = 0.62 with echocardiography) (Chetham 2003).

2.2.3 Origins of the Impedance Cardiography Waveform

Many authors highlight concerns regarding the origin of thoracic impedance changes. The exact region or origin in the thorax that contributes to thoracic impedance change is still controversial and not well understood (Peura, Penney, Arcuri, Anderson & Wheeler 1978, Schuster & Schuster 1984, Geddes & Baker 1989, Patterson 1989, Wang & Patterson 1995, Critchley 1998, Newman & Callister 1999, Taylor, Timmons & Hines 1999). Multiple regions of the thorax have been suggested to generate several different impedance signals which sum to give the impedance variations observed.

These include:

- blood volume changes due to left ventricle ejection into the aorta,
- blood volume changes of the atria and ventricle,

- lung volume changes,
- blood resistivity and cell structural changes,
- aortic and pulmonary blood flow.

The Kubicek equation however, assumes contributions to the measured impedance are only due to changes in the blood volume of the ascending aorta during left ventricular ejection.

Controversy regarding the origins of blood volume changes contributing to the thoracic impedance change has been evident since early development. Blood volume changes from organs other than the aorta have been shown to significantly alter the measured thoracic impedance. Theoretical and experimental models have been published simulating the effect of changes in the atria and ventricles of the heart, lungs, large and small arteries and veins, and skeletal muscle. Contributions of up to 61% from the lungs, 23% from the large arteries and 13% from skeletal muscle volume changes have been reported using a 3D electrical model of the thorax (Patterson 1985). In a further study, the 3D model was enhanced with magnetic resonance images obtained at end diastole and end systole (Wang & Patterson 1995). The net contributions were categorized into three areas. These are structural changes of the heart and arteries (4%), arterial and venous flow induced blood resistivity changes (57%) and lung resistivity changes due to blood volume changes (39%). These results suggest that the impedance signal is a mixed representation of many inseparable factors and may not be reliable for the calculation of stroke volume.

A number of studies investigating the origin of the impedance change in the thorax confirm these results. Various models of the impedance of the thorax have been published (Sakamoto, Muto, Kanai & Iizuka 1979, Kosicki,

Chen, Hobbie, Patterson & Ackerman 1986, Kim, Kim, Baker, Pearce & Won Ky Kim 1988) and findings confirm that the changes in thoracic impedance are primarily due to:

- blood volume changes in the heart
- inhomogeneous and complex geometry of the organs in the thorax
- change in lung resistivity due to blood volume changes in the lungs
- blood resistivity changes induced by flow
- structural changes and movement of organs
- volume changes in the aorta and arteries leading to expansion
- volume changes in the veins

Impedance changes of 4% each for volume changes in the lungs, heart and aorta have been modelled with a 3D model at the surface on the thorax (Sakamoto et al. 1979). A theoretical impedance time signal modelled on the changes in aorta volume flow along with changes in heart volume, induced blood resistivity and blood volume in the lungs also successfully simulates most features of the measured waveform (Kosicki et al. 1986). It has also been reported that the primary influence on the impedance change results from blood volume changes in the lungs (Wang & Patterson 1995, Taylor et al. 1999). Other 3D finite element modeling shows that blood volume changes in the ventricles induce greater impedance changes than blood volume changes in the lungs. The impedance change is linearly related to blood volume changes in the aorta and flow induced blood resistivity changes may contribute as much as 40% of volume changes in the aorta (Kim et al. 1988).

In addition these sources don't occur at the same time during the cardiac cycle which further increases the complexity.

Measurements made with band and spot electrodes in various configurations have also been shown to capture the impedance of different regions with varying sensitivities. The impedance waveforms may look similar, but the origin of the signal may not be the same (Kauppinen, Hyttinen & Malmivuo 1998). Wang, Haynor & Kim (2001) further developed this to investigate the source of impedance changes for both band and spot electrode configurations. Blood volume changes in the major vessels and resistivity changes in blood and lungs were found to contribute to a uniform decrease in impedance, while ventricular contraction increased impedance non-uniformly. A spot electrode configuration is concluded to allow a better detection of ventricle volume change.

These highlighted studies are just a few that demonstrate the widespread disagreement on the origins of the ICG. Perhaps the most widely investigated source of impedance changes as explored by many authors is the resistivity changes in flowing blood measured longitudinally in the direction of flow (Critchley 1998). This is predicted to be caused by changes in the orientation of the red blood cells as blood pulses. The orientation effect can be defined as variations in the electric resistivity of blood as a result of variation in orientation of the red blood cells during flow in the contributing blood vessels. Many authors (Liebman & Bagno 1968, Dellimore & Gosling 1975, Sakamoto & Kanai 1979, Ninomiya, Fujii, Niwa, Sakamoto & Kanai 1988, Visser 1989, Fujii, Nakajima, Sakamoto & Kanai 1999) have investigated the physical properties of blood and confirmed the phenomena associated with the presence of red blood cells. It has been shown that resistivity changes in the ascending and descending aorta have the largest effect

on the thoracic impedance change, 27% and 34% of total vessel contribution respectively (Wang & Patterson 1992). In addition, no impedance changes have been recorded for cell free substances such as plasma or saline (Liebman, Pearl & Bagno 1962).

The presence of this effect can contribute as much as 60% of the $\frac{dZ}{dt}_{max}$ waveform (Newman & Callister 1999). Thus blood volume variations and the orientation effect are both equally important, each contributing to nearly half of the impedance change. The calculation of stroke volume in impedance cardiography assumes that resistivity is constant and that impedance changes are caused solely by volume changes in the contributing blood vessels. However, Raaijmakers, Marcus, Goovaerts, De Vries, Faes & Heethaar (1996) have experimentally demonstrated, using MRI scans to determine vessel radius, that the resistivity of blood varies throughout the cardiac cycle. Therefore the effect of flow dependent impedance changes is to reduce the accuracy of impedance cardiography. Flow induced blood resistivity changes are also non linear; thus significant errors may be introduced in the calculation of stroke volume (Wang & Patterson 1995).

A new equation to calculate stroke volume using impedance cardiography developed by Bernstein & Lemmens (2005) assumes that $\frac{dZ}{dt}_{max}$ relates directly to the first time derivative of the velocity induced blood resistivity variations and therefore $\frac{dv}{dt}_{max}$. The derivation of the equation assumes that the transthoracic impedance is a parallel connection of a static base tissue impedance and a dynamic time dependent signal comprising a velocity induced blood resistivity component and vessel volume changes. The results demonstrate that this assumption vastly improves the determination of stroke volume over the Kubicek and Sramek-Bernstein equations when compared to results obtained using thermodilution techniques. This suggests that the as-

sumption of the volumetric origin of the thoracic impedance change may not be adequate and understanding of velocity induced changes in the resistivity of blood will improve impedance cardiography techniques.

2.2.4 Validation of Impedance Cardiography

Many studies have been conducted comparing single frequency impedance cardiography with conventional cardiac monitoring techniques such as dye-dilution methods, thermodilution and the Fick process. While the research detailed in the above sections shows high correlations, the accuracy of impedance cardiography is still questioned particularly in subjects with cardiac abnormalities (Newman & Callister 1999, Schuster & Schuster 1984). Difficulty in performing comparative evaluation arises as the generally accepted cardiac output reference, thermodilution is only accurate to 10 - 20% (Critchley 1998).

Studies comparing impedance cardiography and indicator dilution techniques in normal healthy subjects show a correlation coefficient from 0.7 - 0.9 and a difference of less than 20% (Patterson 1989, Stout, Van De Water, Thompson, Bowers, Sheppard, Tewari & Dalton 2006, Bayram & Yancy 2009). However, breathing, arrhythmias, movements and posture can interfere with an ICG and subjects with abnormal heart function can generate distorted waveforms which reflect such abnormalities. In these instances, it is difficult to determine the required features of the waveform and result in disparities of up to 44% (Newman & Callister 1999, Cotter, Schachner, Sasson, Dekel & Moshkovitz 2006). The non-invasive nature of the technique makes it ideal for monitoring cardiac functions of frail or elderly patients. However it has been shown that correlation decreases as population age increases due to increasing haemodynamic instability (Stout et al. 2006).

Heart failure primarily affects the haemodynamics of the circulation and as a result changes in the morphology of the measured thoracic impedance are to be expected. While this may compromise the determination of the stroke volume, Bour & Kellett (2008) have attempted to correlate abnormalities in the morphology of the ICG waveform with various heart diseases. Recognising different patterns present in the ICG allows differentiation between normal and abnormal cardiac function. Left ventricular systolic dysfunction has also been assessed by observing differences in the ICG using a new parameter called systolic amplitude (SA) which can be calculated from $\frac{\frac{dZ}{dt}max}{Z_0}$ (DeMarzo, Calvin, Kelly & Stamos 2005, DeMarzo, Kelly & Calvin 2007). This parameter is also associated with the shape of the waveform and has shown to be a better indicator of left ventricular systolic function than cardiac output. Further to this DeMarzo & Calvin (2007) compared ICG waveforms of patients with various heart diseases to the typical $\frac{dZ}{dt}$ waveform generated from a normally functioning heart. Deviations from this normal pattern were considered to be indicative of heart disease. An abnormal $\frac{dZ}{dt}$ waveform during systole would indicate systolic dysfunction, while an abnormal $\frac{dZ}{dt}$ waveform during diastole would indicate diastolic dysfunction. A sensitivity of 94% was achieved in identifying the presence of a strucural or functional disorder but could not be used to identify the specific cause. These studies show the potential for use of the morphology of the ICG waveform to predict cardiac abnormalities.

In general, most validation studies have found reasonable correlation between impedance cardiography and other invasive methods. In addition to assessments of accuracy, clinical evaluations include repeatability and the ability to provide trend data over time. Impedance cardiography tends to be fairly accurate in identifying SV changes with higher reproducibility than

thermodilution techniques (Stout et al. 2006, Visser 1989, Van De Water, Miller, Vogel, Mount & Dalton 2003, Newman & Callister 1999, Nowakowski, Palko & Wtorek 2005). Other clinical applications of impedance cardiography include assessment of blood pressure and central venous pressures, extent of pulmonary congestion and origin of dyspnea (Bayram & Yancy 2009).

Methodological variations such as electrode placement, impedance processing equations and subject characteristics more than likely contribute to the varied correlations and agreements to conventional methods. Although difficulties with current techniques have limited the applications to research, advances in technologies suggesting greater accuracy should lead to clinical acceptance such as cardiac monitoring during surgery. Acceptance should continue to improve with further advancements in the technique (Moshkovitz et al. 2004).

2.3 Flow Induced Blood Resistivity Changes

It has been identified that a significant proportion of the thoracic impedance change can be attributed to blood flow rate dependent changes in the resistivity of blood. The changes in the resistivity of blood as a function of velocity have been investigated by many authors.

2.3.1 Red Blood Cell Effects

Flow related impedance changes have been suggested to be a result of various phenomena; however, it is agreed that it is the presence of the ellipsoidal red blood cells that initiates the impedance change. This is confirmed as saline, haemolysed blood or plasma demonstrate no measurable impedance change with flow changes (Sigman, Kolin, Katz & Jochim 1937, Liebman

et al. 1962, de Vries, Langendijk & Kouw 1995, Fujii et al. 1999, Visser, Lamberts, Korsten & Zijlstra 1976). Reported cell changes inducing an impedance change include:

- the break-up of rouleaux formations [1],
- changes in the cell-free zone or boundary layer [2],
- axial accumulation [3],
- cell deformation and,
- changes in cell orientation.

The effect of velocity on the electrical conductivity of blood has been investigated from as early as 1937 (Sigman et al. 1937). In this study, it was experimentally shown that the resistivity of both bovine and canine blood was altered when blood began to flow. Sigman et al. (1937) attributed this effect to the break up of rouleaux formations by shear forces during flow. However, rouleaux formation is absent in bovine blood (Visser 1992), suggesting that rouleaux break up is not the cause of the impedance change. The cell free zone has also been shown to have a negligible effect on the impedance of blood when the tube diameter or the thickness of the rectangular conduit is larger than 1 mm (Sakamoto & Kanai 1979). Cell deformation has also been ruled out as a primary cause of the impedance change (Visser 1992).

Axial accumulation has been shown to be negligible by comparing experimental results with theoretical results based on a mathematical analysis of two attributed factors: axial accumulation and the orientation effect

[1] Rouleaux formation is the aggregation of RBCs into cylindrical stacks

[2] The boundary layer is the cell free zone that exists close to the walls of a tube in which no cells are present

[3] Axial accumulation is cell migration towards the centre of the tube

(Liebman et al. 1962). A maximum experimental increase in conductance of 8% was achieved, while the calculated results predicted a maximum increase in conductance of 20.5% and 5.46% due to axial accumulation and orientation of cells respectively. If the orientation effect is disregarded, the difference between experimental and theoretical results is still large and shows that axial accumulation only occurred to about 40% of the predicted theoretical magnitude. Since orientation of the cells also contributed, axial accumulation must have occurred to an even lesser extent. It is therefore concluded that axial accumulation is of negligible magnitude.

The change in orientation of red blood cells induced by shear flow is therefore concluded to be the primary influence on the absolute impedance of flowing blood.

2.3.2 Red Blood Cell Orientation

Due to their biconcave shape, changes in orientation of red blood cells will cause changes in blood resistivity. For example, in stationary blood red blood cells are orientated randomly due to Brownian motion and resistivity is isotropic. During flow in rigid, circular, long, straight tubes, every element of a Newtonian viscous fluid flows in a series of laminae parallel to the walls of the tube. As velocity increases, the cells experience a higher velocity variation across their surface. To minimise this shearing stress, cells align in an orientation such that the minimum cross sectional area is experiencing the shear force. The cross sectional configuration of the blood is changed thus altering the resistivity of the flowing blood. Resistivity at full alignment will be anisotropic and will decrease in the longitudinal direction as the electrical current flows through a larger cross section of conductive plasma. An example of cell orientation in both stationary and flowing blood is shown in Figure

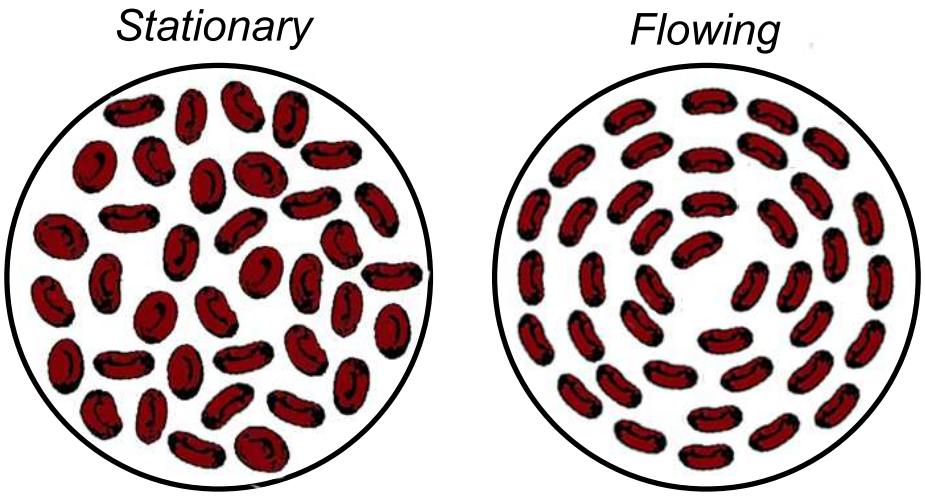

Figure 2.6: Simplified red blood cell orientation during stationary and flowing blood

2.6 looking down the length of the cylindrical tube.

The implications of velocity induced resistivity changes of blood for impedance cardiography are unknown. At the end of diastole (low blood flow) the red blood cells are oriented randomly in response to reduced shear rates. This is the condition of highest resistivity. During the rapid ejection phase of early systole, red blood cells will align parallel to the direction of flow. This is the condition of lowest resistivity (Bernstein & Lemmens 2007). The notches of the ICG signal corresponding to opening and closing of the aortic valve have also been reported to be due to conductivity changes of blood caused by changes in the orientation of red blood cells (Visser et al. 1993).

Traditionally impedance cardiography measurements are taken at 50 kHz. However it has been shown that the orientation effect is dependent on the applied current frequency (de Vries et al. 1995). At higher frequencies, the flow induced orientation effect of the red blood cells flowing through rigid tubes becomes negligibly small (0.5% change in admittance at 20 MHz for

haematocrit of 0.2). This is because at low frequencies, the current passes through only the extracellular fluid, while at high frequencies, the current passes through both the extra- and intra-cellular fluid. Thus it is expected that changes in cell orientation (and intra-cellular fluid) at high frequencies will not influence the impedance. Confirming this, it was found that the effect of red blood cells on the electrical properties of blood in steady flow almost disappeared at frequencies higher than beta dispersion (Ninomiya et al. 1988). From this it can be concluded that impedance cardiography measurements made at high frequencies are immune to the effects of orientation changes and are for the most part caused by changes in blood volume.

Impedance measurements made at high frequencies are known to be unreliable, but perhaps the BIS approach may provide useful information of the resistance at infinite frequency, R_∞, which will not be plagued by blood resistivity variations. Conversely, the resistance at DC, R_0, should provide more sensitive information of the blood resistivity variations caused by changes in red blood cell orientation and thus more physiological information may be extracted from the waveform. It is also possible that a combination of the two may be used to isolate the resistivity changes.

2.3.3 Steady Flow

Many studies have found a resistivity dependence on the shear rate profile for blood flowing at constant rates through rigid tubes (Liebman et al. 1962, Dellimore & Gosling 1975, Ninomiya et al. 1988, Edgerton 1974, Visser 1992, Sakamoto & Kanai 1979). It has been shown both experimentally and theoretically that as flow increases, longitudinal resistivity decreases from that of stationary blood. An example presented by Visser (1989) is shown in Figure 2.7. For higher values of shear, a point will be reached at which

flow induced viscous forces no longer affect the resistivity. At this point, all red blood cells are assumed to be in parallel orientation and thus, an increase in velocity will not change the orientation of cells or the measured impedance. This saturation point has been reported to occur at a range of different shear rates and velocities and varies with the type of flow and geometry of the tube. In two examples, this occurs at a shear of approximately 200 s^{-1} (Visser 1989, Sakamoto & Kanai 1979) while another example reports a velocity of 5 $cm.s^{-1}$ (Liebman et al. 1962). Resistivity changes below the saturation velocity have shown to be both proportional and exponential to the steady state velocity. These results also show that the magnitude of the resistivity change is also dependent on the haematocrit.

2.3.4 Pulsatile Flow

Blood flow through arteries is pulsatile in nature and so steady flow investigations are limited in their in-vivo applications. For example, in one study, the resistivity changes from stationary blood were measured at 8% for steady flow and only 2% for pulsatile flow at similar shear rates (Liebman et al. 1962). This identifies a significant difference between pulsatile and steady flow. Additional studies have reported similar results (Sakamoto & Kanai 1979) in which red blood cells are not able to orient in response to rapid changes of high pulse rate. That is, the peak to peak resistance change decreases with the increase of sinusoidal flow pulse rate. This has important implications for impedance cardiography as the blood pumped through the aorta is pulsatile and may explain why many steady flow studies overestimate the orientation effect.

In tube flow, the laminae that respond to pressure changes first are those nearest the wall and the laminae towards the axis of the tube fol-

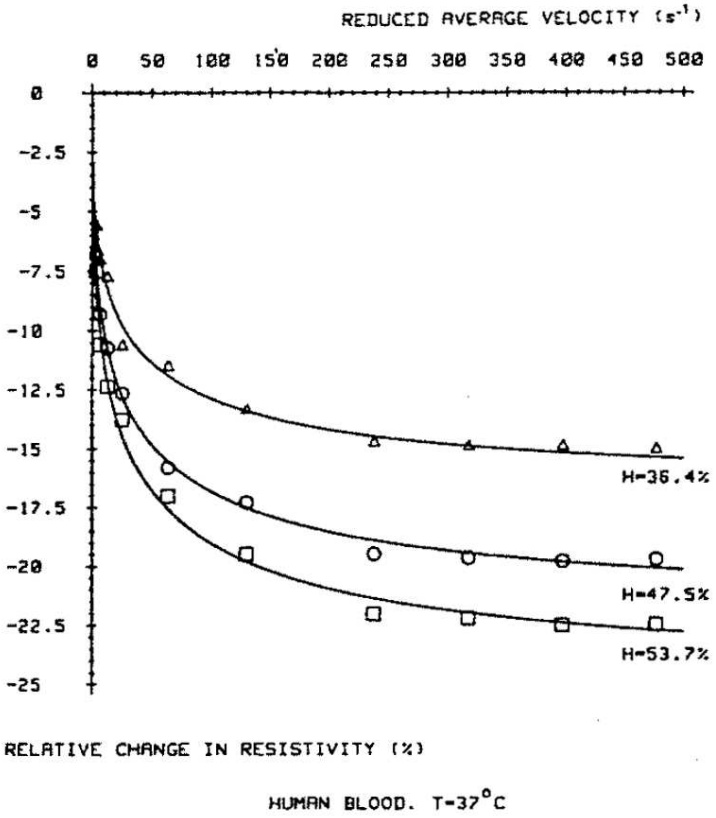

Figure 2.7: Relative change in resistivity of human blood as a function of the reduced average velocity for different haematocrit values (Visser 1989)

low (McDonald 1974). The laminae near the wall have a low velocity due to the effect of viscosity. Hence these laminae have low momentum and reverse easily when the velocity gradient reverses. Closer to the axis, the momentum becomes higher so there is a larger lag between the pressure gradient and the movement of laminae in the centre of the tube. As the frequency of the pressure pulse increases, there is less time for the movement to be translated through to the axial laminae and the velocity profile becomes flattened in the central axial region. This means the laminae are subject to a lower shear than during steady flow at the same average velocity. This explains the pulse dependence of the conductivity change as red blood cells do not experience

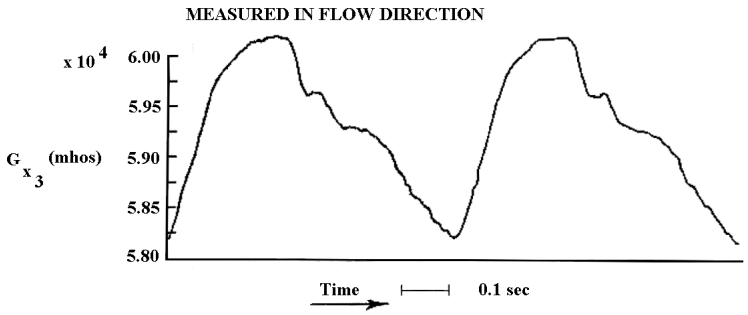

Figure 2.8: Conductivity in the direction of flow in a rectangular measuring conduit during accelerating and decelerating flow (Dellimore & Gosling 1975)

the same shear forces and thus do not have a chance to orient in response to the increase in flow.

Conductance measurements of pulsatile flow taken in a rectangular conduit (Dellimore & Gosling 1975) have shown changes in conductivity are dependent on red blood cell shape as well as axis ratio, haematocrit, shear rate (induced by flow velocity) and the rate of change of shear rate with time (flow acceleration and deceleration) in addition to red blood cell orientation. Figure 2.8 shows the effect of flow acceleration and deceleration on changes in the conductance measured in the longitudinal direction during pulsatile flow presented by Dellimore & Gosling (1975). The arrows show the direction of flow change. As the flow accelerates, the conductivity increases and as the flow decelerates, the conductivity decreases. However, the conductivity is not the same at the same average velocity, during acceleration and deceleration.

In addition to this, it has been found that in time varying flow, the time for orientation and disorientation differ largely (Visser 1989). In accelerating flow, the resistivity change is synchronous with the change in flow. However in decelerating flow, an exponential decay appears to exist in which the time constant does not significantly differ for the different driving flow velocities. This phenomenon is confirmed by additional published experimental results

for pulsatile blood flow (Sakamoto & Kanai 1979).

These results demonstrate that analysis of steady flow is not sufficient to fully understand the conductivity changes recorded in impedance cardiography and a further relationship between acceleration and conductivity needs to be investigated. It should also be noted, that the shear rate profile and thus the orientation of red blood cells is different in tubes with different cross sections. The aorta can be assumed to be of circular cross section and thus measurements in a rectangular conduit do not adequately reflect the physiological environment. Doubts also arise as to the accuracy inherent in predicting flow velocities from conductance measurements because of the variety of additional factors that influence changes in blood conductivity.

Experimental results comparing simultaneous pulsatile rigid tube impedance with the corresponding pulsatile impedance of an artery able to distend with volume changes have also been reported (Peura et al. 1978, Sakamoto & Kanai 1979, Shankar, Webster & Shao 1985). These show directly that the morphology of the artery impedance pulse is a combination of the blood volume changes measured in the artery and the red blood cell orientation effect measured in the rigid tube. It has also been demonstrated that while both blood volume and blood resistivity changes contribute to the morphology, they occur out of phase such that the blood resistivity contribution at the height of the impedance pulse is less than 5.5% (Shankar et al. 1985). This raises concerns as to the level of error introduced by the assumption used in impedance cardiography that the blood has a constant resistivity.

Through theoretical expansion of the parallel conductor model and experimentation involving dogs, it was shown that the average variation in blood conductance during the cardiac cycle was 7.5% (Visser et al. 1988). This was

made up of 4.5% from orientation effects and 3% by blood volume variations. This shows that up to half of the heart synchronous impedance variations during impedance cardiography may be due to orientation effects.

2.3.5 Anisotropic Properties

Stationary blood is an isotropic medium. Red blood cells are oriented randomly and so the conductivity of stationary blood is the same in all directions. The resistivity of flowing blood however, displays anisotropic properties and is a tensor rather than a scalar. That is, the resistivity differs according to the direction of measurement due to the alignment of red blood cells. This has been shown to be the case in flow through rigid rectangular conduits (Dellimore & Gosling 1975), Couette flow [4] (Fujii et al. 1999) and Poiseuille flow through rigid cylindrical tubes (Visser et al. 1976). Limited investigations have been made of the orthogonal impedance of blood flow through rigid cylinders due to the difficulty presented by the geometry in allowing easy tetra-polar measurements to be taken. Other studies that measure orthogonal resistivity of blood in rectangular conduits or Couette flow have different shear rate profiles due to differences in geometry and thus are difficult to compare.

In a cylindrical tube there exists three cylindrical co-ordinates: longitudinal, z, radial, r, and azimuth, θ. The shear rate in the tube is symmetric around the longitudinal axis. As shear rate is the most important factor in determining red blood cell orientation and therefore resistivity, it can be concluded that resistivity will also be symmetric around the longitudinal axis. Thus the resistivity is reduced to a two dimensional analysis.

The impedance of mammalian blood in pulsatile flow through rigid cylin-

[4] Couette flow is laminar flow between boundaries of which one is moving

drical tubes has been measured in two orthogonal directions and shown to act in opposite directions. As the flow increases, the conductivity in the longitudinal direction rises while the conductivity in the horizontal radial direction falls due to orientation changes of red blood cells (Visser et al. 1976). The radial change is smaller in magnitude than the longitudinal changes.

Modelling and experimental work completed for the orthogonal impedance of blood flowing through a cylindrical tube showed that each element of the conductivity change tensor contributed to the measured impedance only if the corresponding electric field was non zero (Wtorek & Polinski 2005). This demonstrates that the anisotropic properties of flowing blood are important to impedance cardiography. The electrode placement in impedance cardiography means that the electric field generated between the neck and abdomen is in essence vertical in a standing patient. When considering the flow of blood through the aorta in the thorax, the blood flows into the ascending aorta, around the aortic arch and into the descending aorta. Flow in the ascending and descending aorta is essentially parallel to the applied electric field, thus longitudinal conductivity changes will affect the measured impedance. Flow through the aortic arch is essentially perpendicular to the electric field and thus changes in radial conductivity will also affect the measured impedance, but in the opposite direction. This may explain why errors in measurements made in-vivo are not as great as those predicted from simplified models. It also identifies the importance of understanding both the longitudinal and radial conductivity changes in flowing blood.

2.4 Summary

It is evident from the literature that impedance cardiography is still not widely used in clinical settings. The technique has potential, but more basic experimental work is needed on the interpretation of waveforms in order to provide more reliable and meaningful clinical information. A major reason for the delay in acceptance of impedance cardiography in a clinical setting is that the origin of the impedance changes is still not well understood (Geddes & Baker 1989, Patterson 1989, Wang & Patterson 1995, Critchley 1998, Newman & Callister 1999, Taylor et al. 1999, Faes, Raaijmakers, Meijer, Goovaerts & Heethaar 1999, Visser et al. 1993). Not only is there is some disagreement as to the specific organs that are responsible for the volume change, but other phenomena such as orientation of blood cells and respiration have also been attributed to the occurrence of impedance changes.

The literature reviewed demonstrates that one of the most widely researched sources of impedance error is the resistivity change observed in flowing blood (Visser et al. 1988, Liebman et al. 1962, Liebman & Bagno 1968, Sakamoto & Kanai 1979, Dellimore & Gosling 1975, Visser 1989, Visser 1992, Hoetink et al. 2004, de Vries et al. 1995, Ninomiya et al. 1988, Edgerton 1974). Many studies conclude that the presence of red blood cells causes the resistivity of the blood to change as the orientation of the cells change. The effect of flow is to alter the state of orientation of the cells and thus the resistivity is also affected. Variations in resistivity caused by changes in orientation of the cells can contribute to as much as half of the impedance change observed in impedance cardiography.

Although much work has been published on this effect, previous studies have concentrated primarily on quantifying impedance change for constant flow rates. Because the blood flow through the heart is pulsatile in nature,

these studies are not adequate. The characteristics of pulsatile flow are different from that of steady flow due to its viscous nature and need to be taken into account. Prior to conducting this research, no studies on theoretically modelling the impedance of blood in pulsatile flow or quantifying experimental results for pulsatile flow through cylindrical tubes had been completed. Thus investigations to reveal a greater understanding of the acceleration and deceleration effects of pulsatile flow on resistivity of blood should lead to improved impedance cardiography techniques.

Literature has shown that the events of the cardiac cycle are complex and difficult to measure (Katz 1977, Geddes & Baker 1989, Pedley 2003). Impedance methods allow the measurement of the effects of these events by recording changes in impedance. The $\frac{dZ}{dt}$ signal has many distinct peaks and notches that are repeated from cycle to cycle and appear to be related to periodic events in the cardiac cycle such as opening and closing of valves. This indicates that ICG waveforms may contain more information on cardiac health and function than just the stroke volume. The information contained within the timing relationship of the ICG may be of more value than the amplitude of the signal (Meijer, Boesveldt, Elbertse & Berendse 2007). These variations may originate from resistivity changes due to changes in rate of blood flow caused by physiological events in the heart. Understanding the contribution to the morphology of the waveform will be of significantly worthwhile in clinical investigations. Also, diseases of the heart and heart valves (such as stenotic valves) can cause predictable abnormalities in flow of blood from the heart. It is likely that such abnormalities will result in detectable variations in the impedance cardiogram. The non-invasive nature of impedance cardiography makes it highly suitable for use in diagnosis of such patients.

Chapter 3

Experimental Impedance of Blood Measured in Rigid Tubes

3.1 Design

In order to understand the flow effect of red blood cell (RBC) orientation on impedance cardiography waveforms, the relationship between the impedance and velocity of blood has been investigated. In this chapter the experimental relationship is explored using an in-vitro mock circulatory system to pump blood through rigid tubes. The impedance and flow rate of the blood was measured synchronously in real time. From the flow rate, the velocity and acceleration of the blood were determined.

Measuring the impedance of blood flowing through rigid tubes isolates the effect of flow changes on the impedance by removing volume changes occurring in-vivo. The remaining impedance changes are assumed to be due solely to the effect of flow induced variations in red blood cell orientation. This begins the first step in understanding the effect of red blood cell orientation changes during flow on impedance cardiography waveforms.

The purpose of the mock circulatory system was not to exactly mimic the in-vivo performance of the circulatory system, but rather to generate physiological flow as closely as possible, while maintaining well known and reproducible flow properties (Hoskins, Anderson & McDicken 1989). The system was designed to simulate pulsatile blood flow through the aorta over the pulse rate and flow velocity range similar to that found in a normal adult.

3.1.1 Flow Generation

The system was designed to generate pulsatile blood flow over a range of pulse rates, stroke volumes, and tube radii. The velocity profile in normal arteries is known to be laminar and ranges in profile from flat to parabolic during the cardiac cycle (McDonald 1974). Pulsatile flow can be generated by a number of different means such as a peristaltic roller pump, a gear pump, or a piston pump (Hein & O'Brien 1992). Gear pumps can cause significant damage to suspended cells (Hoskins et al. 1989) while peristaltic pumps cause minimal damage to suspended cells. However the required flow rates were not attainable using peristaltic pumps available at the time of experimentation. Instead, the Harvard Apparatus Pulsatile Blood Pump for Large Animals and Haemodynamic Studies was used. It is a positive piston pump with specifications shown in Table 3.1.

PARAMETER	HARVARD PUMP	REQUIREMENT
Volume Flow	0.15 L/Min - 10 L/Min	2 - 8 L/Min
Stoke Volume	0.015 L - 0.1 L	0.06 - 0.1 L
Pulse Rate	10 - 100 bpm	60 - 72 bpm
Systolic/Diastolic Ratio	25/75 to 45/55	35/65
Accuracy	2%	5%
Reproducibility	0.5%	5%

Table 3.1: Harvard Apparatus Pump Specifications

3.1.2 Entrance Length

To ensure laminar flow within the tube, impedance measurements were taken at a location after which the flow was able to stabilise through an entry length, L. This entry length can be calculated a number of ways for steady flow.

Laminar Flow

$$L = 0.04d \cdot Re \qquad \text{(McDonald 1974)} \tag{3.1}$$

$$L = \frac{0.16\rho}{\pi\mu}Q \qquad \text{(Hoskins et al. 1989)} \tag{3.2}$$

Turbulent Flow

$$L = m.d \qquad \text{(Nakayama \& Boucher 2000)} \tag{3.3}$$

where d is the diameter of the tube, Re is the Reynolds Number, ρ is the fluid density, μ is the dynamic viscosity of the fluid, Q is the volumetric flow rate and m is a scaling factor between 25 and 40.

For pulsatile flow, the absolute entrance length is more difficult to specify. The Womersley number (α_w) is an indication of the extent to which the velocity profile in laminar flow differs from the Poiseuille profile. The entrance length of unsteady flow has been found to vary over the duration of the pulse, equivalent to the corresponding steady flow entrance lengths when the Womersley number is low (He & Ku 1994). However, as the Womersley number increases, the entrance length becomes more uniform during the pulsing cycle and tends to the entrance length of the mean flow of the pulse.

Experiments performed by Visser (1989) generated reversed flow through

a tube length where the measurement location was close to the entrance. It was found that flow was similar to that measured when flowing forward through the entire entrance length. This suggests that entrance effects in pulsatile flow may not be as important as initially expected. Therefore, due to the simplicity in calculation, equation 3.3 was used to determine the entrance length, AB. The final design is shown in Figure 3.1. The current injecting electrodes are labelled B and E and the sensing electrodes are labelled C and D. Electrode G is used along with electrode D for bi-polar measurements. For a tube of 12.7 mm inner diameter the following dimensions were used:

$$AB = 0.51 \ m$$

$$BC = 0.02 \ m$$

$$CD = 0.01 \ m$$

$$DE = 0.02 \ m$$

$$EF = 0.32 \ m$$

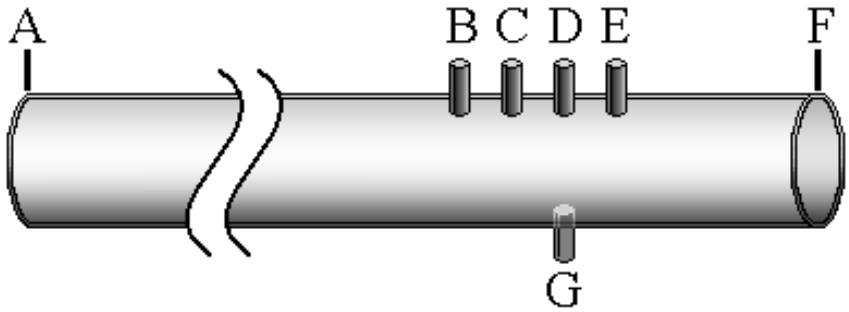

Figure 3.1: Entrance length of measurement tube showing location of electrodes

3.1.3 Impedance Measurements

To measure the impedance of flowing blood, an ImpediMed Imp SFB7^{TM} was used. The ImpediMed Imp SFB7^{TM} is capable of measuring the impedance at 256 frequencies at a single point in time. This device was also modified to allow rapid measurements to be taken at a single current frequency at a sample rate of about 1 kHz. This is a single channel tetra-polar device.

To measure the impedance, electrodes are required to make contact with the blood. Large electrodes directly inserted into the measuring tube will disturb the flow pattern and polarisation will occur on the metallic surface (Grimnes & Martinsen 2000). Thus the electrode were made flush with the tube walls so as not to alter the developed flow. The electrodes were constructed of platinum to minimise polarisation effects.

Visser (1989) and de Vries et al. (1995) both implemented four circular ring electrodes mounted within the tube of a cylindrical measuring cell in order to maintain developed flow. A circular ring electrode is able to sit flush, surrounding the fluid while cells over the entire cross sectional area are able to contribute to the measured impedance. Due to difficulties in manufacturing circular ring electrodes within the wall of the tube and maintaining a liquid tight tube, this geometry was abandoned for the present study. Instead, four probe electrodes were mounted with one end flush with the developed flow.

3.1.4 Flow Sensing

The flow was measured using a Transonic TS410 Tubing Flow meter and a ME-PXN-Series inline flow probe. This device comes pre-calibrated for blood, directly measures the volume rate of flow, and can be externally triggered. In this instance, the flow sensor was triggered by the impedance

measurement made using the ImpediMed Imp $SFB7^{TM}$. The low pass filter setting on the Transonic flow meter was set at 40 Hz. In addition, the collected data was also passed through a digital low pass filter with a cut-off of 10 Hz. Fourier analysis showed that the flow signal was composed of frequencies predominantly below 10 Hz and no significant information was lost in filtering.

While the velocity profile gives more information relevant to the impedance of the blood, measurement was limited to the spatial average velocity over the tube. The spatial average velocity is the average velocity of all laminae across the tube at any moment. This is different from the mean velocity which is the average velocity over the flow cycle time. The volumetric flow rate was converted to a spatial average velocity by dividing by the cross sectional area of the tube.

3.1.5 Tube Radius

Many published studies have made use of a rectangular measuring chamber (Dellimore & Gosling 1975, Liebman & Bagno 1968, Ninomiya et al. 1988, Sakamoto & Kanai 1979). However, flow through a cylinder more closely resembles the flow patterns through the human arterial system. Therefore the measuring chamber chosen was a cylindrical tube. The measurement tube radius was varied during testing but the majority of measurements were made within a 6.35 mm radius tube (12.7 mm diameter).

The tube was constructed of rigid Perspex to eliminate impedance changes due to blood volume changes. The average diameter of the aorta is 25 mm which is larger than the 12.7 mm tube implemented. The cross sectional area of the aorta (i.e. diameter) changes as the heart ejects blood. As rigid tubes were used to remove the effect of volume changes on impedance in

this study, the diameter of the tube (regardless of size) does not truly reflect all physiological conditions. Therefore little importance has been placed on meeting this requirement. As it was easier to generate larger peak velocities in smaller tubes within the limitations of the pump, the 12.7 mm diameter tube was used.

The remaining connecting tubing in the system was relatively stiff as excessive elasticity would distort the signal due to reflected pressure waves (Hoskins et al. 1989). Thus the connecting tube used was made of PVC or silicon.

3.1.6 Stationary Cell

An isolated stationary cell was used to measure the impedance of the stationary blood. This was based on the design by Visser (1992) and is shown in Figure 3.2.

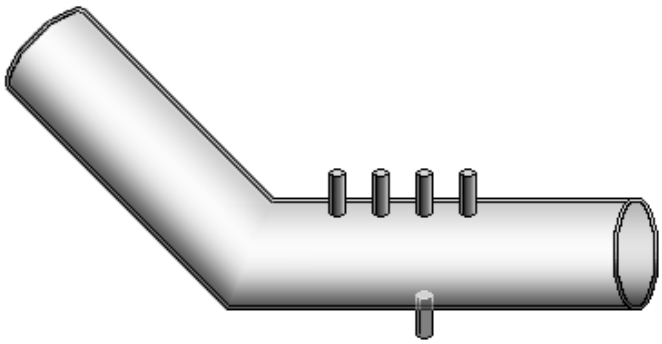

Figure 3.2: Measurement tube for stationary blood

3.1.7 Temperature Control

The conductivity of blood has been shown to be temperature dependent (Jaspard & Nadi 2002, Mohapatra & Hill 1975, Tjin, Xie & Lam 1998) due to changes in the mobility of ions with temperature. As the temperature increases, the impedance of blood decreases. In one example the resistivity of blood decreased from 165 $\Omega.cm$ to 150 $\Omega.cm$ with an increase in temperature from 34^oC to 41^oC.

Thus the temperature of the blood was kept at a constant level. As room temperature was climate controlled and the easiest to maintain during experimentation, data collection was generally performed at this temperature. The effects of temperature were also assessed by varying the temperature of the blood. This was achieved by immersing the collection reservoirs in temperature controlled water baths.

3.1.8 Blood

Bovine blood was used in this study as a model for human blood. Bovine blood is the most easily obtainable animal blood available in large quantities (up to 8 litres) that most closely resembles the size of human RBCs (major axis length of 8 μm and 5.5 μm respectively). Heparin was added to prevent coagulation of the cells.

At low shear rates, the viscosity of bovine blood (6.6 mPa.s) is considerably less than human blood (33.5 mPa.s) (Windberger, Bartholovitsch, Plasenzotti, Korak & Hienze 2003). This difference is thought to be due to the higher degree of aggregation of RBCs to form cylindrical rouleaux occurring in human blood. At higher shear rates, the rouleaux formations are broken up by shear stresses and the viscosity of both human and bovine blood

are of similar magnitude (4.8 mPa.s and 6 mPa.s respectively) (Windberger et al. 2003)).

The presence of rouleaux in human blood may alter the impedance in Poiseuille flow at very low shear rates (Dellimore & Gosling 1975). At low shear rates, the velocity profile of Poiseuille blood flow through venules is flattened rather than parabolic (Bishop, Nance, Popel, Intaglietta & Johnson 2001). This effect is less noticeable at high shear rates when rouleaux are disaggregated. As the present study investigated the impedance of pulsatile blood and the effect of pulsatile flow is also to flatten the velocity profile, it is expected that the lack of rouleaux formation in bovine blood had a negligible effect on the measured impedance.

The resistivity changes of bovine blood have been shown to be similar to those of human blood (Visser 1989). This rules out rouleaux formations as a cause of impedance change in flowing blood. In addition, most studies reported the use of a magnetic or mechanical stirrer to keep the blood in motion and avoid any effects such as rouleux formation or settling due to gravity. It has been suggested that in stationary blood, erythrocytes tend to orient with their axis of symmetry in the vertical direction due to gravitational settling (Visser 1989). This will affect the conductivity of blood and can be countered by shaking or vibrating the blood. A mechanical stirrer was used in the source reservoir in the present research.

3.1.9 Orthogonal Measurements

Previously, impedance measurements of blood flowing in circular tubes have been primarily longitudinal measurements along the direction of blood flow. In order to investigate the changes in the impedance of blood across the direction of flow, an orthogonal measurement needs to be taken along the

radial axis. The measurement of orthogonal impedance has been reported in the literature for blood flowing through rectangular conduits (Dellimore & Gosling 1975) and cylindrical tubes (Visser et al. 1976). The geometry of the cylindrical tube used by Visser et al. (1976) was such that an electrode was located in the centre of the tube, obstructing the flowing blood and compromising the development of the shear profile.

In order not to disturb the flow pattern, electrodes must be maintained in a flush position with respect to the flowing blood. In a circular tube, only two electrodes are able to make contact with the blood across the diameter of the tube, one on each side of the tube as shown in Figure 3.2.

The use of only two electrodes constitutes a bipolar measurement. In a bipolar electrode configuration, the current is injected via the same electrode from which the voltage is sensed. Polarisation effects are more evident in measurements of this nature. Polarisation is defined as the electric field induced disturbance of the charge distribution in a region (Grimnes & Martinsen 2000). Thus the absolute results cannot be compared directly with the standard tetra polar longitudinal measurements, however conclusions can be drawn by examining the nature of the impedance response to flow for both measurement configurations.

Previous literature suggests that the longitudinal impedance of flowing blood is only a function of the radius of the tube (Visser 1989). This is because the erythrocytes will align with the minimum cross sectional area undergoing the shearing force. In a cylindrical tube, this shear is symmetric about the longitudinal axis. Thus it can be assumed that the impedance of flowing blood will not be a function of the azimuth, however there have been no published experimental results confirming this assumption.

The orthogonal impedance of flowing blood has also been theoretically

modelled by Wtorek & Polinski (2005) using the Geselowitz relationship for an anisotropic medium. This study was limited to the impedance change at the instant the blood begins to flow.

3.2 Methods

3.2.1 Final Implementation

Eight litres of bovine blood were pumped through rigid tubes from one reservoir to another, as shown in Figure 3.3. This open loop set up was required as closed loop measurements were affected by interference on the impedance signal due to the additional current path between the electrodes. The blood was pumped through silicon tubing using the Harvard Apparatus Pulsatile Blood Pump for Large Animals and Haemodynamic Studies. The impedance was measured in a Perspex rigid tube (12.7 mm diameter) with 4 platinum electrodes using an ImpediMed Imp SFB7. This device was modified to make rapid measurements at 1 ms intervals for a period of up to 30 seconds at a single current frequency. Flow rate was measured by a Transonic ME13 PXN Inline Sensor and TS410 Tubing Flow meter. The temperature of the blood was maintained at constant temperature (room temperature or maintained using a programmable water bath) and the haematocrit of the blood was measured using a Coulter Counter or spin down techniques.

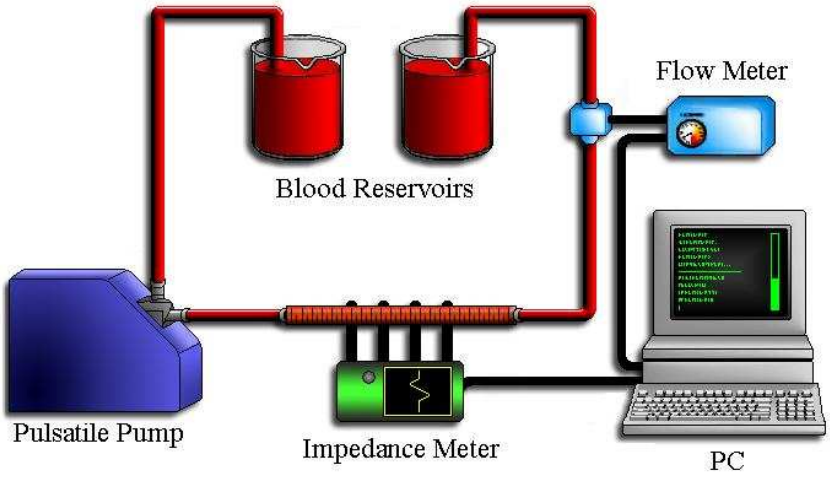

Figure 3.3: Experimental Mock circulatory System

3.2.2 Orthogonal Measurements

To investigate the anisotropic properties of the flowing blood, impedance measurements were recorded in the direction orthogonal to the direction of flow. Orthogonal bipolar measurements of flowing blood were recorded for a pulse rate of 73 bpm and stroke volume of 20 ml through a 12.7 mm diameter tube (h = 44 %, temperature = 19^oC). Measurements were taken across the diameter parallel to the horizontal axis, with the tube rotated by 45 degrees clockwise and with the tube rotated by 45 degrees counter clockwise. This is demonstrated in Figure 3.4. Previous studies report the impedance in one radial direction only.

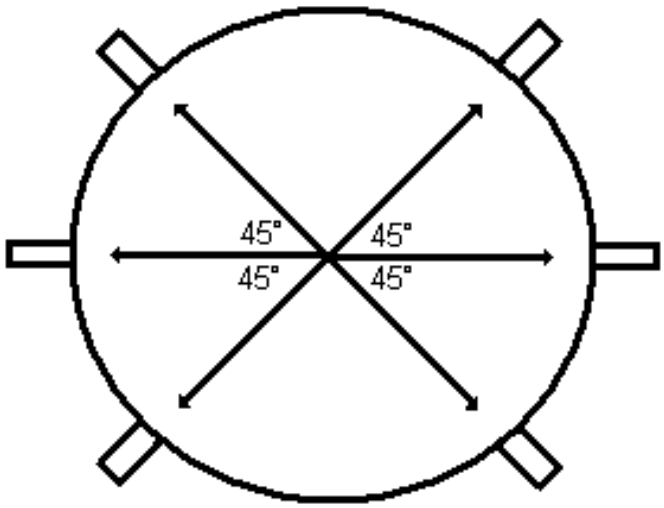

Figure 3.4: Direction of Orthogonal Measurements Recorded

3.2.3 Parameter Variations

Experimental data were collected over a range of parameters. The velocity of the flowing blood was altered by varying the pulse rate and the stroke volume of the pump to be representative of the human heart. The shape of the velocity pulse was altered by varying the systolic/diastolic ratio of the pump. The impedance was measured at a number of current injection frequencies. The haematocrit of the blood was varied by adding volumes of physiological saline to the whole blood. It was found that large additions of saline decreased the viscosity of the blood and in turn affected the flow properties. As a result, only small volumes of saline were added to vary the haematocrit. The temperature of the blood was varied by immersing both the source and sink reservoirs in temperature controlled water baths. Insulation was wrapped around the tubing and the heated blood was pumped around

the tubing for a period of time prior to taking impedance measurements. The tube radius was also varied. Each parameter was varied while maintaining standard values for the remaining parameters as shown in Table 3.2.

PARAMETER	STANDARD VALUE	VARIATIONS
Pulse Rate	70 bpm	20 - 100 bpm
Stroke Volume	40 ml	20 - 60 ml
Systolic Ratio	35/65	45/55 - 25/75
Current Frequency	5 kHz	5 - 500 kHz
Haematocrit	40 %	36 - 46 %
Temperature	19^oC	$19 - 35^oC$
Tube Diameter	12.7 mm	9.5 - 19 mm

Table 3.2: Experimental parameter variations

3.3 Results and Discussion

Prior to data collection of blood, saline was pumped through the system and the impedance measured. No variation with flow was recorded.

3.3.1 Stationary Blood

The impedance of stationary blood was measured using the apparatus shown in Figure 3.2. Both multi-frequency and single frequency measurements were recorded. In both cases, blood was measured with the longitudinal axis of the stationary tube in a vertical and horizontal orientation to ensure adequate mixing of the blood. An example of the multi-frequency data for stationary blood is shown in Figure 3.5. The SFB7 measures the impedance from 3 kHz to 1000 kHz, however the characteristic frequency of bovine blood is in the order of 1500 kHz. There is therefore insufficient experimental results to accurately describe the impedance locus as would be expected from Figure 2.2.

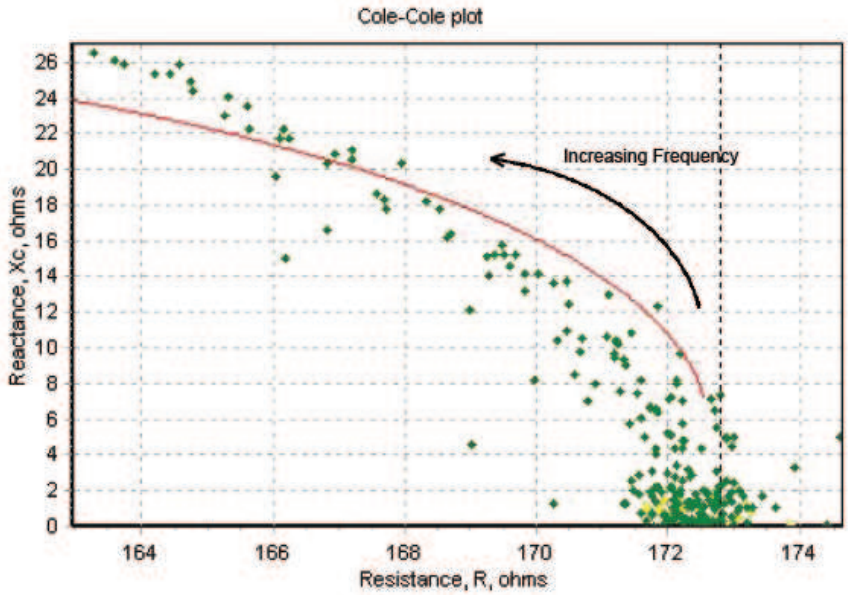

Figure 3.5: Multi-frequency impedance of stationary bovine blood where the green dots show the raw data points and the red line shows the fitted impedance locus (d = 12.7 mm, h = 44%, T = 19 °C)

The theoretical resistance at 0 Hz (R_0), impedance at 5 kHz (Z_5) and other Cole parameters were calculated for each measurement. The resistivity (ρ) was also calculated by dividing R_0 by the cross sectional area of the tube. A summary including mean and coefficient of variation (CV) is shown in Table 3.3. Random orientation of the cells is verified by the small difference between results obtained in the horizontal and vertical orientations ($\leq$1.5%).

Many authors publish data determining the resistivity of stationary blood as a function of temperature and haematocrit. The resistivity of blood has been calculated using these relationships for the experimental conditions (H = 44 %, T = 19^oC) existing during stationary blood measurements (see Table 3.4).

The measured resistivity in the present research is consistent with that calculated from published studies for bovine blood. The resistivity deter-

Orientation	R_0 (Ω)	R_∞ (Ω)	f_c (kHz)	Z_5 (Ω)	ρ (Ω.cm)
Horizontal	173.8	133.1	1968	174.9	220.2
Horizontal	173.6	137.9	1729	174.7	219.9
Horizontal	173.8	132.6	2071	174.9	220.2
Mean	173.7	134.5	1922.7	174.8	220.1
CV (%)	0.1	2.9	175.4	0.1	0.1
Vertical	171.8	129.8	2118	172.7	217.6
Vertical	171.2	139.1	1825	172.2	216.9
Vertical	171.1	137.3	1902	172.7	216.7
Mean	171.4	135.4	1948.3	172.5	217.1
CV (%)	0.4	4.9	151.9	0.3	0.5
Difference of Means	2.4	0.9	25.7	2.3	3.0
% of Avg	1.4%	0.6%	1.3%	1.3%	1.4%

Table 3.3: Summary of Cole parameters for stationary blood at a temperature of 19 ^{o}C

Details	Equation	ρ ($\Omega.cm$)
(Geddes & Sadler 1973) Bovine blood, H = 0-70%, T = 37^oC, f = 25kHz	$\rho = 54.5e^{0.02H}$	131
(Mohapatra & Hill 1975) Human blood, H = 16-52.5%, T = 22-40^oC, f = 100kHz	$\rho = (6.272H + 75.176)$ $-(0.104H + 1.467)T$	236
(Tjin et al. 1998) Porcine blood, H = 18-49%, T = 33-42^oC	$\rho = (4.823H + 63.812)$ $-(0.045H + 0.810)T$	223

Table 3.4: Published studies investigating the resistivity of stationary blood, H = 44 (%), T = 19 (^oC)

mined using Geddes & Sadler (1973) is much lower than the resistivity measured at 19^oC in the present study. However their equation was developed from data at 37^oC and it is expected that the resistivity would increase with a decrease in temperature. The remaining published relationships that include the variation of temperature give a closer approximation to that measured in this study (217 - 220 Ω), despite the different current frequency used to measure the impedance. This is explained as erythrocytes are known to be non-conductive ellipsoids when placed in electric fields with frequencies up to 100 kHz (Trautman & Newbower 1983).

The characteristic frequency (f_c) of human blood is in the order of 700 kHz to 1 MHz. Ulgen & Sezdi (1998) determined the characteristic frequency of stationary blood as 937 kHz. However the characteristic frequency measured in the present work (1948 kHz) is almost double this value. This increase may be explained as the characteristic frequency has been shown to increase after sedimentation begins (Grimnes & Martinsen 2000). Fifteen minutes after sedimentation begins, the characteristic frequency of blood has been shown to be 1.2 MHz, increasing to 1.5 MHz, 90 - 270 minutes after sedimentation begins. While every effort was made to minimise sedimentation, the presence of sedimentation during these experimental measurements is also supported by the measurements example shown in Figure 3.6.

Figure 3.6 shows an example of data collected experimentally. It shows that as the blood begins to flow after about five seconds, the impedance decreases from the stationary impedance. However, when the flow returns to zero, the impedance continues to increase beyond that of the stationary starting impedance. This suggests that the erythrocytes did not begin from an initial random orientation, but rather may have experienced some settling. This may be because the blood was not constantly stirred during

measurement time to avoid electrical interference on the impedance signal. Other published studies maintained constant agitation of the blood through vibrations to prevent settling and sedimentation (Visser 1992, Geddes & Sadler 1973).

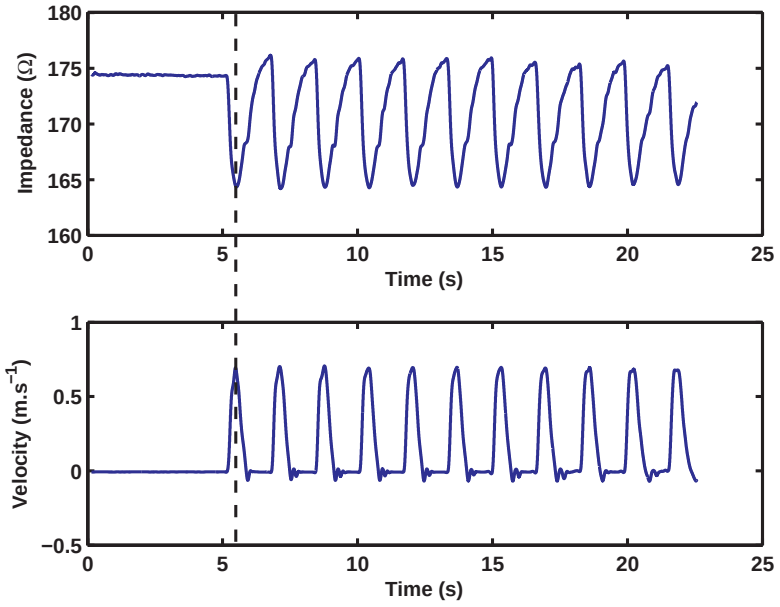

Figure 3.6: Stationary and flowing blood collected experimentally

Sigman et al. (1937) showed a similar effect to the present study for bovine blood in which at low flow rates, the resistance of blood increased. This effect was not observed for canine blood. Sigman et al. (1937) attribute this to an electrode effect. To remove this effect the electrodes were removed from contact with the flowing blood and placed in contact with stationary blood in side arms of the flow tube. For the purposes of the present study, this was not considered an option as this may have altered the flow profile through the tube and modify the measured impedance.

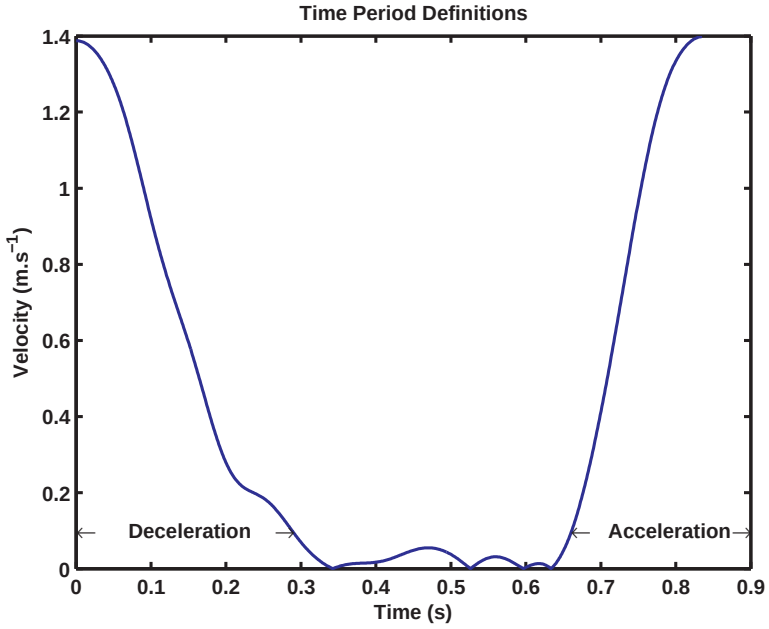

Figure 3.7: Definition of deceleration and acceleration flow phases in an example velocity pulse wave

3.3.2 Impedance of pulsatile blood flow

To aid in analysis, two distinct flow phases were identified. These were: a) the acceleration phase, defined from the time when the blood velocity begins to rise to the time where the peak of the velocity occurs, and b) the deceleration phase, defined as the time from the peak of the velocity to the time when the velocity begins to rise again. This is shown graphically in Figure 3.7.

The flow and impedance were recorded simultaneously while the blood was pumped from one reservoir to the other. Both the flow and impedance signals were filtered using a low pass filter with a frequency cut-off of 10 Hz to remove additional unwanted noise on the signals. Figure 3.8 shows an example of the ensemble averaged experimental results for impedance and velocity of pulsatile bovine blood. The ensemble average is the average velocity calculated for a number of consecutive velocity pulses. The average

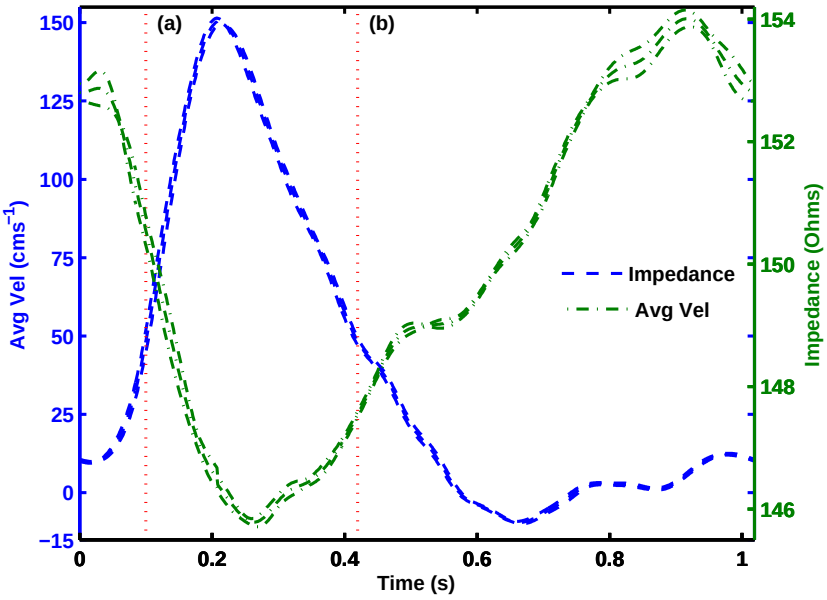

Figure 3.8: Ensemble averaged results ($\pm\sigma$), H=45%, d=12.7mm, pulse rate=60bpm, f=5kHz, ratio=35/65 (a) t=0.1s (b) t=0.42s

velocity is represented by the dashed line and the impedance is represented by the dot-dashed line. The standard deviation of results is also shown.

An example of the impedance and velocity, along with the derivative of impedance and acceleration of the flowing blood over a time period of five seconds is shown in Figure 3.9 for a pulse rate of 72 bpm. This shows explicitly that the measured impedance of blood flowing through rigid tubes changes in a repeated pattern corresponding with the pulsatile velocity of the blood. These results share common characteristics with previously published data such as that of Dellimore & Gosling (1975). Results collected over a range of cardiac parameters such as pulse rate, stroke volume and systolic to diastolic ratio demonstrate similar characteristics.

It can be seen that the impedance responds instantaneously to increases in velocity during the acceleration phase. For each pulse, as the blood accel-

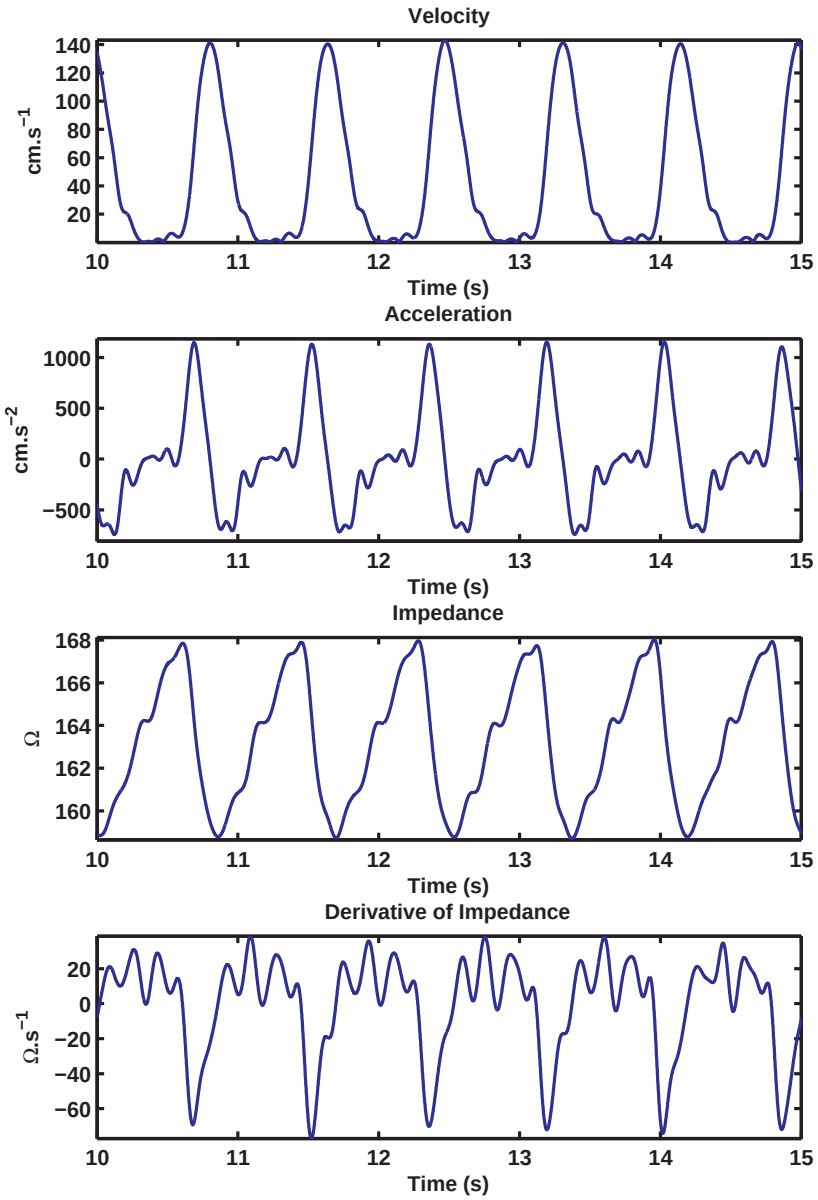

Figure 3.9: Velocity and impedance of bovine blood, H = 44.25%, d = 12.7 mm, T =19^oC, bpm = 72

erates, the impedance decreases until the velocity reaches a peak. During the deceleration phase, as the velocity begins to decrease, the impedance of the blood increases at a decayed rate. This is able to be seen more explicitly at low pulse rates by comparing the conductivity of the blood with the absolute velocity as in Figure 3.10. At low pulse rates, the time between consecutive acceleration phases is longer and the velocity of the blood returns to a stationary flow in between pulses. In this case, the cells have a longer period of time to continue disorientating from their aligned position before they begin to realign due to an increase in velocity. The decay effect can then be easily seen. The observation of this decay effect suggests that there exists a different relationship between the impedance and velocity of the blood during the acceleration and deceleration phases. In Figure 3.8, it can also be seen that the impedance is different for the same spatial average velocity, during the acceleration and deceleration phases such as at time (a) 0.1 s and (b) 0.42 s indicated by the vertical dotted lines.

It is also interesting to note that without the presence of volume changes, the negative peak impedance derivative occurs simultaneously with the peak acceleration of the blood in Figure 3.9. This is in corroboration with investigations by Bernstein & Lemmens (2005) who assume that the peak rate of change of blood resistivity, $\frac{d\rho}{dt}$, is the origin of the peak derivative of the thoracic impedance $\frac{dZ}{dt}$, rather than blood volume changes. Due to the orientation of the cells, Bernstein & Lemmens (2005) assumed the derivative of the resistivity of blood ,$\frac{d\rho}{dt}$, to represent the velocity of the blood and therefore, that $\frac{dZ}{dt}$ is due to the peak acceleration of blood through the aorta. The simultaneous occurrence of the in-vitro peak blood velocity and the impedance derivative presented here for flow through rigid tubes provides further substantiating evidence that $\frac{dZ}{dt}$ measured during IC is due to peak aortic blood

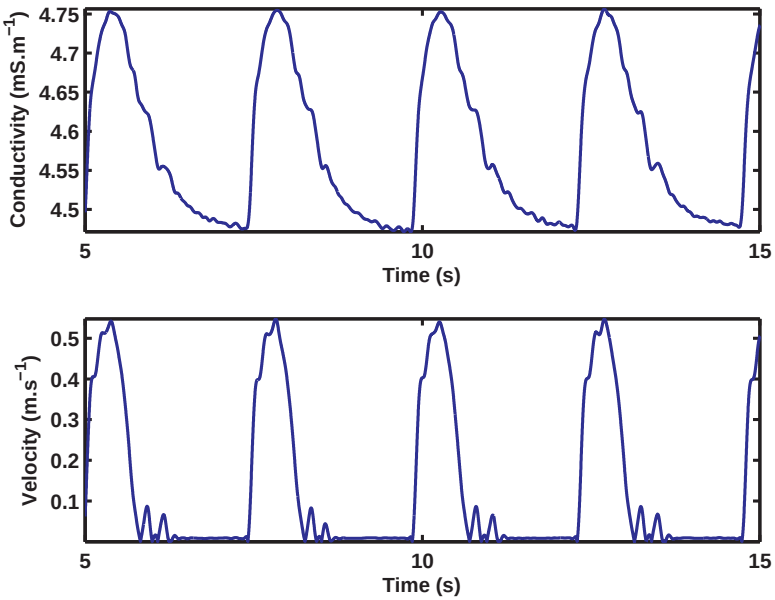

Figure 3.10: Conductivity and velocity of bovine blood, H = 44%, d = 12.7 mm, T =19^oC, bpm = 24

acceleration represented by the peak blood resistivity change.

Figure 3.11 provides further demonstration that the velocity affects the impedance of blood. Both plots show the flow and impedance of blood when pulsing at 48 bpm. The setting for the flow generation are the same, however in the lower plot, the velocity contains greater fluctuations at low velocities. Consequently, the impedance of the lower plot reflects these fluctuations.

An example of the flow and impedance data collected for varying pulse rates is shown in Figure 3.12. It can be seen that changing the shape and pulse rate of the velocity, changes the impedance response. The maximum impedance for each pulse (occurring at the minimum velocity, close to zero), decreases as the pulse rate increases. Despite the similarity in velocity, the maximum impedance varies with pulse rate. This is believed to be due to the shorter time period therefore the cells do not get a chance to fully

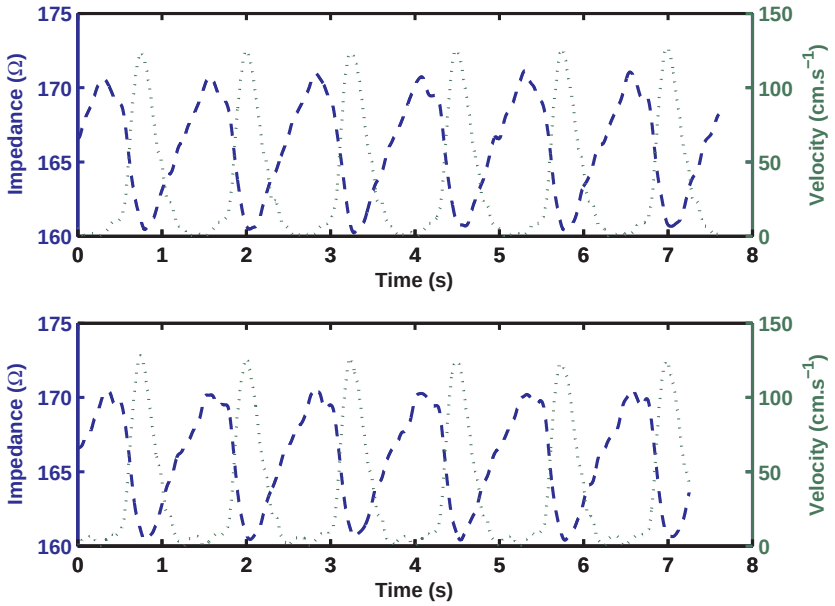

Figure 3.11: Velocity and impedance of flowing blood, H = 44%, d = 12.7 mm, pulse rate = 48 bpm, frequency = 5 kHz

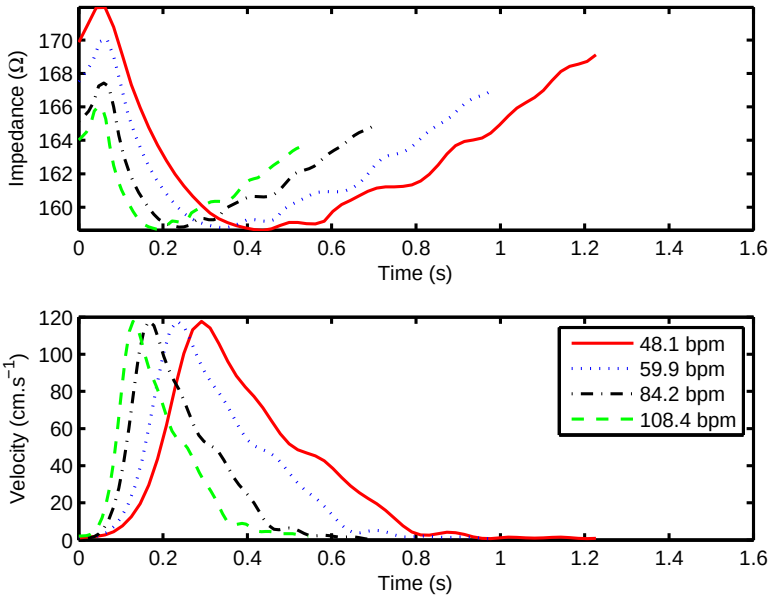

Figure 3.12: Velocity and impedance of bovine blood for various pulse rates, H = 45%, d = 12.7 mm, T = 19^oC

disorientate before the blood begins to flow again. As a result, the cells maintain alignment ensuring a larger conductive cross section of plasma and a lower impedance. This reinforces the idea that the cells never completely disorientate during physiological flow.

The minimum impedance (measured at the maximum velocity) decreases as the pulse rate increases. Before the cells get a chance to fully align at the peak velocity, the flow begins to decrease and the cells do not necessarily achieve full alignment. However, the cells will maintain some momentum and so the variation in impedance due to pulse rate at the peak velocity is not as large as that seen for the minimum velocity.

Due to the inverse relationship between velocity and impedance, it would be expected that the maximum flow over the cycle would correlate well with the minimum impedance of the cycle. This is shown in Figure 3.13 for blood flow through the 12.7mm tube with a haematocrit of 44%. In this case, both the stroke volume and pulse rate were increased in order to increase the peak velocity. The data are shown over the physiological range of expected flow velocities and the relationship between the peak velocity and minimum recorded impedance is linear with a correlation coefficient of -0.85.

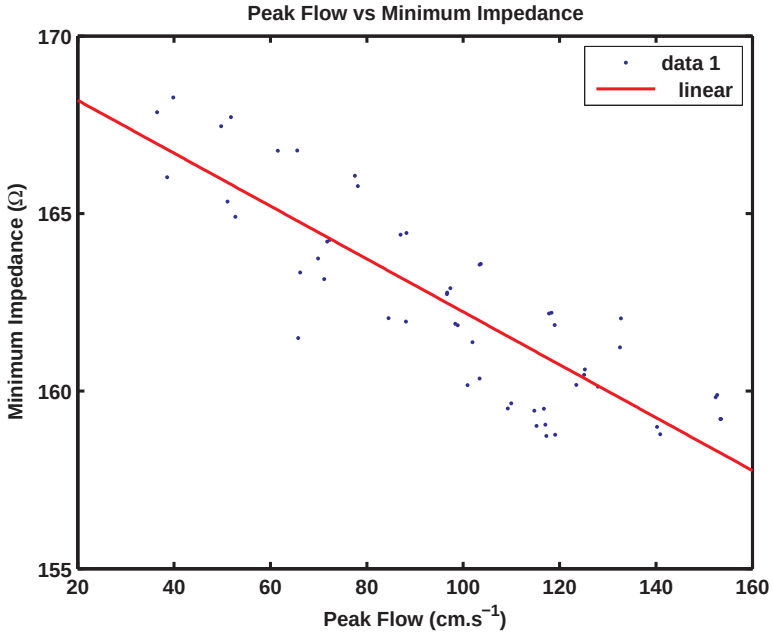

Figure 3.13: Minimum impedance with peak velocity for bovine blood, H = 44%, d = 12.7 mm

Time Frequency Characteristics

Results published by the author (Gaw, Cornish & Thomas 2009*b*) are further detailed in this section.

To understand fluctuations in the measured impedance, frequency decomposition such as a Fourier transform provides information in the frequency domain. However, the Fourier transform assumes that the frequency content of a signal remains constant over time whereas the spectral content of the impedance signal varies over time. The continuous wavelet transform (CWT) maps a signal into both the shift (time) and scale (frequency) domains. This provides an additional dimension of information about the orientation effect of pulsatile blood flow through rigid tubes. The technique has been used to detect characteristic points of ICG waveforms more reliably (Wang, Sun & Van De Water 1995, Shyu, Lin, Liu & Hu 2004, Zhao Shuguang & Min 2005)

and therefore may help to identify repeated fluctuations.

The CWT of a signal s(t) is defined in Equation 3.4 where the function Ψ (Equation 3.5) is the mother wavelet.

$$W_s(a,b) = \int_{-\infty}^{\infty} s(t)\Psi^*_{a,b}(t)dt \tag{3.4}$$

$$\Psi_{a,b} = \frac{1}{\sqrt{a}}\Psi\left(\frac{t-b}{a}\right) \tag{3.5}$$

The wavelet used in this analysis is the Daubechies wavelet, N = 10, see Figure 3.14 (Debnath 2002). This wavelet is scaled by parameter a and time shifted by parameter b to create a family of daughter wavelets $\Psi_{a,b}$. These wavelets are used to analyse the signal in time for the frequency content where b is a representation of time in the signal and a is a representation of frequency. $W_s(a,b)$ computes the two dimensional continuous wavelet coefficients of magnitude of the signal s(t) at real, positive values of a and b.

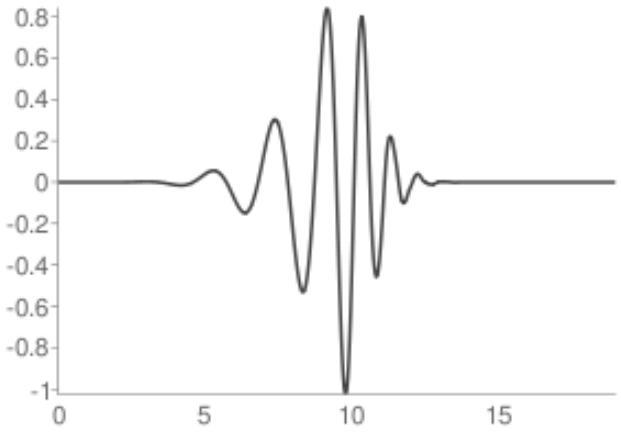

Figure 3.14: Daubechies wavelet, N = 10

A pseudo-frequency can be approximated by the scaling factor using the following equation.

$$F_a = \frac{Fc}{a\delta} \tag{3.6}$$

where Fc is the centre frequency of the mother wavelet, a is the scale factor and δ is the sampling period.

An example of the two dimensional CWT for flow data with a pulse rate of 72 bpm is shown in Figure 3.15. These parameters are representative of all pulse rates tested. The Fourier transform is displayed in Figure 3.15 (a) with frequency on the vertical axis and transform magnitude on the horizontal axis. The time signal is displayed in Figure 3.15 (c) with velocity magnitude on the vertical axis and time on the horizontal axis. The CWT is displayed in Figure 3.15 (b) with the vertical axis equivalent to the frequency axis of Figure 3.15 (a) and the horizontal axis equivalent to the time axis of Figure 3.15 (c). This plot shows the magnitude of the flow signal decomposed into time and frequency components using a contour plot. This plot shows high magnitudes around the pulse rate frequency of 1.2 Hz over the entire duration of the time signal. Some higher frequency components are also found at times when the flow is fluctuating close to zero.

An example of the CWT for the simultaneous impedance data is shown in Figure 3.16. This figure shows that the impedance signal captures similar frequencies to those contained in the flow signal; in particular, the dominant pulse rate frequency and additional higher frequencies.

Figure 3.15 and Figure 3.16 show that the CWT of the impedance signal is very similar to the CWT of the velocity signal and that frequency components in both signals occur during similar time periods of the measurement. This suggests that the impedance signal contains many of the frequency fluc-

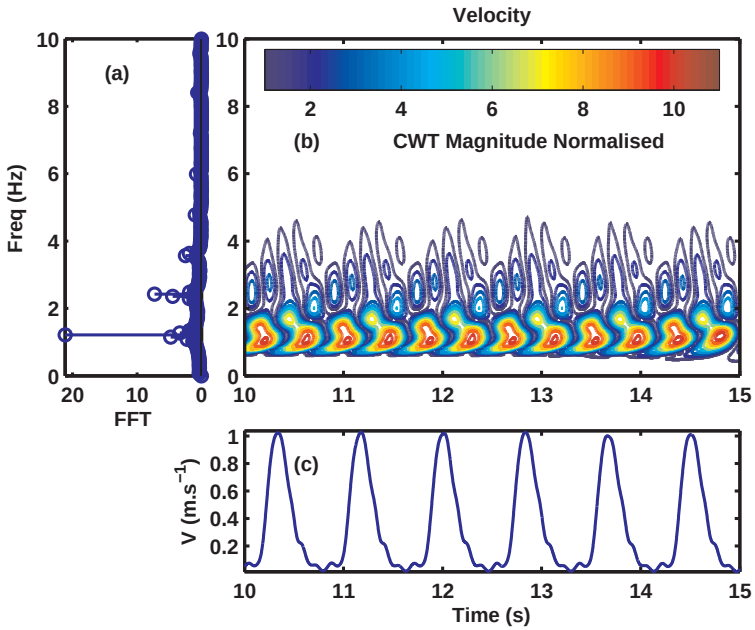

Figure 3.15: Time frequency analysis of velocity (72 bpm, H = 44%, D = 12.7 mm, T = 19 ^oC) (a) Fourier transform (b) contour plot (c) time signal

tuations of the flow velocity. The magnitude of the CWT of the impedance signal is not as large as the CWT for the velocity signal, particularly for frequencies above 2 Hz. This suggests that the impedance is similar to a low pass filtered version of the velocity signal.

To determine how similar the frequency components of the flow and impedance signals are over time, the correlation of the CWT frequencies for impedance and flow shown in Figure 3.15 and 3.16, were calculated at each time step. The results are shown in Figure 3.17 for four pulses. This shows the correlation in frequency components of the signal at each point in time and the corresponding flow velocity, acceleration and impedance. This correlation shows that the impedance signal contains a large proportion of the frequency components found in the flow signal during some periods of the pulse. During other periods, the signal frequencies have a lower correlation.

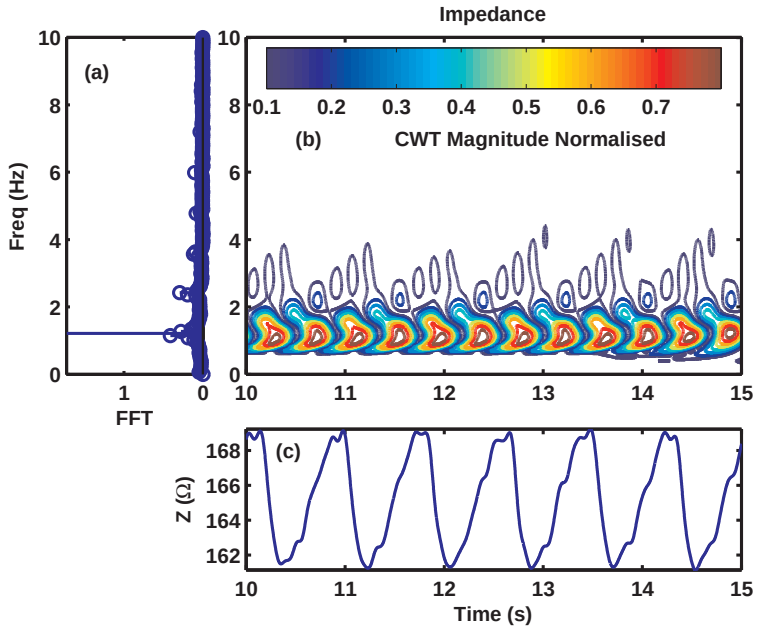

Figure 3.16: Time frequency analysis of impedance (72 bpm, H = 44%, D = 12.7 mm, T = 19 ^oC) (a) Fourier transform (b) contour plot (c) time signal

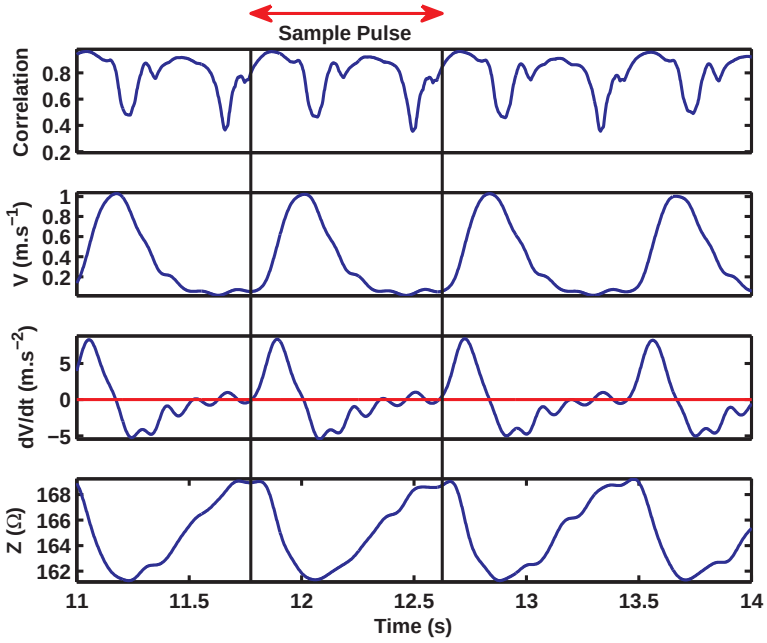

Figure 3.17: Correlation of frequency content between impedance and flow signals over time (72 bpm, H = 44%, D = 12.7 mm, T = 19 ^oC

The correlation between frequency content of the impedance and flow signals in Figure 3.17 is analysed from the beginning of a sample pulse. The period of maximum correlation occurs around the time of the maximum acceleration of the flow. At this point, the cells are aligned and responding to changes in the flow. The correlation of frequency content begins to decrease considerably at the point of maximum velocity and zero acceleration. At this point, the flow begins to slow down however the high inertia of the cells as they flow at high velocities maintains the cells in alignment. The impedance does not respond quickly to the change in direction of acceleration and the minimum correlation occurs quickly after this. Once the cells begin to disorientate due to the reduced shear forces of the lower flow velocity, the correlation increases and the impedance signal responds to fluctuations in the velocity signal again. The correlation subsequently begins to decrease around the time that the minimum velocity is reached. At this time the cells are experiencing a minimum shear force and are least affected by velocity changes. They will be in their most disorientated state during the cycle at this point. The frequency correlation then begins to increase again to a maximum during acceleration.

When the flow changes from a positive acceleration to a negative acceleration as in the point of maximum velocity, the driving velocity force on the cells is now in the opposite direction. The cells take time to respond to this changing force due to their own inertia, and as a result orientation changes are delayed. Thus velocity fluctuations are not contained in the impedance signal at this time. The same occurs when the flow changes from a negative acceleration to a positive acceleration.

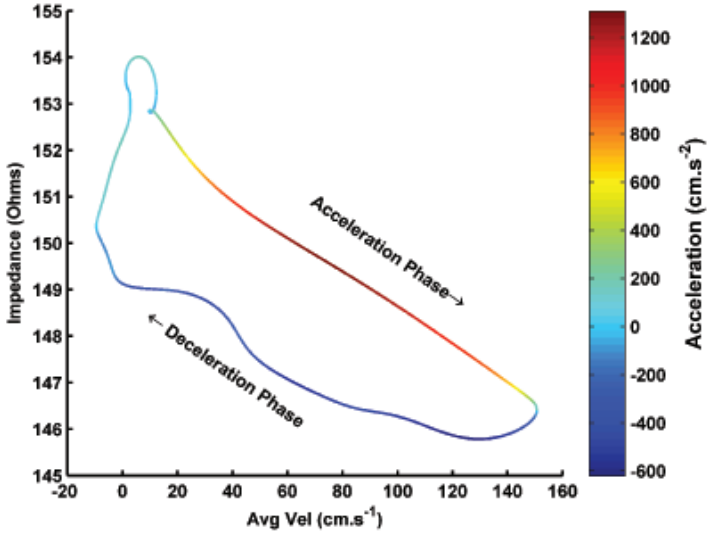

Figure 3.18: Impedance vs velocity with acceleration indicated by colour, h = 45%, d = 12.7 mm, 60 bpm, frequency = 5 kHz, ratio = 35/65

3.3.3 Impedance of pulsatile blood during accelerating flow

The relationship between impedance, velocity and acceleration varies during the cardiac cycle. Figure 3.18 shows an example of this relationship for the pulse shown in Figure 3.8. This plot shows clearly the relationship between impedance and velocity. The acceleration is indicated by a variation in colour according to the colour bar. This figure shows that the relationship between impedance and velocity is difficult to define over the entire duration of the pulse. It appears to be non linear at low velocities and during deceleration, but is clearly linear during the acceleration phase.

The relationship between impedance and velocity during the acceleration phase has been isolated. This relationship has been found to be highly linear over all pulse rates (e.g. $r^2 = 0.99$, for a pulse rate of 60 bpm). Similar trends have been shown by Visser (1989). Stop flow experiments in which

the velocity is made to flow in a repeating square waveform, demonstrate that impedance responds instantaneously to velocity increases or accelerations.

Closer analysis of the linear regression coefficients shows that the magnitude of the slope of the best fit line ($\frac{\delta Z}{\delta v}$) decreases as peak velocity increases. Figure 3.19 shows an exponential relationship between the best fit slope and the peak pulse velocity ($r^2 = 0.89$) with 95% confidence bounds. This relationship demonstrates that changes in velocity have less effect in changing the impedance at higher velocities than they do at low velocities. This is explained by the saturation point detailed in Section 2.3.3 that occurs at high velocities when all red blood cells are aligned. Any increases in velocity will no longer affect the impedance. The saturation point has been previously reported in published literature (Visser 1989, de Vries et al. 1995, Liebman et al. 1962, Liebman & Bagno 1968, Sakamoto & Kanai 1979, Visser 1992, Hoetink et al. 2004). These results for the acceleration phase suggest the relationship between impedance and velocity shows similar trends as that during steady flow.

3.3.4 Impedance of pulsatile blood during decelerating flow

Results published by the author (Gaw, Cornish & Thomas 2009*a*) are further detailed in this section.

Exponential decay of impedance has been shown to occur when flow is stopped due to the delay in disorientation of the cells when high shear rates no longer force the cells to align during flow. Visser (1989) characterised the decay by a relaxation time constant (τ) that is representative of the rate of disorientation of the cells. It was found by Visser (1989) that the time constant did not significantly differ for the different velocities used as

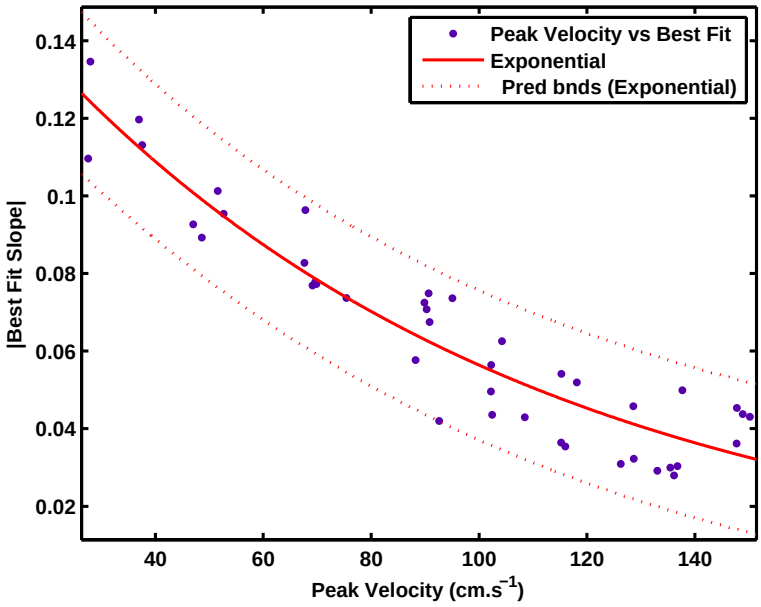

Figure 3.19: Relationship between best fit slope and peak velocity for various pulse rates

the initial constant flow rate. As part of stop flow experiments reported by Bitbol & Leterrier (1982) it was demonstrated that the rate of orientation of red blood cells increases during acceleration with a time constant too short to be measured. After the flow was stopped, a decay process began in which the time constant for disorientation was of the order of 1 second.

Pulsatile blood flow more closely approximates blood flow as it is pumped by the heart. Pulsatile flow consists of changing acceleration and deceleration of flow over a length of time rather than instantaneous step responses. Therefore the time constant for the relationship between impedance and velocity for pulsatile blood flow through rigid tubes was examined.

The time constant of a system characterizes the approach of an exponential function to a steady state value. This can be a decreasing or increasing exponential function. In the case of exponential decay, the time constant is

defined physically as the time taken for the system step response to fall to a factor of $\frac{1}{e}$ or 36.8% of its initial value. That is, how rapidly an exponential function decays. To calculate the system time constant, a first order linear time invariant model can be assumed. The general solution of this is shown in Equation 3.7.

$$y(t) = y_0 e^{\frac{-t}{\tau}} \tag{3.7}$$

To calculate the time constant of the impedance in the case of pulsatile flow, a first order linear differential equation is assumed (Equation 3.8).

$$\dot{\sigma}(t) = -\frac{1}{\tau}\sigma(t) + \frac{K}{\tau}v(t) \tag{3.8}$$

where $\sigma(t)$ is the output conductance, $v(t)$ is the input velocity, K is the system gain and τ is the exponential decay time constant. In order to correctly define τ as exponential gain or decay based on polarity, the conductance is used. This model incorporates the impedance in addition to the velocity and is therefore more applicable in the presence of pulsatile flow.

To convert this to discrete time, the difference equation can be determined by assuming:

$$\begin{aligned} \dot{\sigma}(t) &= \frac{\sigma(t_k) - \sigma(t_{k-1})}{\delta t} \\ \sigma(t) &= \sigma(t_{k-1}) \\ v(t) &= v(t_{k-1}) \end{aligned} \tag{3.9}$$

where $\delta t = t_k - t_{k-1}$. Substituting $k = t_k$, the final difference equation is shown in Equation 3.10.

$$\sigma(k) = \left(1 - \frac{\delta t}{\tau}\right)\sigma(k-1) + \left(\frac{K\delta t}{\tau}\right)v(k-1)$$
$$\sigma(k) = a\sigma(k-1) + bv(k-1) \tag{3.10}$$

The time constant and gain factor can be calculated using Equation 3.11.

$$\tau = \frac{\delta t}{1-a}$$
$$K = \frac{b}{1-a} \tag{3.11}$$

To calculate τ and K, the coefficients were solved using least squares regression (mean square error ≤ 0.0001 in all cases). The time constant was calculated for the deceleration phase of each velocity pulse and averaged over a number of velocity pulses. The system gain was calculated over the entire duration of the pulse. This was repeated for a range of pulse rates and stroke volumes to vary the peak velocities.

The calculated values of τ are shown in Figure 3.20 for the deceleration phase for five pulse rates with varying stroke volumes. This shows τ calculated for each pulse, averaged over a number of pulses and plotted against the average peak velocity of the pulse. This data shows that as a general trend for each pulse rate, the time constant decreases as the peak pulse velocity increases. This decrease is faster at lower peak velocities and appears to plateau at higher peak velocities.

The values of τ reported by Visser (1989) did not significantly differ for the different driving velocity step input. However, Figure 3.20 shows that for each pulse rate, the time constant decreases as the peak velocity increases.

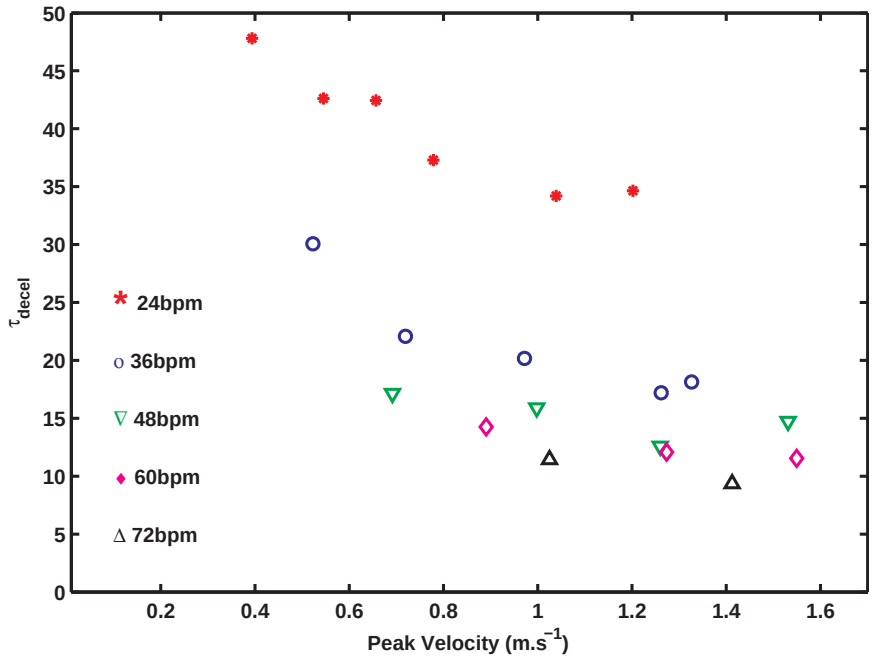

Figure 3.20: Deceleration phase time constant with peak velocity for a number of pulse rates, h = 44%, T = 19 ^oC, SR = 35/65, d = 12.7 mm

This is believed to be because the cells are undergoing pulsatile flow rather than stop flow. During pulsatile flow at a constant pulse rate, an increase in peak velocity generates a faster deceleration. The cell orientation responds faster to this greater deceleration and τ decreases. The decrease of τ during the deceleration phase due to an increase in pulse rate can be explained by the shorter period of the velocity pulse. As the pulse rate increases, the cells have less time to disorientate before the next velocity pulse begins to re-orientate the cells.

The system gain, K calculated over the entire duration of the signal is shown in Figure 3.21 for varying pulse rates. The system gain displays an exponential relationship to peak pulse velocity. The pulse rate does not have a large influence on K.

The exponential decay of K seen in Figure 3.21 confirms the familiar

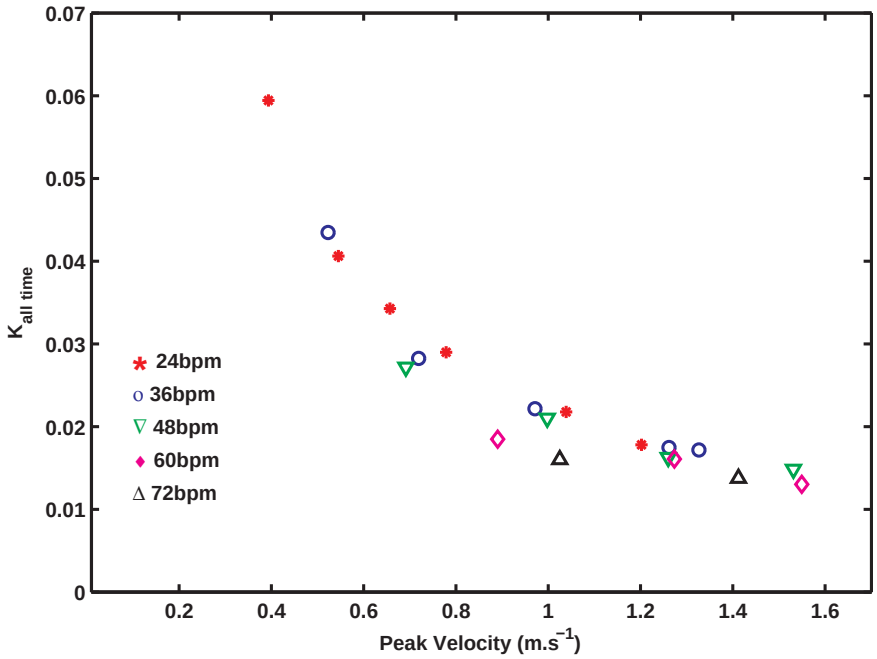

Figure 3.21: Variation in system gain with peak velocity for a number of pulse rates, h = 44%, T = 19 ^oC, SR = 35/65, d = 12.7 mm

concept of the saturation velocity (Liebman & Bagno 1968, Ninomiya et al. 1988, Sakamoto & Kanai 1979, Visser 1992, Liebman et al. 1962, de Vries et al. 1995, Visser 1989). At this velocity the cells become fully aligned and an increase in velocity will no longer affect the measured impedance.

3.3.5 Orthogonal Measurements

Orthogonal impedance and longitudinal flow velocity of bovine blood was recorded across the radial of the tube at a horizontal angle as well as 45^o clockwise and 45^o counter clock wise (Figures 3.22 - 3.24). As orthogonal measurements in this set-up were bipolar, they were affected by polarisation impedance and the stationary impedance was difficult to measure due to a polarisation drift. Therefore the impedance measured across the radials are shown as a percentage change from the average impedance measured over the

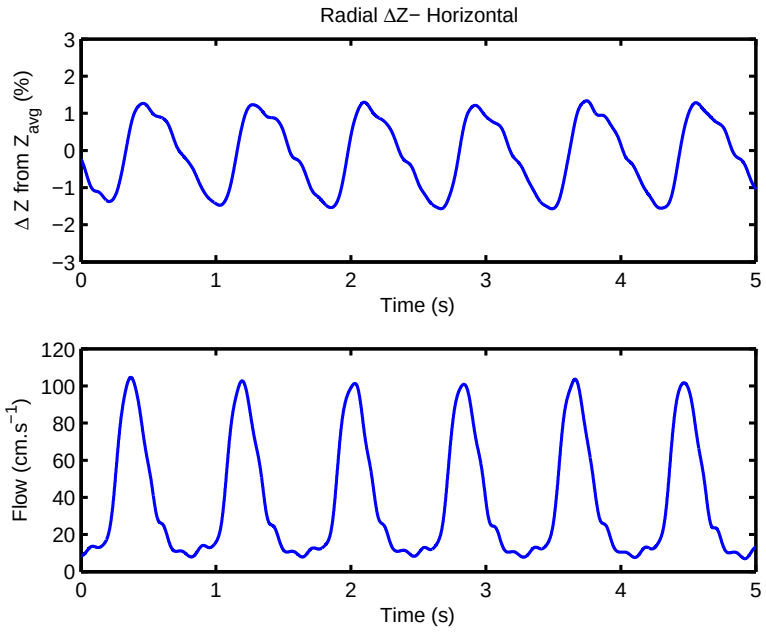

Figure 3.22: Velocity and radial (horizontal) impedance change (from average) of bovine blood

time period. To compare to the longitudinal measurements, the longitudinal measurement were also presented in this way as shown in 3.25.

In the case of flow through rigid cylindrical tubes axial symmetry occurs. As expected, the impedance responses recorded across the radial of the tube is opposite to that measured longitudinally. That is, as the flow increases, the impedance also increases in all three radial cases. This is because as the red blood cells respond to changes in shear rate, they will align in an axisymmetric pattern around the longitudinal axis (see Figure 3.6). The magnitude of the change in impedance is essentially equivalent for each radial and longitudinal case. This experimental response confirms that the red blood cells align in a symmetric pattern around the longitudinal axis of the tube due to axisymmetric flow. In addition, these results suggest that the blood has been adequately stirred and no gravitational settling is occurring

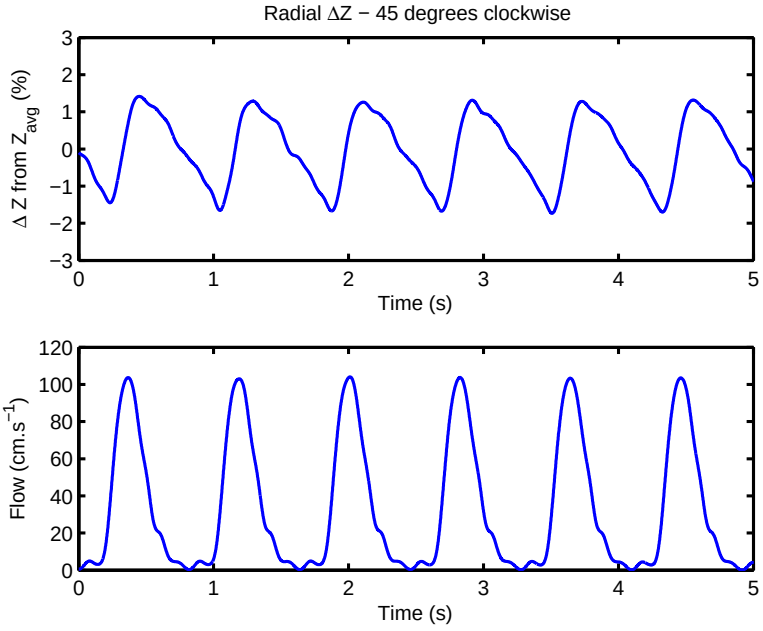

Figure 3.23: Velocity and radial (45^o clockwise) impedance change (from average) of bovine blood

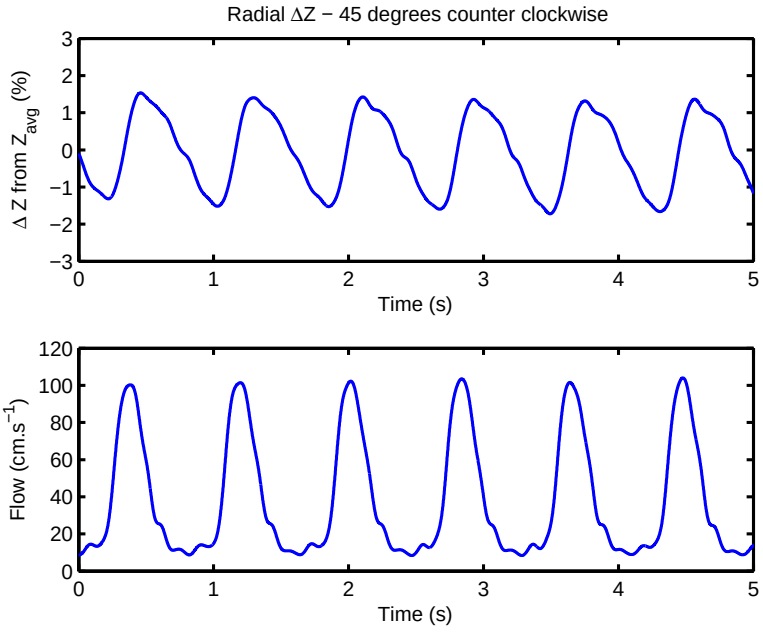

Figure 3.24: Velocity and radial (45^o counter clockwise) impedance change (from average) of bovine blood

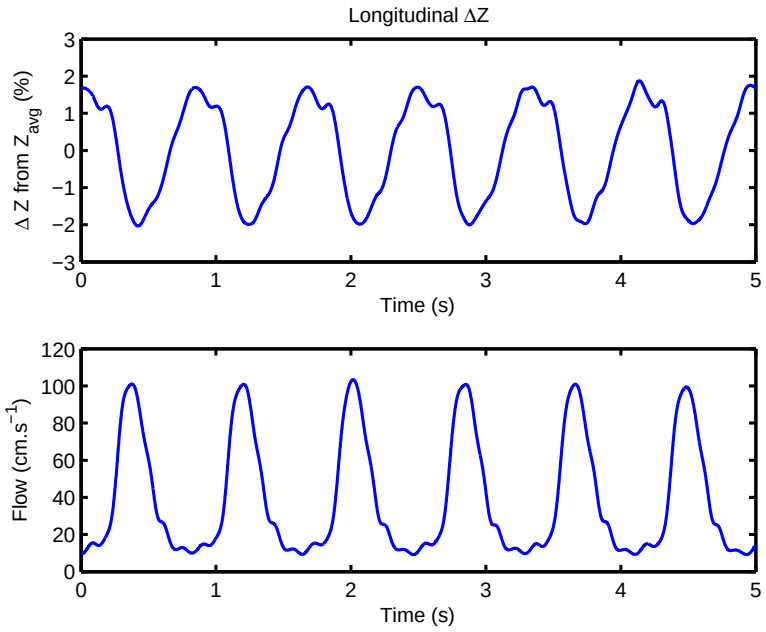

Figure 3.25: Velocity and longitudinal impedance change (from average) of bovine blood

during measurements despite previous evidence that settling does occur.

The radial impedance also displays similar decay characteristics as the longitudinal impedance measured during flow. The radial impedance response follows the velocity at a delayed rate indicating that the change in orientation of cells affect the impedance in both the longitudinal and radial direction in a similar fashion as would be expected.

3.3.6 Future Considerations

There are a number of further improvements that may be made on the design of the experiment in order to generate additional information. The development of a better method of measuring the resistivity of stationary blood while avoiding gravitational settling and ensuring random alignment should be considered. A more appropriate method of taking orthogonal measure-

ments should also be investigated in which a tetra polar measurement can be made. The final consideration is the choice of species from which the blood was collected. Bovine blood does not exactly represent human blood as it does not form rouleaux and blood from a more representative species should be considered.

3.4 Conclusions

As the velocity of blood increases, the measured impedance was shown to decrease as the red blood cell orientation responds to changes in the shear forces. Previous investigations on the electrical characteristics of flowing blood have concentrated on constant flow rates and ignored the effect of acceleration. Experimental relationships between impedance, velocity (during acceleration and deceleration) investigated here demonstrate that acceleration is an important factor in determining the impedance of flowing blood and should not be ignored.

Impedance measurements orthogonal to the direction of the flowing blood verify experimentally that the orientation of red blood cells varies only along the radius of the tube and not with the angle around the central axis. This has not previously been confirmed experimentally and is an important step in confirming the theory of cellular flow through a tube.

Changes in pulse rate have been shown to alter the magnitude of the impedance response. As the pulse rate increases, the peak to peak impedance decreases due to the shorter period of time in which the cells have to respond to changes in velocity. This suggests that the error induced by the assumption of constant blood resistivity in impedance cardiography may be reduced for patients with very high pulse rates.

Time-frequency decomposition of the impedance and velocity of pulsatile blood show similar distributions of the frequency components over time for both the velocity and impedance signals. Good correlation of these distributions occurs for a large proportion of time during the velocity pulse. In particular, the frequency content of signals is well correlated during the acceleration and deceleration phases, but reduces when the flow acceleration changes direction. The similarities have been attributed to the orientation states of the red blood cells during the different flow phases.

Impedance responses during the acceleration phase demonstrate characteristics similar to constant flow responses. The relationship between velocity and impedance during this phase was shown to be linear. During the deceleration phase the relationship between velocity and impedance is more complex. The impedance does not respond as quickly to changes in velocity during deceleration and this response is characterised with a decay time constant. This time constant increases with pulse rate and peak velocity due to changes in the orientation response of cells.

The peak impedance derivative of pulsatile blood flowing through rigid tubes occurs simultaneously in time with the peak acceleration of the blood. In the absence of volume changes, the orientation response of the cells is the only cause of the blood resistivity changes with changes in velocity and acceleration. This provides clear evidence that the $\frac{dZ}{dt}_{max}$ signal measured as part of an ICG comprises contributions from the maximum aortic blood flow acceleration in addition to the peak blood volume change.

Given the experimental results presented here it can be concluded that the impedance signal of flowing blood is largely influenced by the velocity and acceleration of the flowing blood. This suggests that the thoracic impedance signal measured during impedance cardiography will also include informa-

tion related to the velocity of the blood in addition to the currently derived parameter of cardiac output.

Chapter 4

Theoretical Impedance of Blood Modelled in Rigid Tubes

The model presented here has been published by the author (Gaw, Cornish & Thomas 2007, Gaw, Cornish & Thomas 2008). Aside from this publication, no other studies have been found which theoretically model the impedance of blood in pulsatile flow over the length of the cardiac cycle. Previous theoretical and experimental studies have concentrated primarily on quantifying impedance change for constant flow rates. Due to the viscous nature of blood, the flow characteristics of pulsatile blood are different from steady flow. This in turn affects the impedance.

4.1 Background

4.1.1 Basic Fluid Mechanics

The viscosity of a medium is a measure of the internal molecular friction of a fluid and can be considered as a resistance to flow. It is analogous to

the frictional force resisting the relative motion of neighbouring laminae in a fluid and is dependent on the concentration of cells. The tangential shear stress (τ) between the adjacent lamina layers travelling at different speeds is dependent on the shear rate and the dynamic viscosity (μ) of the flowing medium. The shear rate refers to the velocity gradient across the radius ($\frac{dv}{dr}$).

$$\tau(r) = \mu \frac{dv}{dr} \tag{4.1}$$

The kinematic viscosity (ν) can be calculated from the dynamic viscosity where ρ is the density of the fluid.

$$\nu = \frac{\mu}{\rho} \tag{4.2}$$

The motion of fluid through a tube is driven by a local pressure difference along the length of the tube. For steady Poiseuille flow through a rigid cylinder, the relationship between the driving pressure gradient (pressure difference/length) and the flow rate is linear, resulting in a parabolic velocity gradient, $v(r)$, as shown in Figure 4.1 and described by Equation 4.3.

$$v(r) = \frac{G^*}{2\mu}(R^2 - r^2) \tag{4.3}$$

where G^* is the driving pressure gradient over the length of the tube, R is the radius of the tube and r is the distance along the radius from the centre of the tube.

The Reynolds number is a non dimensional parameter that represents the interaction between viscous and inertial forces. It is given by:

$$Re = \frac{vL}{\nu} \tag{4.4}$$

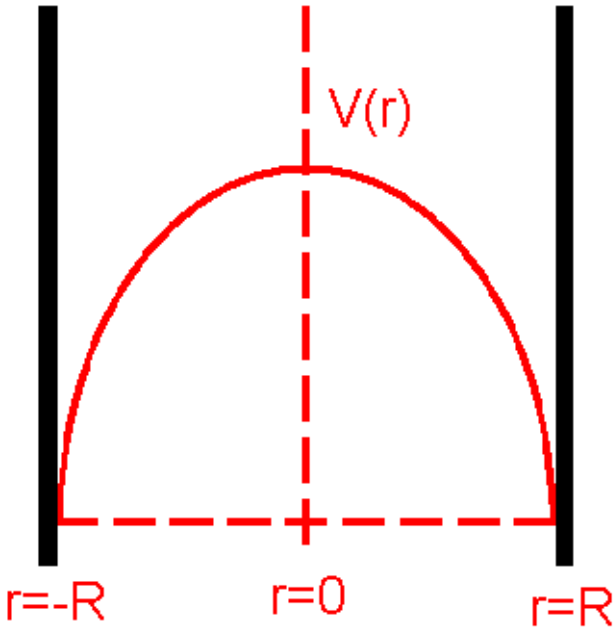

Figure 4.1: Poiseuille flow velocity profile

where L is the characteristic length of the channel (in this case, the diameter of the tube) and v is the average velocity of the fluid.

For blood flow in the body, a time dependent pressure wave propagates along the aorta resulting in pulsatile flow. Flow begins through the ascending aorta when the aortic valves open and blood is ejected from the ventricle. The velocity rises rapidly to a peak from which it falls more slowly. There is a brief period of backward flow as the aortic valve is forced closed and then the blood remains at rest for the rest of the cardiac cycle. Figure 4.2 shows this behaviour.

During oscillatory or sinusoidal flow the relationship between the oscillating pressure gradient and flow velocity is non linear and results in the normally parabolic velocity profile of steady flow becoming distorted during oscillatory flow. The case of oscillatory flow is important as pulsatile flow

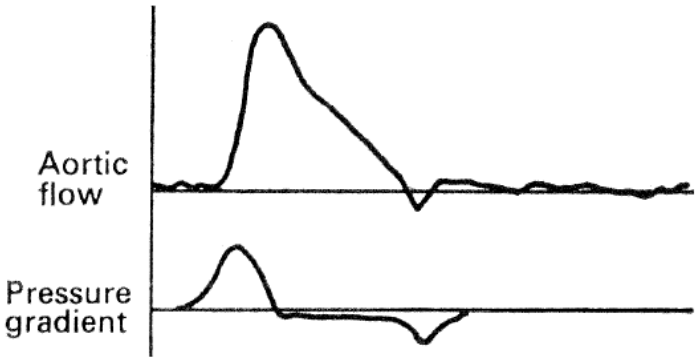

Figure 4.2: Velocity Pulse and Pressure Gradient in the Aorta (McDonald 1974)

can be described through a Fourier series representation by an addition of oscillatory flow signals with different frequencies.

In oscillatory flow, the axial region of the velocity profile is much flatter than the parabolic velocity curve of Poiseuille flow, and the lamina near the walls experience a higher shearing stress. The Womersley number (α_w) is an indication of the extent to which the velocity profile in laminar flow differs from the Poiseuille profile when the fluid is subjected to a time varying pressure gradient at an angular frequency, ω.

$$\alpha_w = R\sqrt{\frac{\omega\rho}{\mu}} \tag{4.5}$$

where R is the radius of the tube, ρ is the density of the fluid, ω is the oscillating frequency and μ is the dynamic viscosity of the fluid.

The Womersley number is a dimensionless number that describes the characteristics of unsteady flow. As α_w increases, the flow deviates further from Poiseuille flow as more of the central region of the velocity profile becomes flattened and significantly higher velocity gradients are found near the walls of the tube. This increase can be brought about by an increase in tube

radius or oscillation frequency.

Caro, Pedley, Schroter & Seed (1978) identified the type of flow based on the Womersley number. For $\alpha_\omega \leq 1$, the flow is considered quasi-steady flow and the velocity profile is parabolic. The flow rate can be determined by the instantaneous pressure gradient and Poiseuille flow. For $\alpha_\omega > 1$, the velocity profile is distorted and the instantaneous flow rate is no longer the same as that predicted on the basis of an instantaneous pressure gradient. Instead the spatial average velocity lags behind the pressure gradient. For $\alpha_\omega > 4$, the phase lag increases and the peak flow becomes less than that predicted by the instantaneous pressure gradient. In normal resting conditions, α_ω for flow through the aorta is approximately equal to 17.6, thus steady flow assumptions are not valid.

4.1.2 Erythrocyte Dynamics

The characteristics of the cell orientation process are difficult to account for. It has been suggested that erythrocytes behave as gyroscopic bodies when they are in motion (Liebman et al. 1962). At low shear rates, the erythrocytes behave as rigid disks, rotating with a periodically varying angular velocity and essentially no deformation. At higher shear rates, the cells behave more like liquid drops undergoing deformation and"tank treading" motion while achieving a stable orientation with respect to the flow (Keller & Skalak 1982, Bitbol & Quemada 1985, Bitbol 1986). Tank treading is the motion of an ellipsoid in which the cell membrane rotates around the interior cell fluid. The rotation velocity of the membrane is dependent on the angle between the rotation axis and the direction of flow. As this angle increases, the rotation velocity increases, creating higher momentum and a stable orientation.

The transition between the two states and the degree of alignment with

the flow is influenced by the shear rate profile across the tube. It is assumed that there are only two well defined states of orientation. These are: erythrocytes with random orientation, as in flipping rigid disk behaviour; and erythrocytes in stable orientation, as in liquid drop behaviour. Bitbol & Quemada (1985) assumed that all erythrocytes in the second state aligned with their major axis within 20 degrees of the flow direction. To simplify the calculations, erythrocytes in this state are assumed parallel to the direction of flow (Hoetink et al. 2004).

For time varying flow, it has been reported that the time taken by erythrocytes to align with the flow and the time taken to disorientate also differ largely (Bitbol & Leterrier 1982, Visser 1989). This is also confirmed by the experimental impedance results observed in Chapter 3 for acceleration and deceleration of blood flow. This can be described as a first order kinetic process which is dependent on the shear rate experienced by the cells. Stop-flow experiments have demonstrated synchronous orientation response with the start of flow (time constant too short to be measured) and a decay of orientation when flow stops, with a time constant ranging in the order of 1 to 100 seconds (Bitbol & Leterrier 1982, Visser 1989). From these results it is concluded that time constants exist for an orientation time that is a function of the haematocrit and shear rate, and a disorientation time that is a function of haematocrit, shear rate and suspending medium viscosity. Brownian motion is expected to be the cause of the disorientation phenomenon, however these time constants indicate that disorientation is more likely to be accelerated by collisions between the particles.

4.1.3 Published Studies

Published theoretical models restricted to steady flow provide a strong foundation from which to model the impedance of pulsatile blood. The conductivity of stationary blood is most commonly modelled using the Maxwell-Fricke equations (Fricke 1924) for spherical particles with known conductance and concentration suspended in a medium of known conductance. The form factor C encompasses the shape and geometry of the particles. Hoetink et al. (2004) have extended the Maxwell-Fricke theory to ellipsoidal particles to explain the flow dependency of the impedance of blood for laminar steady flow in a rigid cylindrical tube. In the model developed by Hoetink et al. (2004) the impedance of the suspension is calculated based on a form factor determined by the orientation and deformation of the cells. These parameters are determined from the shear stress, which is related to the velocity of flow.

The theoretical results presented by Hoetink et al. (2004) closely agree with previously published experimental results for constant flow rates and show that red blood cell orientation and deformation can quantitatively explain the flow dependency of blood impedance in steady flow. Theoretical modelling of the impedance of pulsatile blood proves more difficult as the blood resistivity has been found to change non linearly with the flow velocity (Wang & Patterson 1992).

The Maxwell-Fricke equations have been well validated for steady flow. Application is now extended to pulsatile blood flow in this thesis. The relationship between the amount of deformation which a cell membrane experiences, and the shear stress inducing this deformation is predicted to remain the same regardless of the type of flow. The orientation rate calculated in literature has been based on probability or a linear relationship with shear

rate. These assumptions ignore the kinetics of the orientation-disorientation process and do not provide an accuracte relationship between the shear rate and the proportion of oriented cells. The model developed here aims to improve this flaw.

In pulsatile flow, the spatial average velocity does not necessarily correspond to a unique velocity profile as it does in steady flow. In fact, many different velocity profiles existing in pulsatile flow may produce the same spatial average velocity. Therefore the spatial average velocity cannot be used to determine the shear stress profile and more complicated pulsatile flow dynamics have been investigated here. Thus, the first advancement of the model presented here demonstrates the inclusion of pulsatile flow dynamics, in order to determine the shear rate profile experienced by the cells across the tube.

A method to determine the flow of pulsatile blood through rigid tubes is that shown by McDonald (1974) based on the Navier Stokes equations. This method is an analytical solution and provides the required velocity profiles across the tube. However, it is limited to tubes with standard cylindrical geometry.

4.2 Model Development

The model presented in the current study extends and advances the principles and assumptions used by Hoetink et al. (2004) by incorporating pulsatile flow and orientation effects.

4.2.1 Assumptions

The theoretical modelling assumption (that the resistivity of blood flowing through rigid cylindrical tubes is dependent only on the radius of the tube) is verified by the orthogonal measurements investigated in the experimental chapter. This is because the magnitude of the change in impedance is essentially equivalent for each radial case.

The theoretical model presented assumes blood to be a flowing dilute suspension of oblate ellipsoidal particles (the RBCs) in plasma. Each ellipsoid had one long axes of length $2b$ and one short axis of symmetry of length $2a$ where $a < b$. The behaviour of the RBCs was considered by assuming each cell to be centred in a control volume ($d\Theta$, dr, dL) with small dimensions compared to the tube and surrounded by plasma. These control volumes were then ordered in a regular circular pattern over the cross section of the tube as proposed by Hoetink et al. (2004). An example of a single control volume is shown in Figure 4.3. Flowing RBCs were assumed to remain in two defined states of orientation: random or aligned. Those RBCs with an orientation of $\pm$ 20 degrees to the direction of flow were assumed to be fully aligned with the flow.

Axial accumulation was ignored and blood was assumed to be a Newtonian fluid. Blood was assumed to flow in a pulsatile manner through long, straight, rigid tubes with parameters similar to those of the cardiac cycle. The driving pressure gradient was assumed to be a summation of simple harmonic motion components. The impedance of blood has been shown to be purely resistive below excitation currents of 100 kHz (Visser, Lamberts et al. 1976), thus the excitation current used was assumed to be DC (direct current). Since the RBC membrane acts as a capacitor at DC, no current will flow through the cell, only through the surrounding plasma. The con-

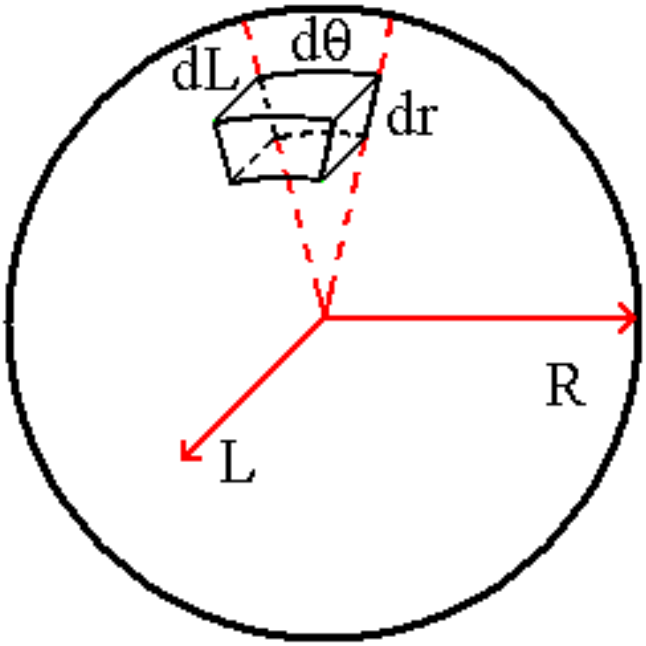

Figure 4.3: Blood flow geometry model

ductivity of the intracellular fluid of the RBC was therefore assumed not to contribute to the blood conductivity.

Further, although turbulence in the blood flow occurs during the cardiac cycle, it occurs for only a very small fraction of the cycle, and then settles quickly to laminar flow (McDonald 1974, Zamir 2000). Consequently, only laminar flow was modelled in this study.

4.2.2 Velocity Profile and Shear Rate

The shear stress experienced by the RBCs, and its variation across the radius, is the most important factor in modelling the conductivity of flowing blood. Fluid flows as a result of a pressure difference over the length of the tube. During flow through rigid, straight cylinders, every element of a Newtonian viscous fluid flows in a series of laminae parallel to the walls of the tube.

Near a stationary surface, the fluid further from the surface is flowing more rapidly than that closer to it. In a tube, this generates a velocity gradient perpendicular to the walls, which is referred to as the shear rate. In steady flow the velocity profile is parabolic across the diameter. In contrast, the presence of an oscillating pressure gradient results in a profile that is much flatter in the central axial region. This is due to the large momentum of the laminae close to the central axial region of the tube which respond slowly to pressure changes. In contrast, laminae near to the wall have less momentum and respond more quickly.

For simplicity, the first step in determining the pulsatile shear rate is to assume the pressure gradient takes the form of simple harmonic motion. This is important because with the aid of the Fourier series, any pulsatile function can be represented as a sum of oscillatory functions. This assumption is valid because the oscillatory flow is linear and takes place under the same conditions as those in steady Poiseuille flow. That is, the cross section of the tube is circular and remains rigid, axial symmetry exists and the fluid velocity is independent of L (Zamir 2000).

Given these assumptions, the equation for the motion of a viscous liquid in laminar flow is derived using the Navier Stokes theorem for the motion of a viscous liquid in laminar flow in a tube of circular cross section is given by Equation 4.6 (McDonald 1974).

$$\frac{\partial^2 w}{\partial r^2} + \frac{1}{r}\frac{\partial w}{\partial r} + \frac{1}{\mu}\frac{\partial P}{\partial z} = \frac{\rho}{\mu}\frac{\partial w}{\partial t} \tag{4.6}$$

where w is the velocity of blood and $w = ue^{j\omega t}$ (u = maximum velocity, ω = angular frequency, t = time), r is the radial co-ordinate, μ is the viscosity of the fluid, P is the pressure, z is the direction of fluid flow, ρ is the density of fluid and t is time.

To model the pulsatile flow velocity and shear rate, the form of the pressure gradient over the length of the tube was initially assumed to be simple harmonic motion and is written in complex form in Equation 4.7.

$$\frac{dP}{dz} = Ae^{j\omega t} \tag{4.7}$$

where $\frac{dP}{dz}$ is the pressure gradient (dyn.cm^{-3}) along the length z of the tube, A is the pressure coefficient (dyn.cm^{-3}), ω is the angular frequency (rad.s^{-1}) of the oscillatory motion, t is time and $j = \sqrt{-1}$. The solution for the assumption of simple harmonic motion is important. Because of it's periodic and finite nature, realistic blood flow time signals can be expressed as a linear combination of individual sine and cosine term, known as a Fourier series.

Rearranging Equation 4.6 and 4.7 gives

$$\frac{\partial^2 w}{\partial r^2} + \frac{1}{r}\frac{\partial w}{\partial r} + \frac{\rho}{\mu}\frac{\partial w}{\partial t} = -\frac{A}{\mu}e^{j\omega t} \tag{4.8}$$

Simplifying this with the assumption that velocity can also be expressed in exponential form, $w = ue^{j\omega t}$ and cancelling the exponential component.

$$\frac{\partial^2 u}{\partial r^2} + \frac{1}{r}\frac{\partial u}{\partial r} - \frac{j\omega\rho}{\mu}u = -\frac{A}{\mu} \tag{4.9}$$

The velocity profile for flow in a tube of circular cross section undergoing an oscillatory pressure gradient, can be solved as a form of Bessel's equation resulting in Equation 4.10 (McDonald 1974, Zamir 2000).

$$v(r)[cm.s^{-1}] = \frac{A}{j\omega\rho}\left[1 - \frac{J_0(\alpha_w y(r) j^{\frac{3}{2}})}{J_0(\alpha_w j^{\frac{3}{2}})}\right] e^{j\omega t} \tag{4.10}$$

This equation was used to determine the velocity of the lamina of liquid at a fraction of the radius, $y = \frac{r}{R}$, from the axis of the tube; where $v(r)$ is the

velocity profile of blood (cm.s^{-1}), r is the radial distance from the central axis of the tube (cm), R is the radius of the tube (cm), ω is the angular frequency of the pressure pulse, ρ is the density of the fluid (g.cm^{-3}), t is time (s) and α_w is the Womersley's number calculated using Equation 4.5.

The corresponding volume flow is calculated by integrating over the cross section of the tube (see Figure 4.3) and is given by:

$$Q(r)[ml.s^{-1}] = \frac{\pi R^2 A^*}{j\omega\rho}\left[1 - \frac{2J_1(\alpha_w j^{\frac{3}{2}})}{\alpha_w j^{\frac{3}{2}} J_0(\alpha_w j^{\frac{3}{2}})}\right] e^{j\omega t} \tag{4.11}$$

The spatial average velocity can be calculated from the volume flow rate by:

$$vel[cm.s^{-1}] = \frac{Q[ml.s^{-1}]}{Area[cm^2]} \tag{4.12}$$

This results in Equation 4.13, (McDonald 1974, Zamir 2000). The spatial average velocity is the average velocity of all laminae flowing through the cross section of the tube at any moment.

$$vel[cm.s^{-1}] = \frac{A}{j\omega\rho}\left[1 - \frac{2J_1(\alpha_w j^{\frac{3}{2}})}{\alpha_w j^{\frac{3}{2}} J_0(\alpha_w j^{\frac{3}{2}})}\right] e^{j\omega t} \tag{4.13}$$

The pulsatile velocity profile can now be used to determine the shear stress profile of the blood. This was found by a differentiation of the velocity profile with respect to the radius (the shear rate), multiplied by the viscosity.

The volume flow derivative (bulk flow acceleration) is calculated by taking the time derivative of the flow.

$$\frac{dQ}{dt}[ml.s^{-2}] = \frac{\pi R^2 A^*}{\rho}\left[1 - \frac{2J_1(\alpha_w j^{\frac{3}{2}})}{\alpha_w j^{\frac{3}{2}} J_0(\alpha_w j^{\frac{3}{2}})}\right] e^{j\omega t} \tag{4.14}$$

A^* is the complex conjugate of A. The derivative of the spatial average velocity can be calculated from the volume flow derivative.

$$\frac{dvel}{dt}[cm.s^{-2}] = \frac{\frac{dQ}{dt}[ml.s^{-2}]}{Area[cm^2]} \tag{4.15}$$

The acceleration profile over the radius is calculated by taking the time derivative of the velocity profile.

$$\frac{dv(r)}{dt}[cm.s^{-2}] = \frac{A}{\rho}\left[1 - \frac{J_0(\alpha_w y j^{\frac{3}{2}})}{J_0(\alpha_w j^{\frac{3}{2}})}\right] e^{j\omega t} \tag{4.16}$$

The shear stress profile can also be determined from the velocity profile by a simple derivation with respect to the radius.

$$\begin{aligned} \tau(r)[N.m^{-2}] &= \mu\frac{dv}{dt} \\ &= \frac{\mu A}{j\omega\rho}\left[\frac{\alpha_w j^{\frac{3}{2}} J_1(\alpha_w j^{\frac{3}{2}})}{J_0(\alpha_w j^{\frac{3}{2}})}\right] e^{j\omega t} \end{aligned} \tag{4.17}$$

This equation successfully encompasses the dynamics of time varying flow and was used to determine both the RBC orientation and deformation at a location r along the radius of the tube.

The shear rate profile has been calculated in the case of an oscillatory flow in simple harmonic motion. The conversion of periodic waveforms such as pressure and flow into pulsatile flow in numerical form is done by Fourier analysis. The calculation of flow from the pressure gradient begins with a resolution of a pressure gradient into its harmonic components by a Fourier analysis. Caro et al. (1978) state that linearity is a good approximation for arteries under physiological conditions.

A linear Fourier series for a fuction that has a period of T is given by:

$$
\begin{aligned}
F(t) &= A_0 + \sum_{n=1}^{n=\infty} (A_n \cos(n\omega t) + B_n(\sin n\omega t)) \qquad (4.18)\\
A_0 &= \frac{1}{T}\int_0^{2\pi} f(t)dt \\
A_n &= \frac{2}{T}\int_0^{2\pi} f(t)\cos(n\omega t)\, dt \; n = 1, 2, 3... \\
B_n &= \frac{2}{T}\int_0^{2\pi} f(t)\sin(n\omega t)\, dt \; n = 1, 2, 3...
\end{aligned}
\qquad (4.19)
$$

where $\omega = \pi/T$ and F(t) is the Fourier representation of the signal f(t) and n is an integer value. For a curve which cannot be described by an algebraic function as in the case of the pressure gradient in physiological blood flow, the curve is divided into $2a$ equally spaced points y_k, and the Fourier coefficients become:

$$
\begin{aligned}
A_0 &= \frac{1}{2a}\sum_{k=0}^{2a-1} y_k \qquad (4.20)\\
A_n &= \frac{1}{a}\sum_{k=0}^{2a-1} y_k \cos\frac{n\pi k}{a} \\
B_n &= \frac{1}{a}\sum_{k=0}^{2a-1} y_k \sin\frac{n\pi k}{a}
\end{aligned}
$$

To derive the total flow due to the pressure gradient, the corresponding flows calculated from each pressure harmonic were summed. Only a relatively small number of harmonics (e.g. 10 harmonics) are required to represent the signal with reasonable accuracy. The final curve also required the addition of a mean flow which was necessary because the summation of a series of sine waves can only sum to zero over a complete cycle (McDonald 1974). In a

Fourier series representation, the constant term A_0 gives the mean pressure value and it was assumed that this generates a steady Poiseuille flow which was added to the oscillating term.

The assumptions made when using these equations are listed below:

- The flow is laminar
- The length of the tube is long compared to the region being studied
- The fluid is homogeneous and does not have anomalous viscous properties
- The flow is through a cylindrical tube whose diameter remains constant
- The flow may be expressed as a sum of harmonic components calculated from the individual harmonic terms of the pressure gradient.
- No slip occurs at the wall

4.2.3 Orientation of RBC

Hoetink et al. (2004) used a simple linear relationship to determine the orientation rate of cells based on the shear rate. However, the characteristics of the cell orientation process are difficult to account for. Equation 4.21 shows an approximate expression for the orientation rate ($f(r)$) as a function of shear rate across the radius of the tube presented by Bitbol & Quemada (1985).

$$\begin{aligned} f(r) &= \frac{n}{n_0} \\ &= \frac{\tau_o^{-1}(r)}{\tau_d^{-1}(r) + \tau_o^{-1}} \end{aligned} \tag{4.21}$$

where n is the number of RBCs with stable orientation per unit volume (in this case, assumed to be oriented parallel to the flow), n_0 is the total number of RBCs per unit volume, τ_o is the time constant for cells changing from random to aligned orientation and τ_d is the time constant for cells changing from aligned to random orientation. Bitbol & Quemada (1985) proposed that the time constant for cell orientation (τ_o) is proportional to the inverse of the shear rate and the time constant for cell disorientation (τ_d) is proportional to the inverse of the square root of the shear rate (Equation 4.22 and 4.23).

$$\tau_o = k_o \left(\frac{dv}{dr}\right)^{-1} \tag{4.22}$$

$$\tau_d = k_d \left(\frac{dv}{dr}\right)^{-\frac{1}{2}} \tag{4.23}$$

4.2.4 Deformation of RBC

Due to the flow induced shear stress profile, the RBC membrane supports the shear stress existing at a distance, r, from the tube axis. As a result the RBC will be deformed with new axis length a_d and b_d. The amount of deformation is indicated by the change in the axis ratio of short to long axes of the cell. Using the property of constant enclosed volume and constant surface area, and the relation between the strain and extension ratio in the direction of the b axis, Hoetink et al. (2004) developed a relationship between cell axis ratio (a_d/b_d) after deformation, and shear stress (Equation 4.24).

$$\frac{a_d(r)}{b_d(r)} = \frac{a_0}{b_0}\left[1 + \frac{\tau(r)b_0}{4\mu}\right] \tag{4.24}$$

A RBC with initial axis lengths of a_0 and b_0 is deformed in the presence of a shearing stress $\tau(r)$ at a distance, r, from the tube axis. The new axial

lengths are a_d and b_d respectively and μ is the surface shear modulus of the cell membrane.

4.2.5 Impedance of Blood

For a single control volume located at a distance r from the axis, the conductivity is calculated using the Maxwell-Fricke equations (Equation 4.25).

$$\frac{\sigma_{cv}}{\sigma_{pl}} = \frac{1-H}{1+(C-1)H} \tag{4.25}$$

where σ_{cv} and σ_{pl} are the conductivities ($S.m^{-1}$) of the control volume and the plasma respectively, H is the haematocrit expressed as a fraction and C is a form factor that depends on the geometry and orientation of the RBC at location r.

For a control volume in which the contained cell is oriented with its short axis (a) or long axis (b) parallel to the electric field, and also the flow direction in the case of longitudinal measurements, C is calculated by Equation group 4.26.

$$\begin{aligned} C_a &= \frac{1}{M} \\ C_b &= \frac{2}{2-M} \\ M(a<b) &= \frac{\varphi - \frac{1}{2}\sin 2\varphi}{\sin^3\varphi}\cos\varphi \\ \cos\varphi &= \frac{a}{b} \end{aligned} \tag{4.26}$$

For cells in random orientation, it is assumed that cells are equally distributed in orientation between the three axes aligned with the flow. C_r is calculated by taking the average of the C values for each axis alignment.

$$C_r = \frac{1}{3}(C_a + 2C_b) \tag{4.27}$$

The deformation of a RBC experiencing different shear stresses is accounted for by using the deformed short to long axis ratio in calculating Equation 4.26. The C factor in the calculation of the control volume conductivity using Maxwell-Fricke equations must encompass the orientation state of the cells. To incorporate the orientation effect, C does not require the precise orientation to be known. It relies on the fraction of aligned cells, $f(r)$ and the fraction of randomly oriented cells, $1 - f(r)$. The calculation of C based on the fraction of aligned cells is introduced in Equation 4.28.

$$C(r) = f(r)C_b + (1 - f(r))C_r \tag{4.28}$$

The bulk conductivity of blood shown in Equation 4.29 is calculated by a summation of the control volume conductivities over the cross section and Ohm's Law.

$$\sigma_{bl}[S.m^{-1}] = \frac{2}{R^2}\int_0^R \sigma_c v(r) r dr \tag{4.29}$$

The conductivity of stationary blood was also calculated using Equation 4.25 where $C = C_r$. This allowed the change in conductivity of flowing blood from the constant conductivity of stationary blood used in impedance cardiography to be calculated using Equation 4.30.

$$\Delta\sigma[\%] = 100\left(\frac{\sigma_{bl} - \sigma_{st}}{\sigma_{st}}\right) \tag{4.30}$$

The impedance of blood is then easily calculated using Equation 4.31 where A is the cross sectional area and L is the length of the tube.

$$Z[\Omega] = \frac{L}{\sigma A} \tag{4.31}$$

4.2.6 Summary

The impedance of time varying blood flow was calculated by determining the flow rate, velocity profile, shear stress profile and acceleration profile using the analytical method detailed in Section 4.2.2 for the desired pulse rate, pressure gradient and tube radius. For each instant in time, the fraction of cells in parallel orientation is determined over the radius using Equation 4.21, and the current shear rate radial profile and orientation and disorientation time constants. For the present study, a disorientation and orientation time constant of the order of 1 was used.

The deformed short to long axis ratio was calculated from the shear stress profile for cells across the radius using Equation 4.24 and along with the fraction of aligned cells is used with the Maxwell-Fricke equations (Equation 4.25 - Equation 4.28) to determine the conductivity of the control volume. This is then integrated across the cross sectional area of the tube to find the bulk conductivity of the flowing blood (Equation 4.29) and the resulting impedance using Equation 4.31.

4.3 Results

4.3.1 Recreation of Published Results

Figure 4.4 shows the application of the steady flow model published by Hoetink et al. (2004) to a pulsatile velocity time signal flowing through a rigid tube of 10 mm at 72 beats per minute (bpm) for a haematocrit of 45%.

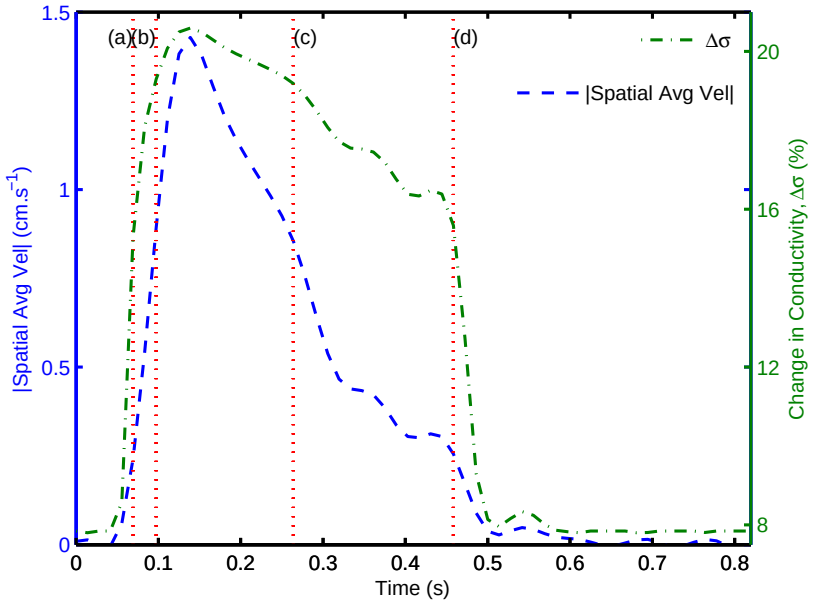

Figure 4.4: Modelled conductivity change from pulsatile average velocity based on steady flow calculations by (Hoetink et al. 2004) over one cardiac cycle, h = 45%, R = 5 mm, pulse rate = 72 bpm (a) t = 0.07 s, spatial average velocity = 0.24 $m.s^{-1}$, $\Delta\sigma$ = 15%, (b) t = 0.10 s, spatial average velocity = 0.89 $m.s^{-1}$, $\Delta\sigma$ = 19%, (c) t = 0.26 s, spatial average velocity = 0.86 $m.s^{-1}$, $\Delta\sigma$ = 19%, (d) t = 0.46 s, spatial average velocity = 0.25 $m.s^{-1}$, $\Delta\sigma$ = 15%,

This result is important because it clearly demonstrates that the steady flow model fails when applied to pulsatile blood flow given the characteristics of the impedance results obtained experimentally in Chapter 3. This is because acceleration is an important factor in determining the conductivity of flowing blood.

In Figure 4.4 the vertical lines labelled (a)-(d) identify times at which the average velocity is the same (times (a) & (d) and times (b) & (c)) under acceleration and deceleration. The corresponding conductivity is the same at both times, however experimental results in Chapter 3 show that this is not an accurate representation. This demonstrates the failure of the steady flow

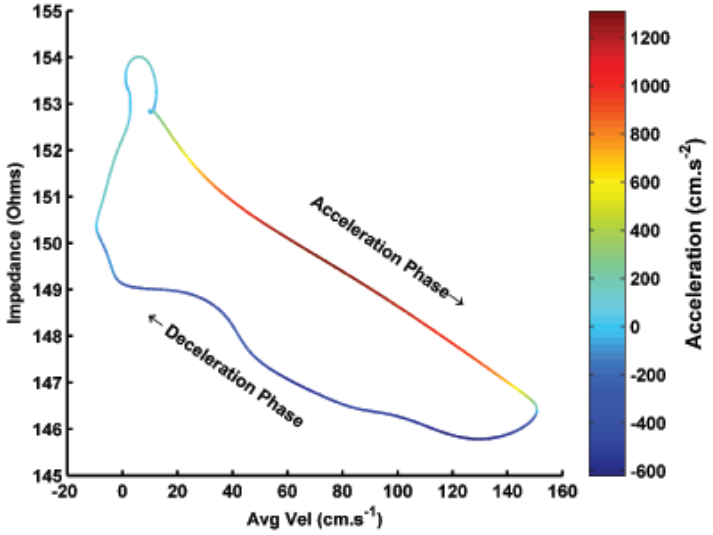

Figure 4.5: Repeat of Figure 3.18: Impedance vs velocity with acceleration indicated by colour, h = 45%, d = 12.7 mm, 60 bpm, frequency = 5 kHz, ratio = 35/65

model when applied to pulsatile blood. This is due to the difference in the shear profile of pulsatile flow that is not captured in steady flow calculations and therefore a model that incorporate pulsatile flow is required.

Experimental results in Figure 3.18, repeated in Figure 4.5 show the impedance of the blood plotted against the average velocity of the blood. This shows that for the same average velocity during pulsatile flow, the conductivity of flowing blood is not the same when the blood is accelerating and decelerating. The same plot is presented for the impedance calculated using the steady model of Hoetink et al. (2004) in Figure 4.6. It can be seen that this model makes no differentiation between acceleration and deceleration and therefore is not adequate in describing pulsatile flow.

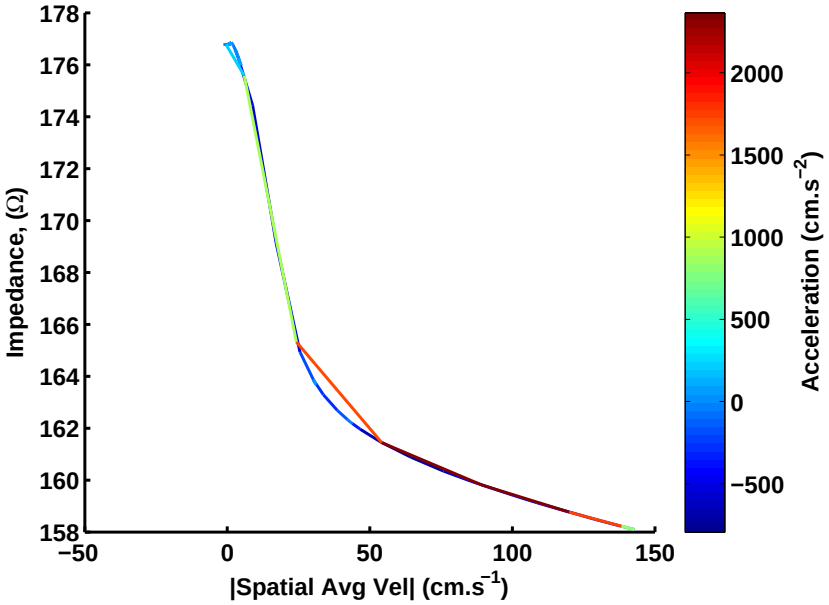

Figure 4.6: Impedance vs velocity with acceleration indicated by colour

4.3.2 Flow Modelling

To model the impedance in this study, realistic flow parameters were selected (see Table 4.1) The flow time signal displayed a peak velocity of approximately 1.4 m.s^{-1} and a normal resting pulse rate of 72 bpm, typical of a healthy adult.

This analytical flow was derived from the pressure gradient across the aorta and is shown for one cardiac cycle in Figure 4.7. The vertical lines labelled (a)-(d) are for the same velocities indicated in Figure 4.4. The acceleration and deceleration phase is also identified. The acceleration phase of the cycle for the absolute spatial average velocity occurs from 0 to 0.14 s and the deceleration phase for the spatial average velocity from 0.14 s to the end of the cycle.

The derived velocity profile and shear stress profile at times (a)-(d) are shown in Figure 4.8. It can be seen that the velocity profiles are not parabolic

Parameter	Description	Value
H	Haematocrit of blood	0.45
ρ	Density of blood	1.055 g.ml^{-1}
ν_{bl}	Viscosity of blood	$\nu_{pl}(1 + 2.5H + 0.0732H)$ P
ν_{pl}	Viscosity of plasma	0.0135 P
σ_m	Cell membrane shear modulus	0.000015 N.m^{-1}
$2b_0$	Major axis length of RBC	8 μ m
$\frac{a_0}{b_0}$	Axis ratio (minor/major)	0.38
N	Number of harmonics	10
f	Frequency of heartbeat	1.2 Hz (72 bpm)
R	Radius of tube	5 mm
k_o	Orientation Constant	3
k_d	Disorientation Constant	1

Table 4.1: Modelling Parameters

as in the case of steady flow, but display characteristics of pulsatile flow such as flattening of the central velocity profile and high shear rates closer to the wall of the tube. It is these characteristics that alter the impedance of the flow and as such, the steady flow model is inadequate in estimating the impedance of pulsatile blood flow. It is also important to note that the velocity and shear stress profiles are not the same at time (a) & (d), and time (b) & (c), despite the fact that they represent the same spatial average velocity at different accelerations.

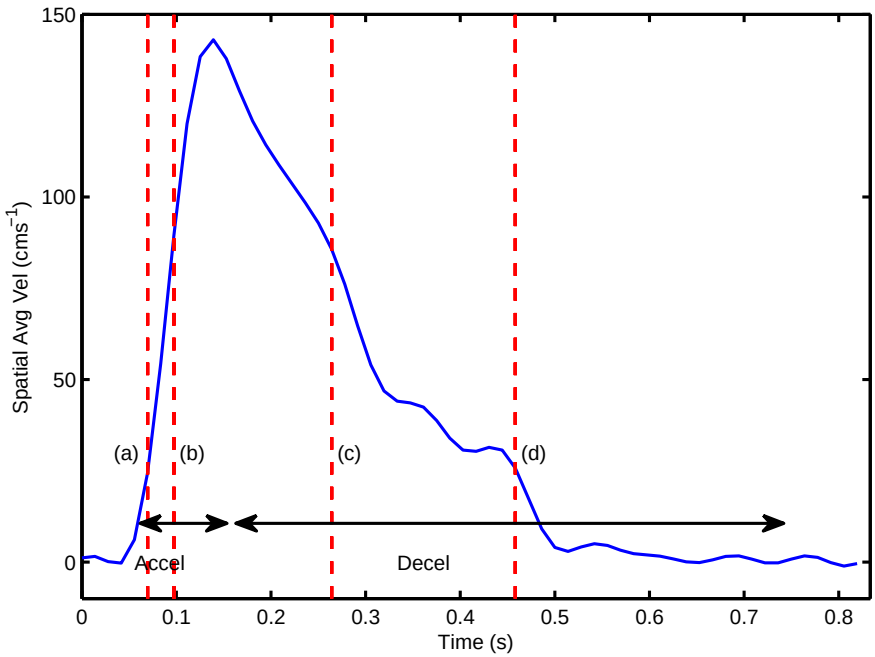

Figure 4.7: Theoretical velocity time signal calculated using analytical techniques for human blood at 37^oC, 72 bpm, $H = 45\%$

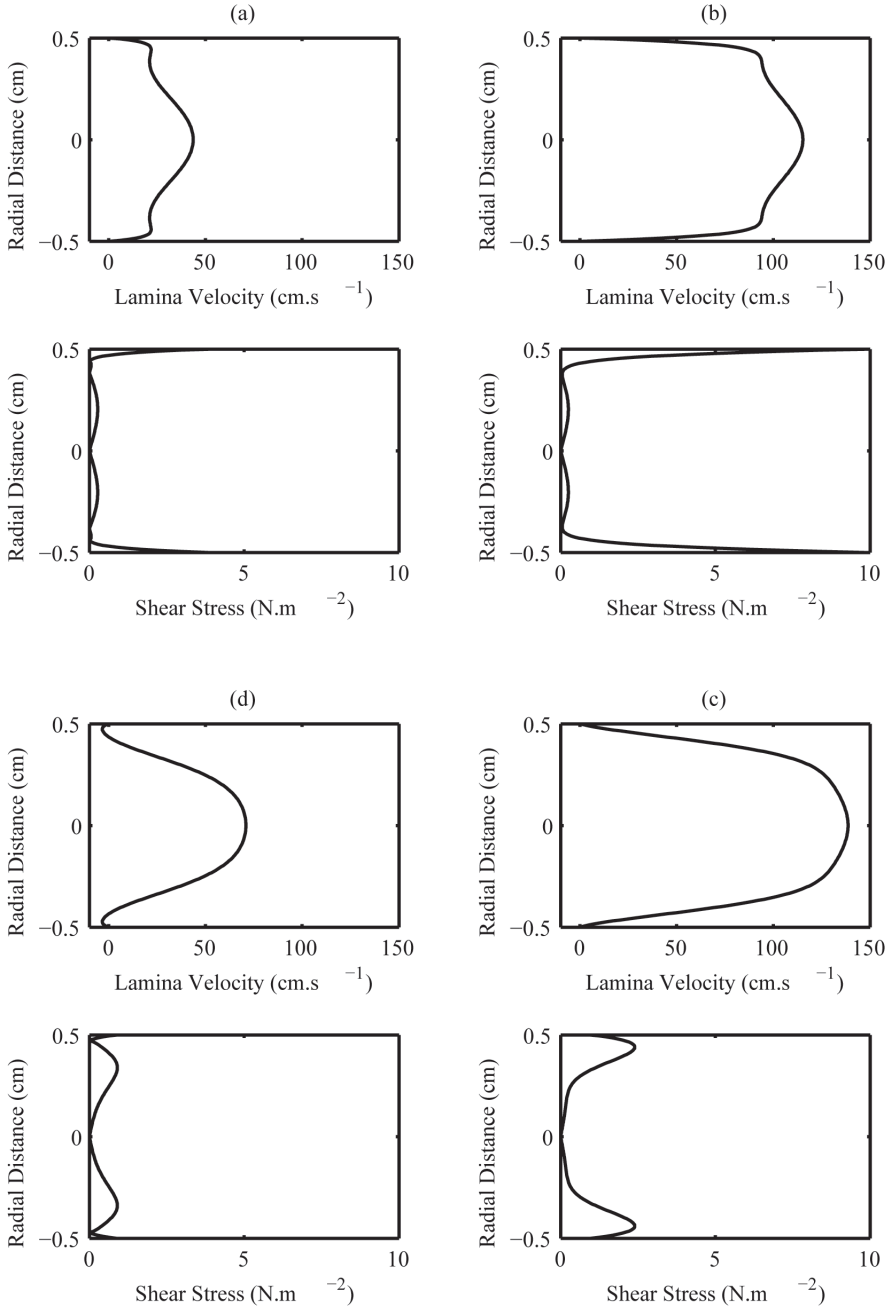

Figure 4.8: Velocity and shear stress profiles at different times during pulsatile flow, (a) $t = 0.07$ s, (b) $t = 0.10$ s, (c) $t = 0.26$ s and (d) $t = 0.46$ s

4.3.3 Impedance Modelling

The result for the impedance of pulsatile human blood over one cardiac cycle is shown in Figure 4.9 (a) by the dot-dashed line with the corresponding absolute spatial average velocity calculated by analytical techniques by the dashed line. The change in impedance as a percentage from stationary blood is also shown in 4.9 (b). The absolute spatial average velocity is used for comparisons to impedance curves because impedance is a non directional parameter. That is, the impedance of blood is dependent on the magnitude of shear contributing to the orientation of the flowing cells rather than the positive or negative direction of the flow. The use of the absolute spatial average velocity is easier for identification of orientation changes caused by velocity and acceleration changes.

The modelled results show that changes in the absolute spatial average velocity affect the impedance of the blood. For the acceleration phase of the data presented, a strong linear relationship between the absolute spatial average velocity and the impedance of the blood is seen ($r^2 = 0.99$). This demonstrates that the changes in impedance follow the changes in spatial average velocity closely. However, during the deceleration phase a delay is evident in the impedance response to changes in absolute spatial average velocity. In addition, the impedance, as well as the percentage impedance change, is also different between acceleration and deceleration of blood at the same velocity, (for example, at times (a) & (d), and (b) & (c) in Figure 4.9). These are all characteristics that have also been identified in the experimental results in Chapter 3.

As part of the modelling procedure, the fraction of aligned cells was calculated over the radius for each point in time. The mean fraction of aligned cells at each time is shown in Figure 4.10. This clearly shows the behaviour

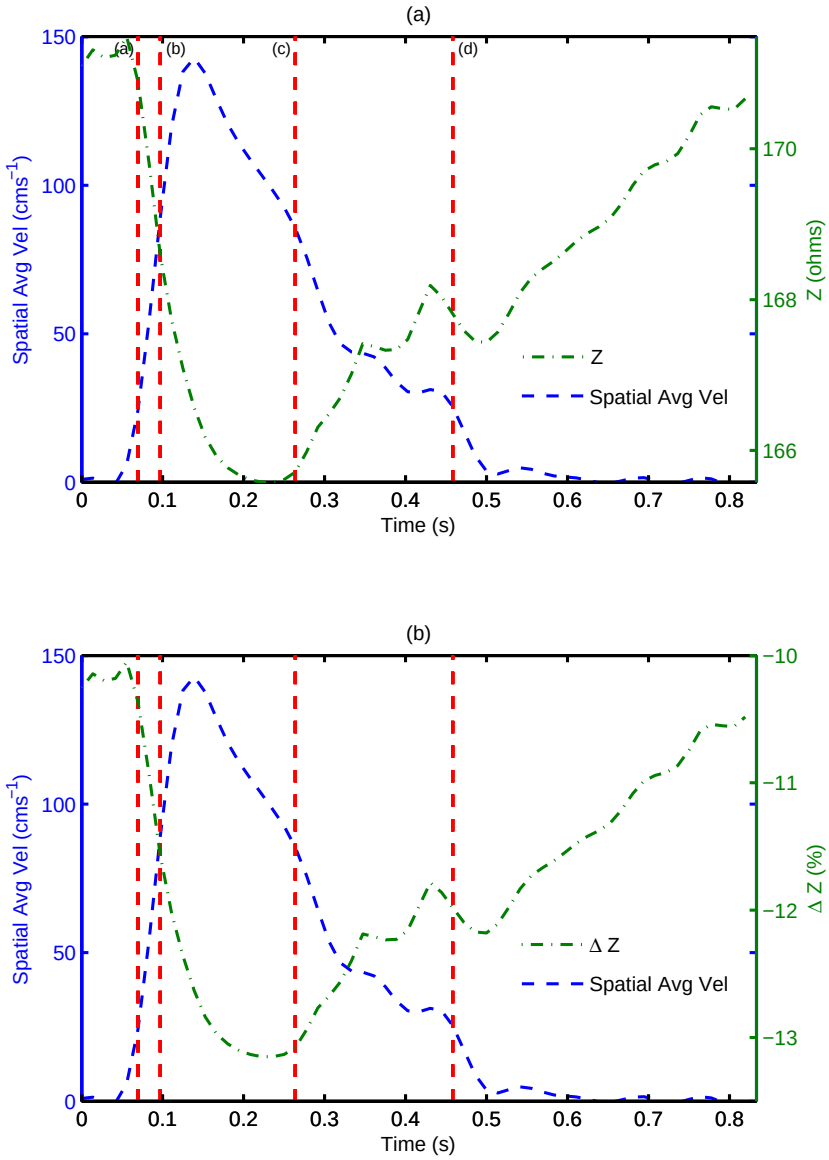

Figure 4.9: Modelled absolute spatial average velocity and a) impedance over one cardiac cycle, b) impedance change from stationary blood over one cardiac cycle, $h = 45\%$, $R = 5$ mm, pulse rate $= 72$ bpm, (a) $t = 0.07$ s, (b) $t = 0.10$ s, (c) $t = 0.26$ s, (d) $t = 0.46$ s

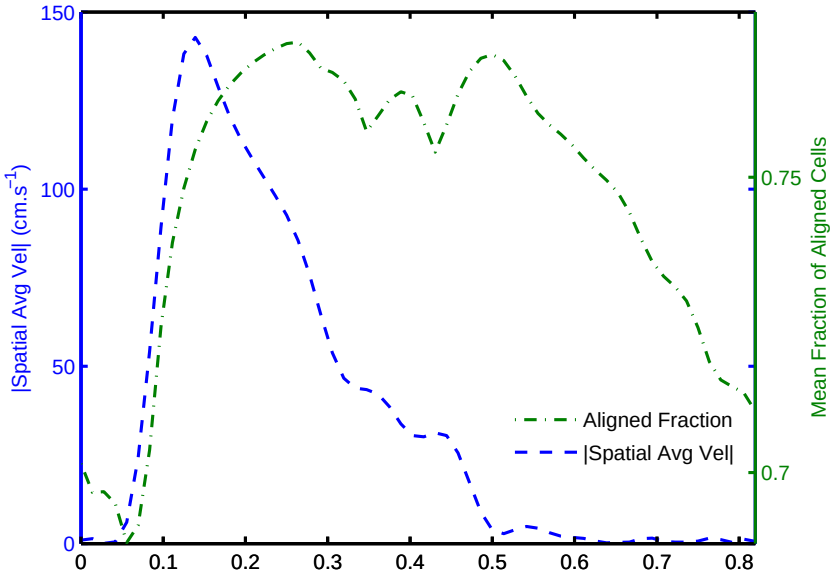

Figure 4.10: Fraction of aligned cells over the cardiac cycle

of the cells during the cardiac cycle. As the flow increases during the acceleration phase, the fraction of aligned cells increases quickly in response to the increase in velocity. However, as the velocity decreases, the number of cells that are fully aligned remains high due to the momentum of the cells. When the flow returns to zero, the fraction of aligned cells decreases as the cells begin to randomly orientate due to Brownian motion.

4.3.4 Verification

The theoretical model has been verified by comparison to experimental results recorded for bovine blood flowing through rigid tubes detailed in Chapter 3. In order to achieve good agreement between the experimental and modelled results, the conductivity and viscosity of plasma were modelled as temperature dependent variables. This was because the parameters used in

the original model were defined at 37^oC.

The temperature dependence of the plasma viscosity is similar to that of water (Shul'man & Makhanek 2005).

$$\begin{aligned} \nu(Poise) &= \nu_0 e^{-\frac{g(T-T_0)}{(T+H)(T+T_0)}} \qquad (4.32) \\ \nu_0 &= 0.0172 Poise \\ T_0 &= 23^oC \\ H &= 111^oC \\ g &= 420^oC \end{aligned} \qquad (4.33)$$

The temperature dependence of the plasma conductivity is approximated by a second order polynomial (Visser 1992).

$$\sigma_p l = 0.335 + 0.405T - 0.000192T^2 \qquad (4.34)$$

In addition, the major RBC axis length of a bovine blood cell (5.5 μm) is smaller than a human cell (8 μm) and the axis ratio used to best represent the experimental results was the original axis ratio found by Visser (1992) ($\frac{a_0}{b_0} = 0.22$). The viscosity of bovine plasma used was 1.73×10^{-3} Pa.s.

Figure 4.11 shows the theoretically modelled impedance for a single pulse and tube of 12.7 mm diameter. The modelled pulse rate was 70 beats per minute (bpm) and haematocrit was 45.5% to represent experimental conditions. The experimental blood was maintained at 22^oC (room temperature). This temperature was more easily maintained and therefore was more reliable during measurement. This temperature was used to model the conductivity

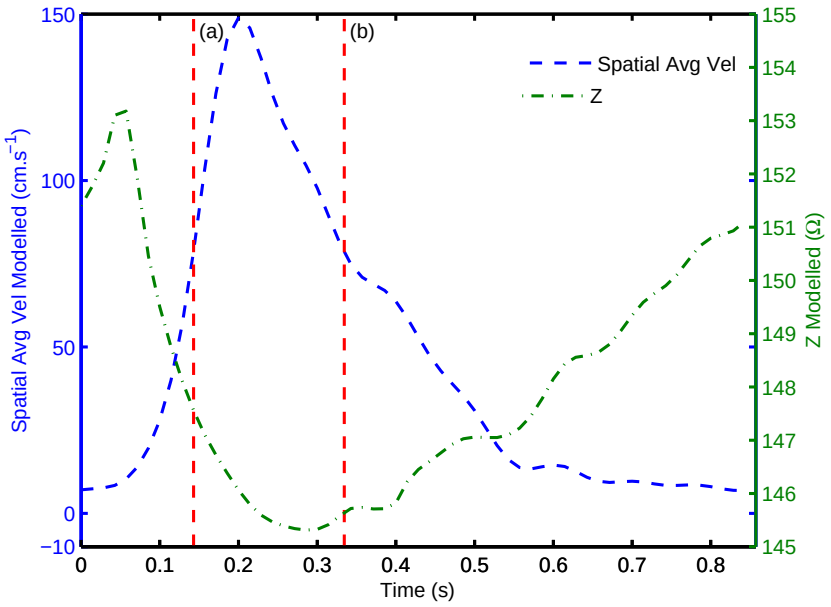

Figure 4.11: Modelled spatial average velocity and impedance of blood over one simulated cardiac cycle, h = 45.5%, d = 12.7 mm, 70 bpm

and viscosity of the plasma. The pulsatile spatial average velocity is shown by the dashed line and the modelled impedance is shown by the dot dashed line. Figure 4.12 shows the experimental results collected under the same conditions for flowing bovine blood. The measured average velocity is shown by the dashed line and the measured impedance is shown by the dot dashed line.

Comparison of the presented results shows that the magnitude and shape of the modelled and experimental impedance time signals are comparable. In addition, both theoretical and experimental results show similar characteristics. Both results show that changes in the average velocity of blood affects the impedance. The correlation between two time series of velocity and impedance was calculated at 0.74 (theoretical) and 0.72 (experimental).

During the acceleration phase of both the theoretical and experimen-

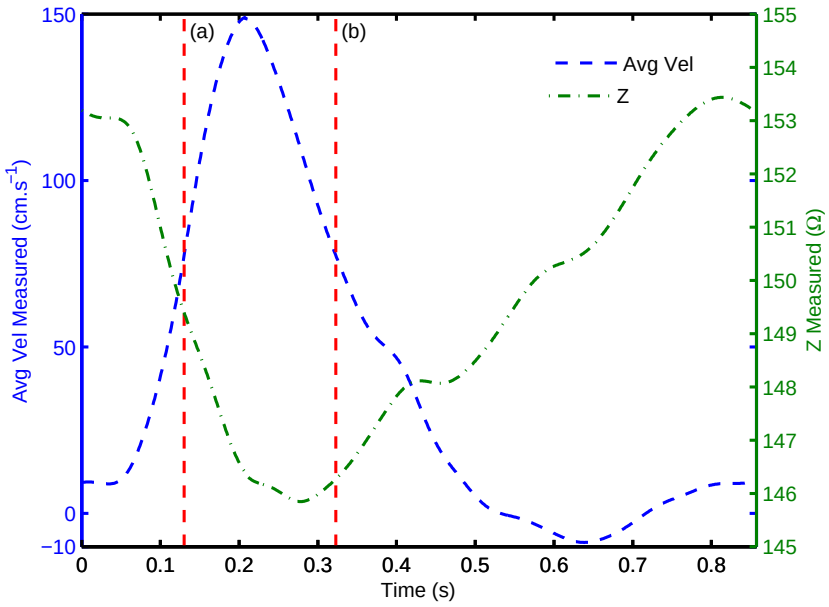

Figure 4.12: Experimental average velocity and impedance of blood over one simulated cardiac cycle, h = 45.5%, d = 12.7 mm, 70 bpm, freq = 5 kHz

tal results, a strong linear relationship between the average velocity and the impedance is seen (r^2 = 0.94 and 0.98 for theoretical and experimental results respectively). During the deceleration phase, a decay is evident in the impedance response to changes in average velocity. In addition, the impedance is also different between acceleration and deceleration at the same velocity, for example, at times (a) and (b), indicated in the experimental and theoretical results in Figure 4.11 and 4.12 by the vertical dotted lines. This is due to differences in the velocity profiles at these times.

The steady flow model developed by Hoetink et al. (2004) was used to calculate the impedance of pulsatile blood flow in Section 4.3.1. However, the impedance of the steady flow model did not capture the differences in impedance due to differences in velocity profile during acceleration and deceleration. The good agreement between the experimental results and results

from the theoretical model developed here, demonstrate that this theoretical model is more satisfactory in estimating the impedance of pulsatile blood flow.

Published stop flow experiments demonstrate that impedance responds instantaneously to increases in velocity, and decays when flow is stopped (Visser 1989). Both the modelled and experimental results of the present study demonstrate this. Both theoretical and experimental impedance results show a linear relationship with velocity during acceleration. During the end of the deceleration phase, the impedance is still changing despite the flow having returned to zero in both cases. This decay effect is also seen earlier in the deceleration phase when the impedance is less than that for accelerating blood at the same velocity such as at time (b) in comparison to time (a) in both Figure 4.11 and 4.12.

Towards the end of the flow cycle, the difference between the theoretical and experimental impedance increases. This is because the difference between the flow rate of the theoretical and experimental blood begins to differ.

4.3.5 Effect of Theoretical Changes in Pulse Rate

Figure 4.13 shows the modelled impedance time signals for one cycle of bovine blood flowing through a rigid tube, diameter of 12.7 mm, 45% haematocrit and varying pulse rates. These time signals have been generated by scaling the initial pressure gradient to ensure that the peak velocity and shape of each time signal remains the same while only the pulse rate varies.

As the pulse rate increases, the impedance time signal retains a similar shape over a shorter period of time. The maximum impedance reached during the cycle (which occurs at close to zero velocity), decreases as the pulse rate

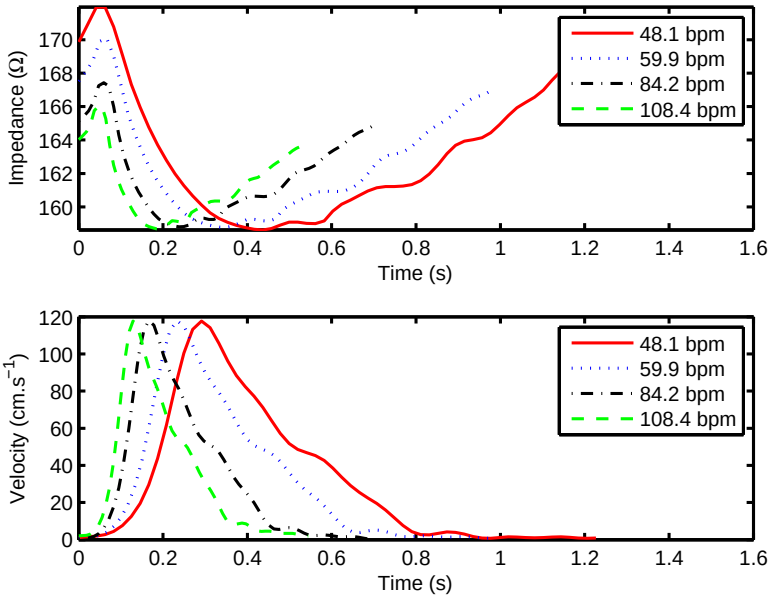

Figure 4.13: Impedance and velocity time signal calculated for varying pulse rates (H = 45%, d = 12.7 mm, T = 19)

increases. This is also evident in experimental measurements for the same flow parameters as shown in Figure 3.12, Chapter 3.

The impedance response at the maximum velocity of the cycle can be explored more robustly using the modelled results. This is because the maximum velocity over the cycle can be better controlled in the modelled case. The minimum impedance (occurring at the maximum velocity), increases as the pulse rate increases. As the pulse rate increases, the period of the cycle shortens and the cells do not have the same length of time to achieve the orientation state induced by the shear stress before the velocity of the blood (and therefore the shear stress) changes and the cells are induced to a new orientation state.

At the time when the flow is approaching zero, the cells do not have a chance to fully disorientate in the shorter time span resulting from a higher

pulse rate. As a result, they are still in a somewhat aligned state and therefore there is more plasma in the cross sectional area resulting in a lower impedance. As the pulse rate increases, the time span becomes shorter and the cells remain more aligned.

As the flow approaches the peak velocity, the cells are at their most aligned. As the pulse rate increases, the time to reach the peak velocity and full alignment decreases and so the cells do not necessarily reach this full alignment. However, as the flow decreases, the cells still maintain forward momentum that continues to provide the shearing force of alignment. As a result the change in magnitude of the minimum impedance is not as great due to pulse rate changes as the magnitude change of the maximum velocity. As a result of these phenomena, the peak to peak impedance change during the cycle also decreases.

4.3.6 Discussion

The features of velocity seen during the deceleration phase are clearly repeated, although delayed, in the impedance change time signal (see Figure 4.9). This suggests that there exist some non linear characteristics throughout the modelled cycle. The relationship between the velocity and impedance over time is shown clearly in Figure 4.14 in the same presentation as the experimental results in Figure 3.18 in Chapter 3 and the steady flow model results in Figure 4.6. This figure shows the absolute average spatial velocity and the corresponding conductivity at each time during the cycle. The spatial average acceleration of the blood is also indicated by the colour map. Figure 4.14 closely resembles the experimental results shown in Figure 3.18, however the steady flow model results in Figure 4.6 do not correlate.

Figure 4.14 confirms that the impedance is linear with velocity during

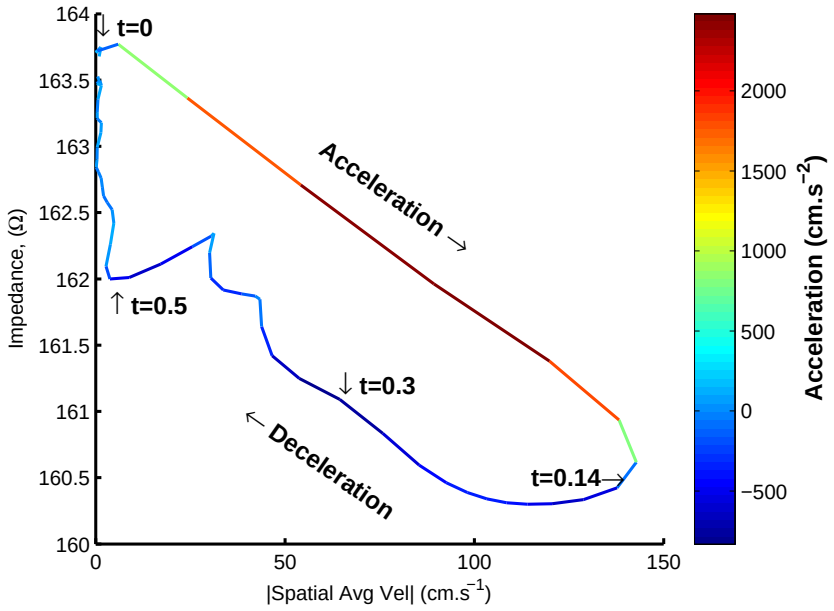

Figure 4.14: Impedance vs absolute spatial average velocity with acceleration indicated by colour variations

acceleration and displays a decayed response during deceleration. The effect of decaying orientation of cells can be seen in the modelling results presented in Figure 4.14 between 0.5 s and the end of the cycle when the absolute spatial average velocity has returned to approximately zero. During this time, the impedance is still increasing. Between 0.14 s and 0.5 s of the deceleration phase, the decay effect is less noticeable but still clearly exists. During this time the blood remains in motion and cells are not able to disorientate freely due to the shear stresses involved.

The important aspect to note from this is that the relationship between the absolute spatial average velocity and the impedance changes during the cardiac cycle. This relationship changes as the spatial average velocity begins to change from accelerating to decelerating. As the blood decelerates, the relationship is no longer the same as that for acceleration and becomes less

linear at lower velocities. Figure 4.14 also shows clearly that the impedance during pulsatile flow is not the same, at any given velocity during acceleration and deceleration. This is suggested to be due to differences in the shape of the velocity profile of the blood during these times. In Figure 4.9 and Figure 4.8 the velocity and particularly the shear stress profiles at times (a) & (d), and (b) & (c), are significantly different. This is despite the fact that the spatial average velocity is the same for each pair of times. At each instant, the cells are changing orientation in response to individual lamina velocities resulting in differences in impedance. This again emphasizes the importance of the velocity profile in determining the conductivity of blood and the inadequate nature of the steady flow model developed by Hoetink et al. (2004).

During oscillatory flow of viscous fluids, it has been previously mentioned that the central axial region of the velocity profile is largely flattened. The central axial laminae act like a solid core with high momentum and therefore resist changes in pressure. Hence the velocity response of the central axial laminae is delayed from that of the bulk spatial average velocity. Conversely the velocity response of the laminae closer to the walls precedes changes in the spatial average velocity. This would suggest that it is the flattened central core of the flowing blood which has the greatest effect on impedance. To investigate this, the cross correlation between two time series was calculated and the value for zero delay recorded. This was completed for each individual radial lamina velocity time signal and the observed impedance time signal. These data are presented in Figure 4.15, together with the correlation of the absolute spatial average velocity and impedance. The higher correlation for laminae with radial fractions less than 0.6-0.7 support this proposal that the central core of the flowing blood is primarily responsible for the impedance.

The impedance dependence on the central axial laminae also explains why

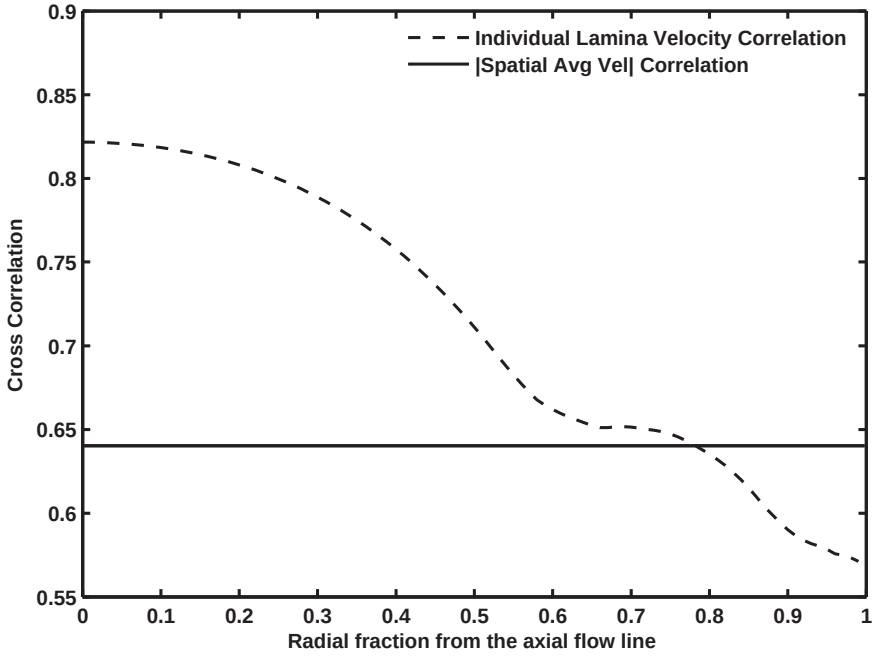

Figure 4.15: Correlation between conductivity and lamina velocity at a fraction of the radius

there is only a small (3%) peak to peak impedance change over the duration of the pulse in Figure 4.9. The flattening effect of the solid core existing in pulsatile flow results in a small variation in velocity across the inner radial laminae. The cells in this region will therefore experience small shear effects and thus the orientation of these cells will be altered only minimally during flow. The consequence of this is a smaller change in impedance over the duration of the pulse. Peak to peak changes of similar magnitudes have also been reported for pulsatile flow (Dellimore & Gosling 1975).

Despite this small peak to peak percentage change modelled, literature suggests that blood flow related resistivity changes are indeed observed in applications such at impedance cardiography (Visser et al. 1988, Visser 1989, de Vries et al. 1995). These impedance changes may be as small as 1 ohm; however they remain significant as it is the patterns found within the time

signal that may prove useful in interpreting physiological causes (Peura et al. 1978).

There is limited literature presenting experimental results for pulsatile blood flow. The experimental results reported by Dellimore & Gosling (1975) (reproduced in Figure 2.8) are for the longitudinal conductance of pulsatile blood flowing through a rectangular tube. Despite the difference in experimental set up, similar characteristics are shared with the modelled results such as instantaneous conductivity response during acceleration and decaying conductance during deceleration. The theoretical results presented in Figure 4.14 of this study also match the general shape of the experimental results reported by Dellimore & Gosling (1975), reprinted in Figure 4.16. In particular the linear relationship between average velocity and conductivity during acceleration, and the decay observed in conductivity during deceleration are evident in both the theoretical model and experimental results presented here and also the experimental results of Dellimore & Gosling (1975).

Without further published results for the change of impedance from stationary flow during pulsatile flow, previously published steady state results (both theoretical and experimental) were used for comparison to the theoretical model presented here. Comparison of the theoretical conductivity results in Figure 4.4 (calculated using steady state methods defined by (Hoetink, Faes et al. 2004)) and Figure 4.9 (b) (calculated using pulsatile flow methods outlined in the present study) for the same spatial average velocity time signal, show that the inclusion of pulsatile flow significantly affects not only the shape of the conductivity time signal, but also the magnitude of the change (e.g. by a factor of almost a half at times surrounding the peak velocity).

The theoretical results of the present study were also compared to pre-

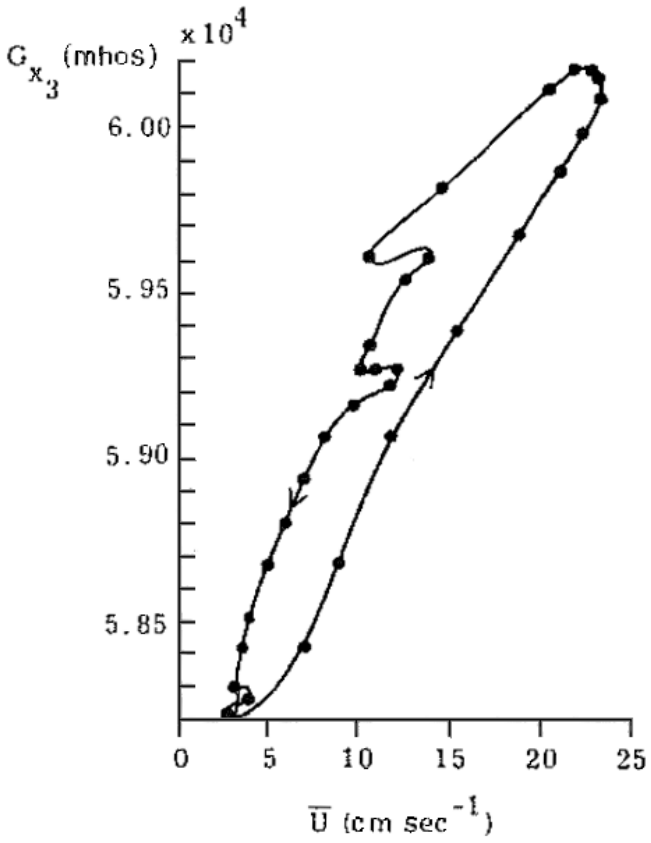

Figure 4.16: Experimental impedance variation with velocity as published by Dellimore & Gosling (1975)

viously published steady flow results. This was achieved by modifying the parameters of the present theoretical model to match those of the previously published experimental configurations. In each case, the theoretically calculated conductivity change at the peak spatial average velocity for pulsatile blood flow was used as a steady state flow comparison. The results show that the theoretical conductivity change is less than that predicted for the same steady flow rates. For example, modelling results presented by Hoetink et al. (2004) demonstrate a 25% change in conductivity at a reduced aver-

age velocity of 500 s^{-1}, tube diameter of 4 mm and haematocrit of 47.5% for human blood. The theoretical model in the present study calculates a conductivity change of only 18% at these parameters.

These differences are due to the characteristics of pulsatile flow and the dependence of the conductivity on the inner axial region. As previously identified, the velocity of the central axial region is delayed from the spatial average velocity. As blood begins to flow, the RBCs do not have time to fully align with the flow before the flow changes direction. As the flow direction changes more often, such as in the case of increased heart rate, the orientation of the RBC is not able to follow the rapid changes in flow. This means that the conductivity does not reach the same as that predicted in steady flow and demonstrates that steady flow models are not accurate in determining the conductivity of pulsatile blood flow.

4.4 Conclusions

Pulsatile flow and cell orientation dynamics have been successfully combined with impedance methods to predict the resistivity changes of pulsatile blood flowing through rigid tubes. The new theoretical model developed here enables the resistivity of blood to be calculated from based on pulsatile velocity and shear profiles. The orientation of the cells has been modelled over the radius of the tube using a direct calculation of the fraction of aligned cells from the shear rate profile. The inclusion of both of these features advances the steady model developed by (Hoetink et al. 2004).

Comparison of the theoretically modelled impedance to the impedance signals collected experimentally verifies the accuracy of this new model under pulsatile flow conditions. It has been shown that the steady flow model

(Hoetink et al. 2004) does not adequately describe the impedance response of pulsatile blood flow as this model predicts the results shown in Figure 4.6. This has been shown to be incorrect in the experimental results of Figure 4.5. Therefore, the mathematical model presented herein for pulsatile flow is the first to theoretically explain the flow dependence of the electrical impedance of blood during pulsatile flow through rigid tubes.

Comparison of the pulsatile theoretical model with experimental data show that the theoretical model successfully simulated features of the experimental time signals that the steady flow model does not. These were: 1) a difference between impedance during accelerating and decelerating flow at the same velocity, 2) a linear impedance response to acceleration, 3) a decay in impedance during deceleration to zero flow, and 4) a variation in impedance with pulse rate. Both the theoretically modelled and experimental impedance data of pulsatile flow also indicate a good cross correlation with the velocity (r=0.72 and 0.74 respectively at a pulse rate of 70 beats per minute).

The theoretical model shows that the velocity profile is the most important factor in determining the impedance of blood. The flowing laminae in the central core of the tube have been shown to be the most influential in determining the impedance. Due to the delay in momentum transfer between the flowing lamina during pulsatile flow, the impedance change from stationary blood (%) has been shown to be less than that for blood flowing at constant flow rates.

Chapter 5

Comparison of Experimental and Theoretical Impedance of Blood in Rigid Tubes

Comparison of the theoretical and experimental results was briefly detailed in Section 4.3.4 under specific conditions. The electrical impedance of stationary blood depends on a number of factors such as: temperature, haematocrit, current frequency of measurement, osmolarity and ionic content. These are in addition to the velocity of flow which can vary depending on the radius of the tube, systolic ratio and pulse rate. The haematocrit of blood, radius of tube and temperature of blood were varied and the theoretical and experimental impedance results were compared. This demonstrates the applicability of the theoretical model over a wide range of parameters.

5.1 Variations in Haematocrit

5.1.1 Impedance of Pulsatile Blood Flow

The experimentally measured and theoretically calculated impedance of pulsatile blood for a variation in haematocrit is shown in Figure 5.1 and Figure 5.2 respectively. Maxwell-Fricke equations predict that the resistivity of a stationary suspension of cells increases as the number of cells increase. This is also the case for pulsatile blood as evidenced in both Figure 5.1 (a) and Figure 5.2 (a) in which the average magnitude of impedance of flowing blood increases as haematocrit increases while the flow pattern remains the same (Figure 5.1 (c) and Figure 5.2 (c)).

Comparison of the experimental and theoretical results (Figure 5.1) shows that the modelled impedance and the experimental impedance for a haematocrit of 46% have similar magnitudes (120 - 130 Ω). As the haematocrit decreases, the impedance decreases due to the decrease in the number of cells resisting the current flow. However, the experimental results are consistently lower than the modelled results. It is expected that this is due to the method used to lower the haematocrit of the blood. The addition of physiological saline ($\sigma = 1.5\ S.m^{-1}$) increased the conductivity of the blood more than if bovine plasma ($\sigma = 1.2\ S.m^{-1}$) were added. This in turn decreased the magnitude of the impedance of the experimental results.

Over the velocity pulse the effect of flow changes on impedance is much larger at higher haematocrit, though the shape of the curves is similar. That is, a larger peak to peak impedance value occurs as the haematocrit increases, while maintaining a similar pattern. Studies reporting changes in the impedance of constant flowing blood also show that the flow dependent change in impedance is larger at higher haematocrit (Visser 1989, Sigman

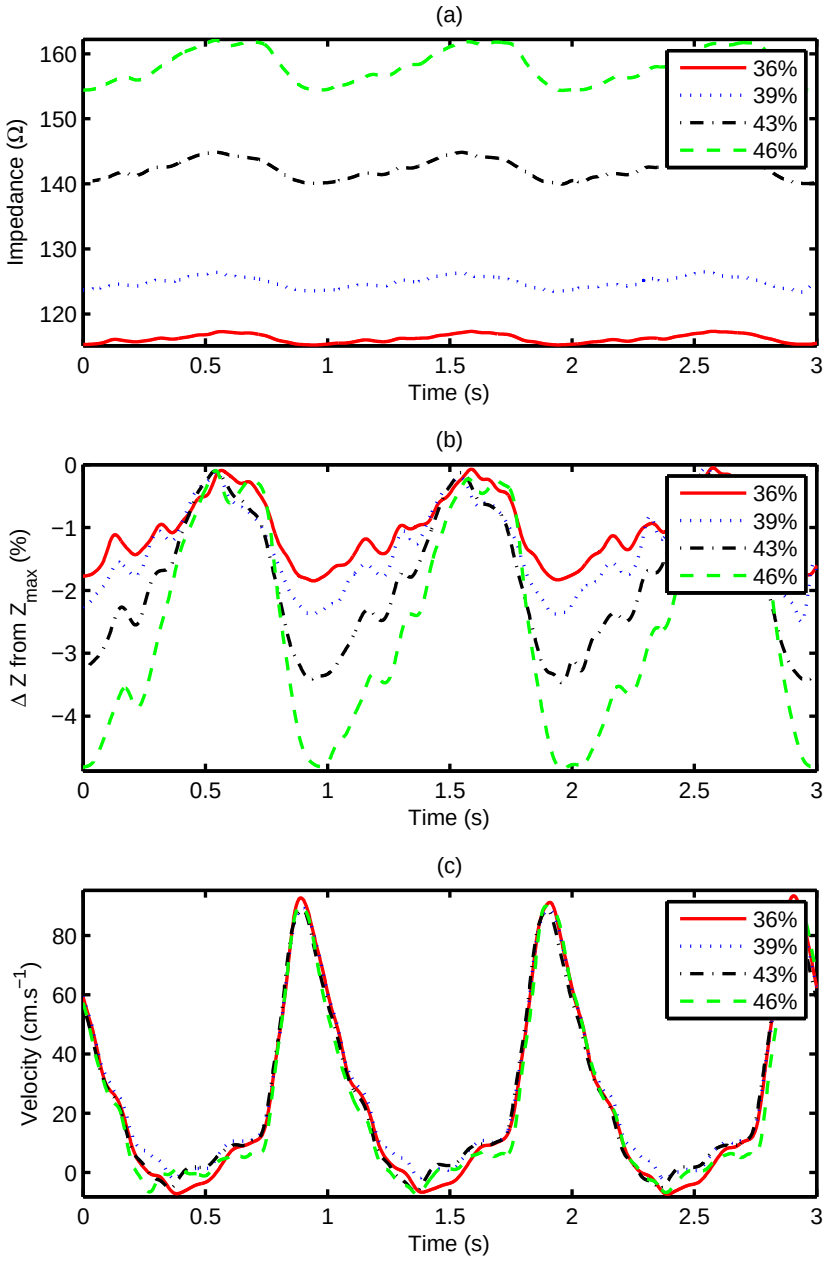

Figure 5.1: The experimental effect of variations in haematocrit on impedance change from random orientation, T = 20 ^oC, Pulse rate = 60 bpm, d = 12.7 mm, H = 36%, 39%, 43%, 46%. Compare Figure 5.2

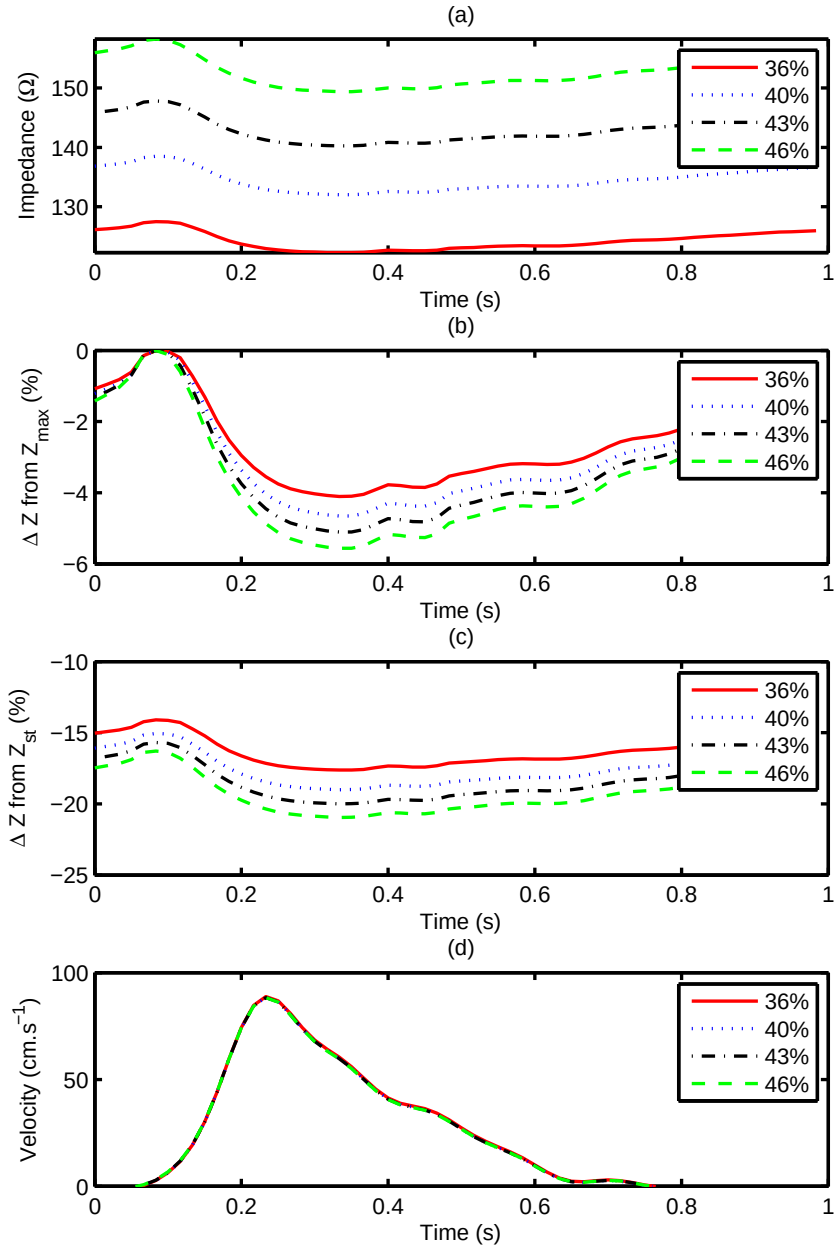

Figure 5.2: The modelled effect of variations in haematocrit on impedance change from random orientation, T = 20 ^oC, Pulse rate = 60 bpm, d = 12.7 mm, H = 36%, 39%, 43%, 46%. Compare Figure 5.1

et al. 1937, de Vries et al. 1995). This is because the presence of more cells means there exists a greater change in the cross sectional area of plasma when the cells begin to orientate. This large difference in plasma cross sectional area between random orientation and aligned flow leads to a larger change in the measured impedance.

The change in impedance from the impedance at the minimum velocity (as a percentage) is shown for the experimental results in Figure 5.1 (b). Published data is traditionally presented as the percentage change in impedance from stationary blood. However, due to difficulties in measuring the impedance of stationary blood as discussed in Section 3.3.1, the change in impedance is calculated as a percentage change from the maximum impedance measured. It is assumed that this occurs at the minimum velocity and the cells are most randomly orientated at this time and therefore closest to stationary. The change in impedance from the impedance at the minimum velocity has also been calculated and is shown in Figure 5.2 (b).

The peak impedance change measured experimentally in Figure 5.1 (b) is less than that for the modelled results in Figure 5.2 (b) (2-4% for experimental results vs 4-6% for modelled results). This can be explained by the difference in viscosity between physiological saline and plasma. The viscosity of saline is approximately half that of plasma. As a result, the addition of saline reduces the viscosity of the surrounding plasma. By decreasing the viscosity, the viscous shearing stress is also decreased and cells experience reduced shearing forces and therefore reduced orientation changes in the experimental results.

In the modelled case, the impedance of stationary blood is easily calculated. Therefore the percentage resistivity change from stationary blood for the varying haematocrit is shown in Figure 5.2 (b). This figure shows that

the general shape of the time signal is not affected by the haematocrit, but rather, increasing haematocrit appears to generate a larger average absolute change in resistivity from stationary blood. Given the good agreement between Figure 5.1 and Figure 5.2, it can be assumed that the experimental results would follow similar trends in the change in impedance from stationary flow due to change in haematocrit.

5.1.2 Time Constant

The deceleration time constant and system gain were calculated for varying haematocrit according to methods described in Section 3.3.4 for both the experimental and theoretical results. The time constant during deceleration is shown as a function of haematocrit for a pulse rate of 72 bpm in Figure 5.3 (experimental) and Figure 5.4 (theoretical). The data points are shown by the asterisk and the line of best fit is shown by the dot-dashed lined. The magnitude of the time constant is similar for both the experimental and theoretical results for 46% haematocrit (10 and 10.5 s respectively).

As the haematocrit increases, the time constant decreases. This can be explained by the increase in the number of cells per unit volume. As the number of cells increases, the number of interactions between the cells also increase. Due to the increase in collisions, the cells will be knocked out of alignment and become randomly orientated at a faster rate than at low haematocrit. This faster disorientation reduces the time constant of decay. As the haematocrit decreases, the time constant does not increase at the same rate for the theoretical results as it does for the experimental results. The time constant for both theoretical and experimental results however, both display a linear trend with respect to haematocrit for the same peak velocity.

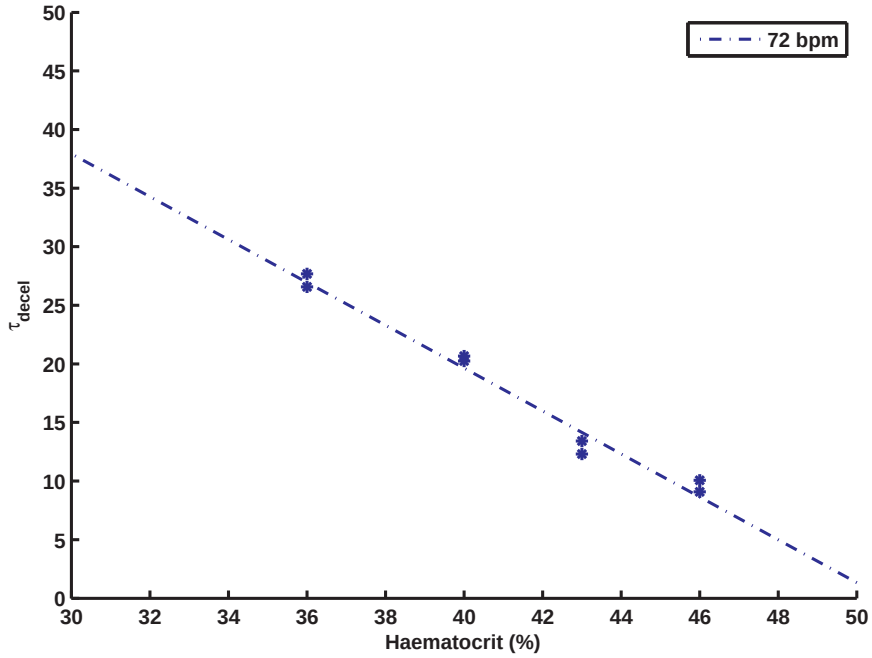

Figure 5.3: Experimental variation in time constant with haematocrit for a pulse rate of 72 bpm

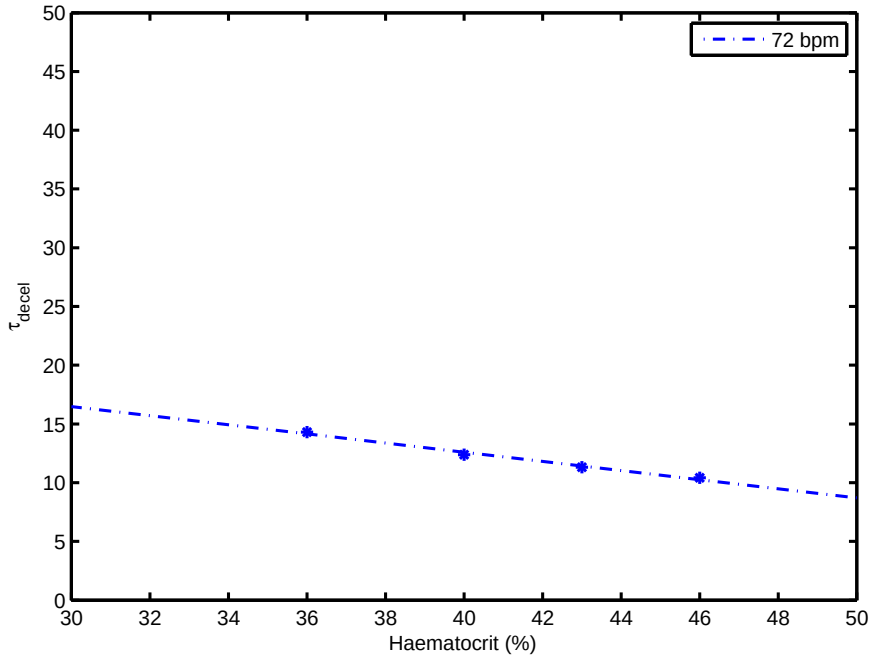

Figure 5.4: Theoretical variation in time constant with haematocrit for a pulse rate of 72 bpm

The peak velocity does not appear to affect the time constant at this pulse rate (for the same haematocrit), however previous data presented in Figure 3.20 for variation in pulse rate suggests that the case may be different for lower pulse rates. (Visser 1989) report for step velocity inputs that for haematocrit of 36.4% and 47.5% the time constant did not significantly differ while for a haematocrit of 53.7%, the time constant increased slightly. This is contrary to results reported here. However the previously published results were reported for stop flow experiments and therefore the differences can be attributed to the use of pulsatile flow in this work.

The system gain, K, over the duration of the pulse is shown as a function of haematocrit for two peak velocities at a pulse rate of 72 bpm in Figure 5.5 (experimental) and Figure 5.6 (theoretical). The data points are shown by the asterisk and the line of best fit is shown by the dot-dashed lined. The order of magnitude of the theoretical system gain is consistent with the experimental system gain. For a given peak velocity, the gain factor decreases as the haematocrit increases. This is because as the number of cells increase, the conductivity will decrease due to the decrease in cross sectional plasma.

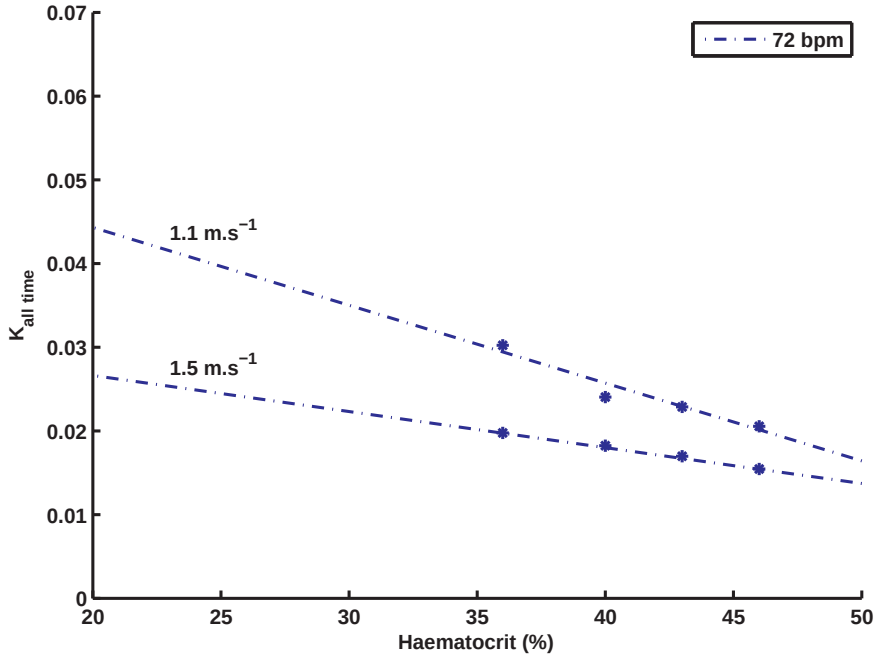

Figure 5.5: Experimental variation in system gain with haematocrit for two peak velocities and a pulse rate of 72 bpm

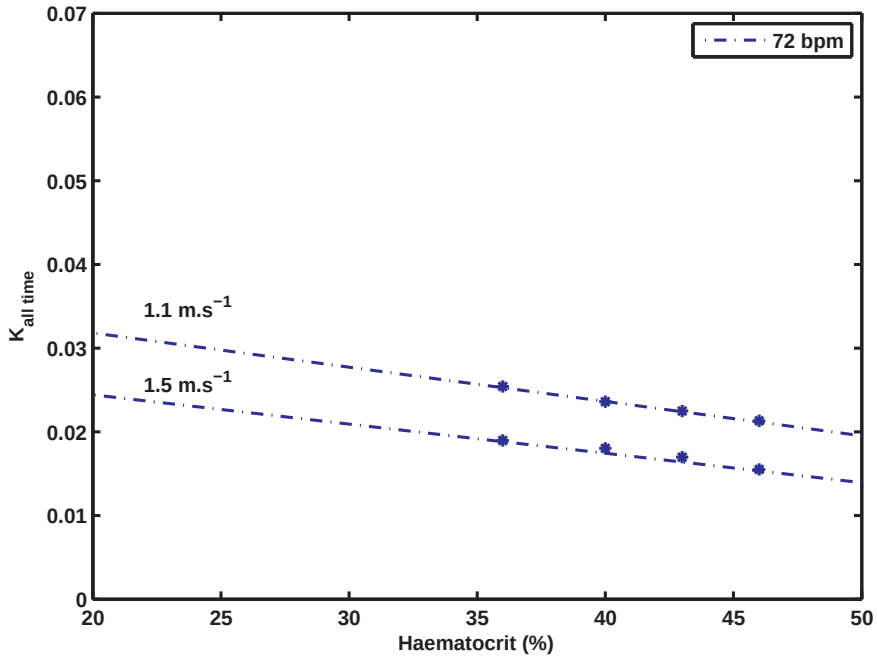

Figure 5.6: Theoretical variation in system gain with haematocrit for a pulse rate of 72 bpm

5.2 Variations in Tube Radius

5.2.1 Impedance of Pulsatile Blood Flow

The radius of the measuring tube was varied in order to determine the effect on the impedance measurements due to orientation changes. Figure 5.7 shows an example of the impedance time signals measured experimentally for tube diameters of 9.5 mm, 12.7 mm and 19 mm for similar spatial average velocity time signals. Figure 5.8 shows the theoretically modelled results.

It can be seen that similar spatial average velocity time signals generate different changes in magnitude of the impedance change for different radii, both experimentally and theoretically. As the tube radius increases, the peak to peak resistivity change across the time signal decreases and the resistivity change from stationary blood decreases (see Figure 5.7 (b) and Figure 5.8 (b)). This can be explained as the same spatial average blood velocity flowing through a small tube will generate higher shear rates than in a larger tube. In particular, while the absolute width of the high shear zone near the wall remains fairly consistent between radii, the fraction of the entire width of the tube that this represents is much larger in a smaller tube. Thus, a higher percentage of cells are becoming aligned in the smaller tube, resulting in a higher impedance change. This greater shearing stress induces a larger change in orientation of the red blood cells for the same spatial average velocity in the smaller tube as shown for the 9.5 mm tube in Figure 5.7 (b) and Figure 5.8 (b).

In addition, the response of cells in the smaller tube is faster. This is because there is a smaller distance for the momentum to be transferred between lamina before all lamina are flowing in response to pressure changes. The lamina begin to flow in turn from the central axis of the tube out to

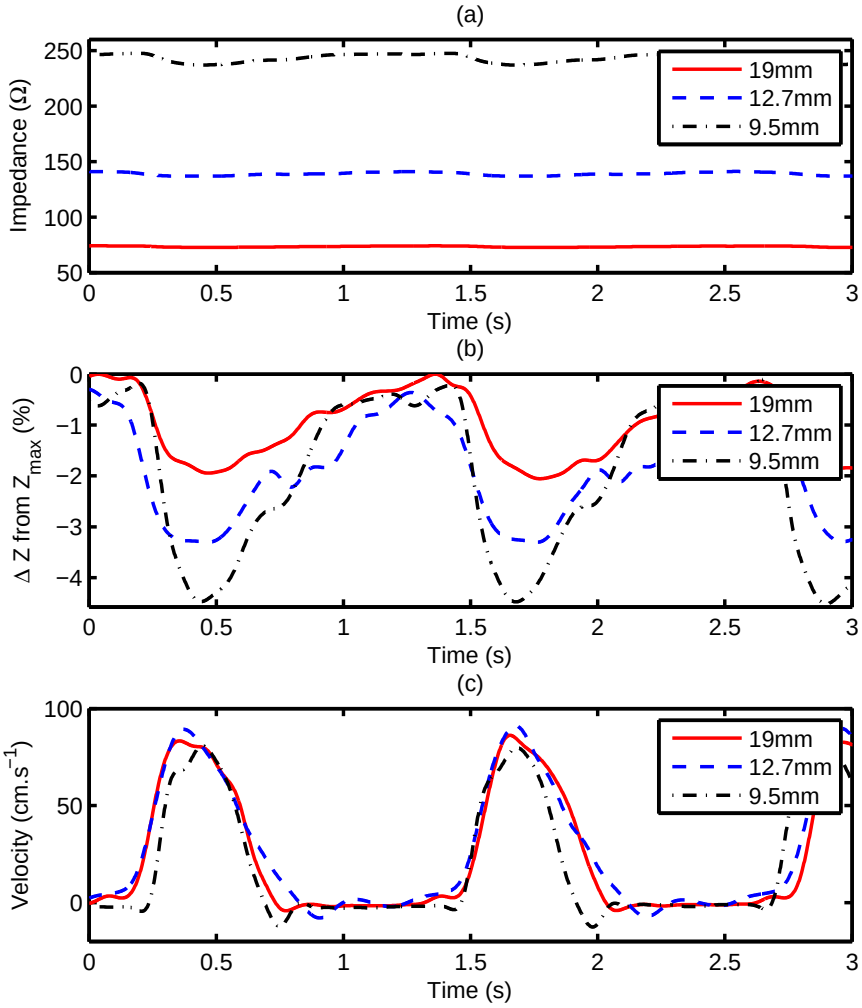

Figure 5.7: The experimental effect of radius variations on the impedance measured for pulsatile blood, h = 40%, T = 20 ^oC, Pulse rate = 48 bpm, diameter = 9.5 mm, 12.7 mm, 19 mm. Compare Figure 5.8

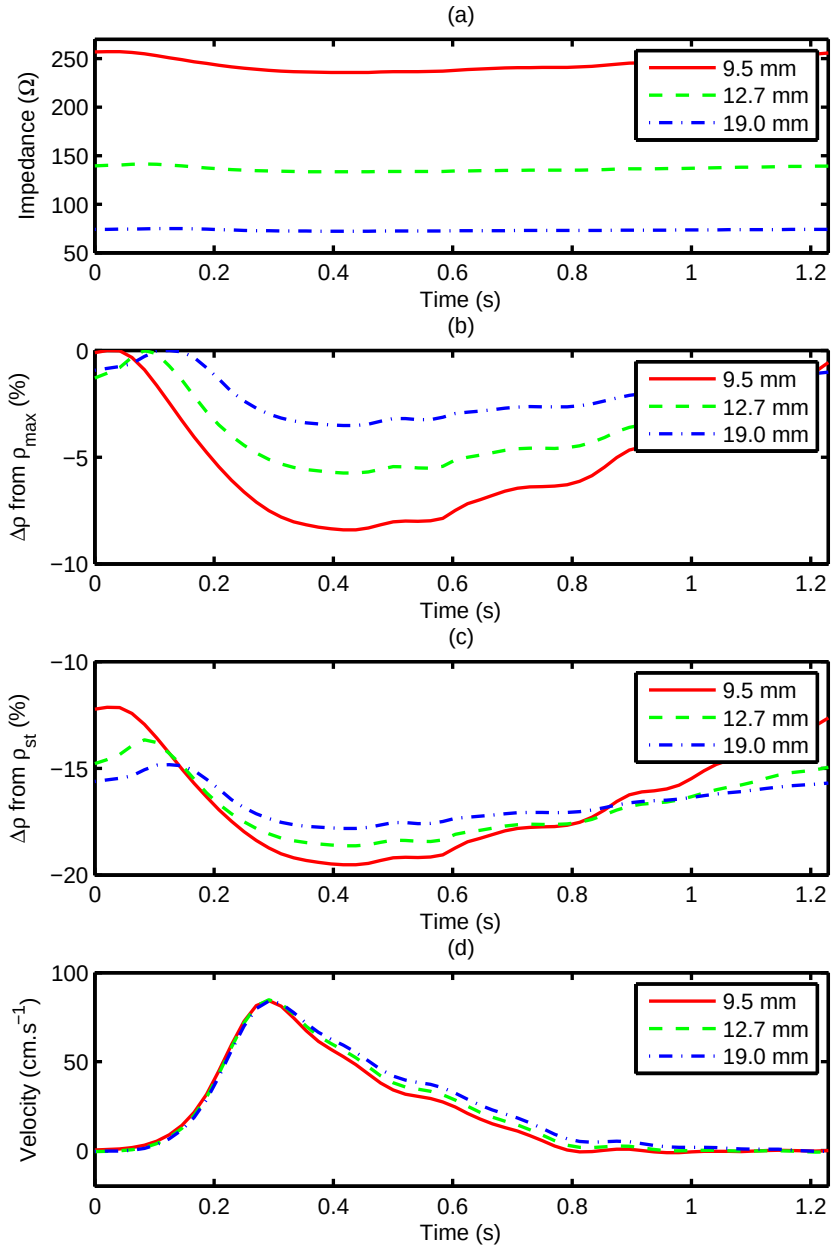

Figure 5.8: The theoretical effect of radius variations on the impedance measured for pulsatile blood, h = 40%, T = 20 ^oC, Pulse rate = 48 bpm, diameter = 9.5 mm, 12.7 mm, 19 mm. Compare Figure 5.7

the tube wall. As a result, for the same amount of time as in a larger tube, more cells as a fraction of the total tube area are able to respond to velocity changes and reorientate. This will result in larger changes in impedance from stationary blood due to the larger fraction of cells changing orientation.

It is suggested using theoretical analysis (Visser 1989, Visser 1992) that the gradient of the velocity profile (or the shear rate) is proportional to the reduced average velocity. For steady flow, the reduced average velocity is the spatial average velocity divided by the radius of the tube, $\frac{<v>}{R}$. Visser (1989) suggests that the reduced average velocity is a better indicator of the resistivity change for constant flow rates as it is a good approximation of the average shear experienced by the cells in the tube. However, this was not verified experimentally or theoretically for varying tube radii.

Figure 5.9 shows the same results as those in Figure 5.7, however in this figure, the resistivity is plotted. In this figure, the resistivity is shown in (a), the resistivity change from minimum flow is shown in (b) and the reduced average velocity is shown in (c). This plot shows that due to the different tube radii, the reduced average velocity and therefore the shear rates experienced by the cells are different for each radii. This is because for the same spatial average velocity, the radius of the tube increases and therefore the average velocity gradient or shear rate reduces. As would be expected, the greatest magnitudes of shear stresses are generated in the 9.5 mm diameter tube and in turn, the greatest orientation change and therefore resistivity change is also measured for this tube.

An example of the measured impedance is shown in Figure 5.10 for blood flowing through the 9.5 mm and 12.7 mm diameter tubes at similar reduced average velocities. It can be seen that the resistivity change measured in both tubes is equivalent, despite the different radii and spatial average velocities.

These results provide further evidence that experimental results collected in small radius tubes are scalable to tubes of physiological relevance comparable to the aorta. This is important because physiological blood flow through the aorta is difficult to mimic in vitro due to the large volumes of blood required. Large volumes of blood are required because of the large aortic radius and high flow rates in vivo.

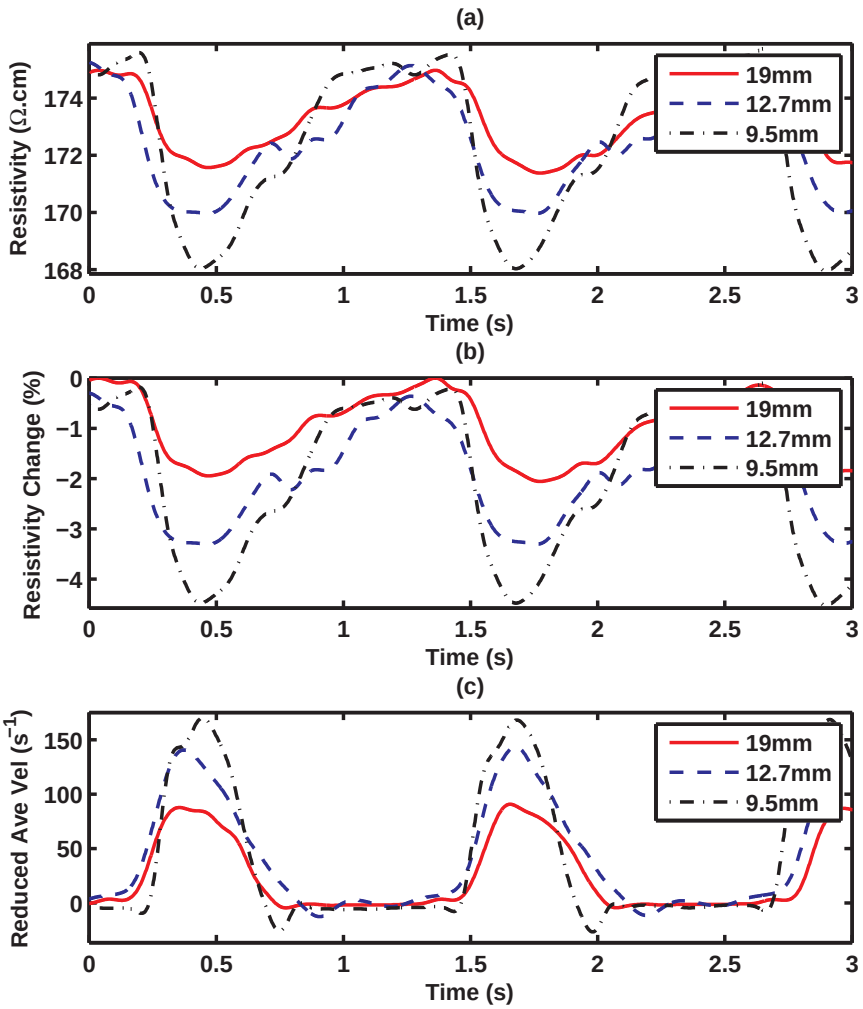

Figure 5.9: The experimental effect of variation of radius on measured resistivity and resistivity change as compared to the reduced average velocity

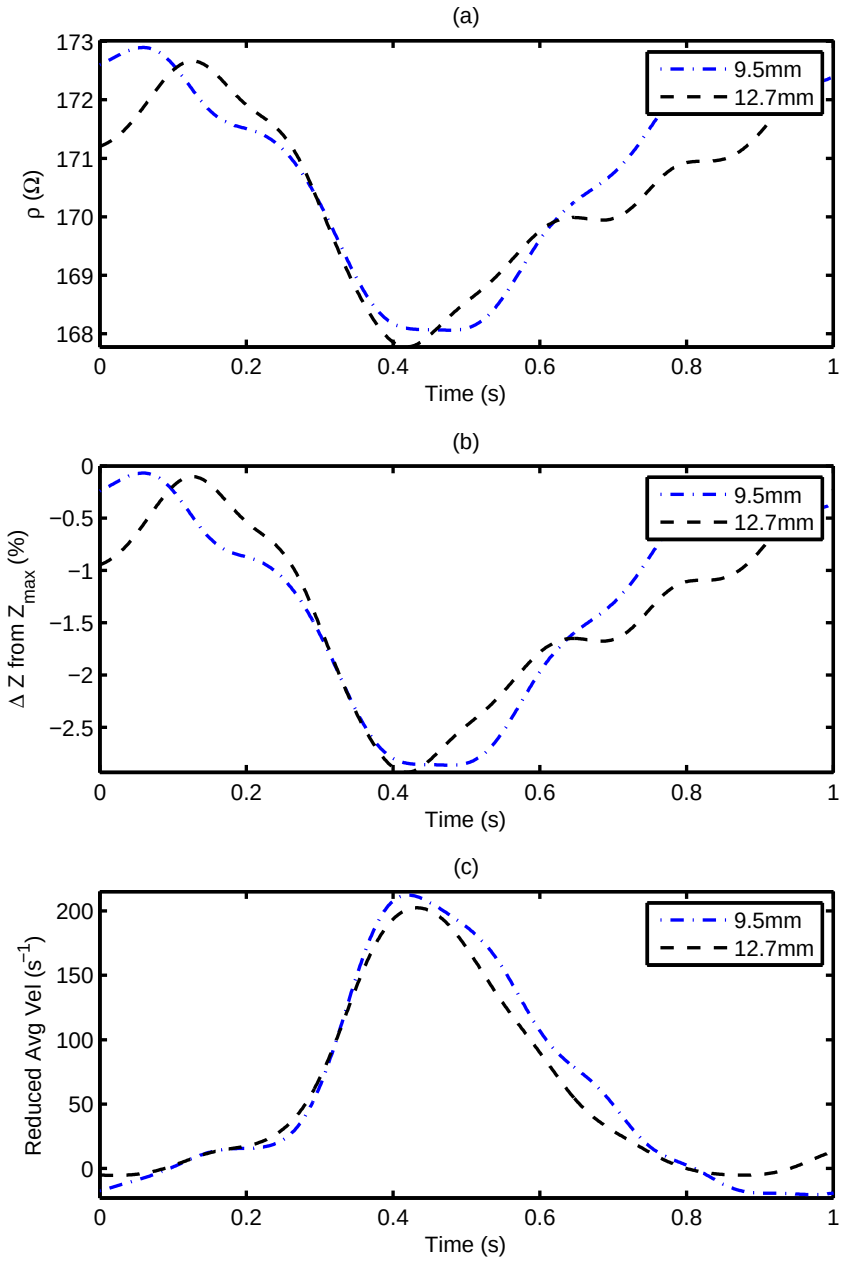

Figure 5.10: The effect of variations in radius on resistivity change for the same reduced average velocity time signal

5.2.2 Time Constant

The variation in deceleration time constant is shown for varying tube radii as a function of the peak reduced average velocity in Figure 5.11 (experimental) and Figure 5.12 (theoretical). No trends are evident in the experimental decay time constant shown in Figure 5.11 and due to the limited range of peak reduced average velocities collected for each tube, it is difficult to make any definite conclusions. Because of this, a spread of standard reduced average velocities have been used to model the theoretical time constant in Figure 5.12.

In this case, the results show that as the tube radius increases, so too does the time constant. The response of cells in a tube with a smaller radius is quicker due to the shorter distance that the momentum must be transferred between the lamina before the central axial core begins to move. Therefore, a larger percentage of cross-sectional area will contain cells that disorientate faster as the momentum is transferred across the radius. This in turn reduces the time constant during deceleration.

The experimental and theoretical system gains shown in Figure 5.13 and Figure 5.14 both display the same exponential saturation characteristics with peak reduced average velocity as that displayed in Figure 3.21 in Chapter 3. The experimental results suggest that the radius does not affect the gain of the system, however the theoretical results show clear separation in gain between the tube radii at lower reduced average velocities. This difference is expected to be due to the limited range of peak velocities in the experimental results at low velocities.

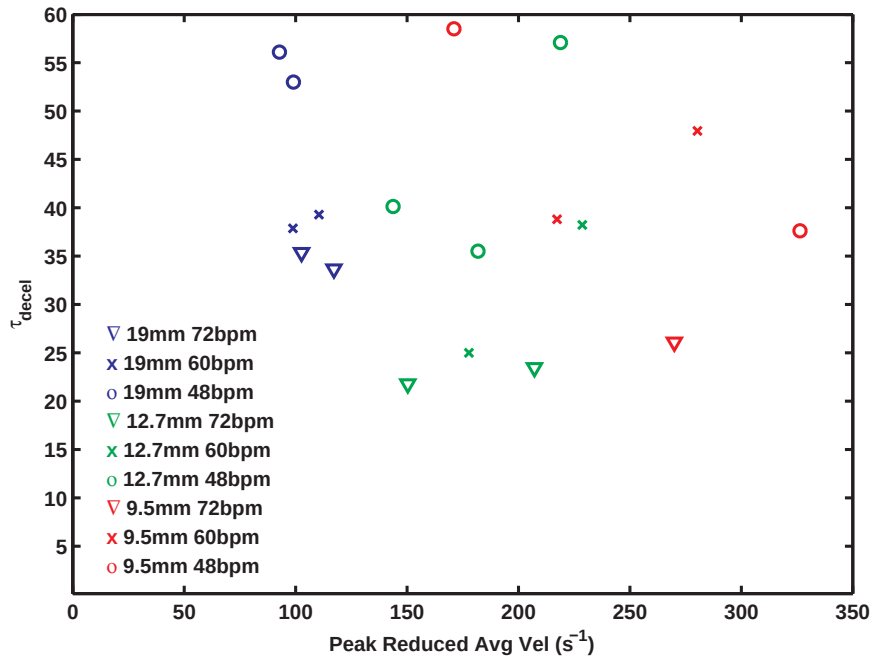

Figure 5.11: Experimental variation in τ_d with peak reduced average velocity, h = 40%, T = 19^oC, SR = 35/65, f = 5 kHz

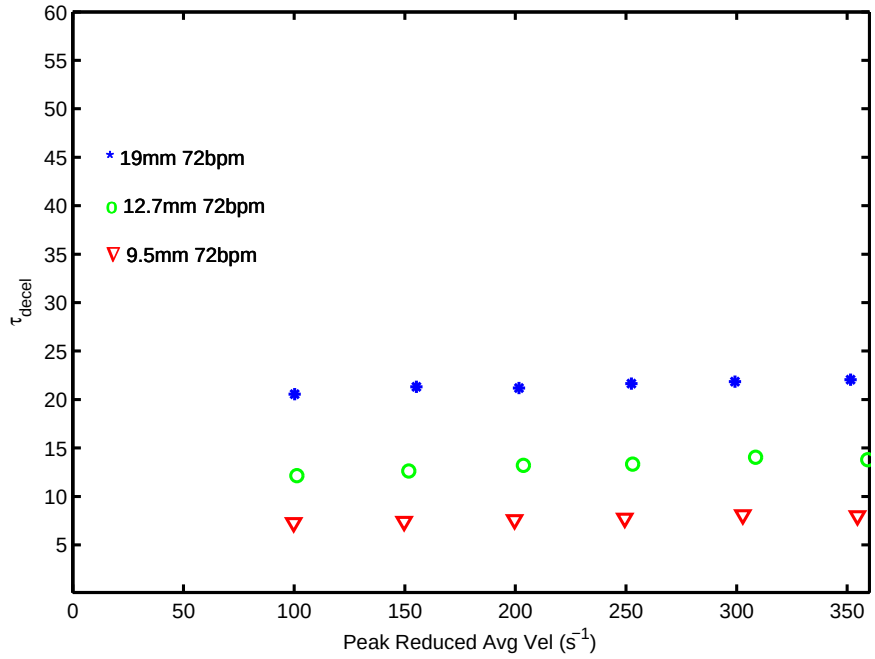

Figure 5.12: Theoretical variation in τ_d with peak reduced average velocity , h = 40%, T = 19^oC, SR = 35/65, f = 5 kHz

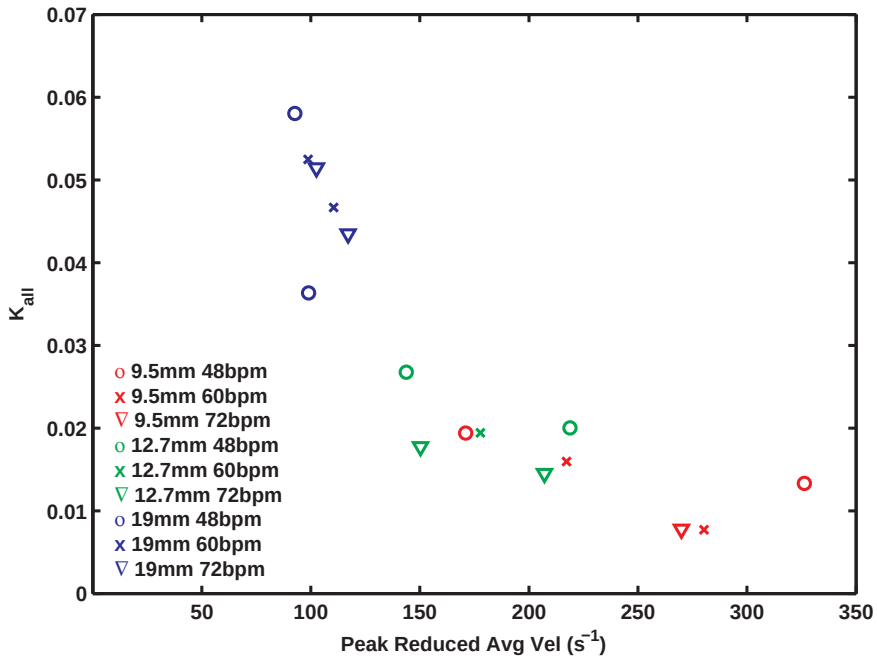

Figure 5.13: Experimental variation in K with peak reduced average velocity during the entire pulse, h = 40%, T = 19^oC, SR = 35/65, f = 5 kHz

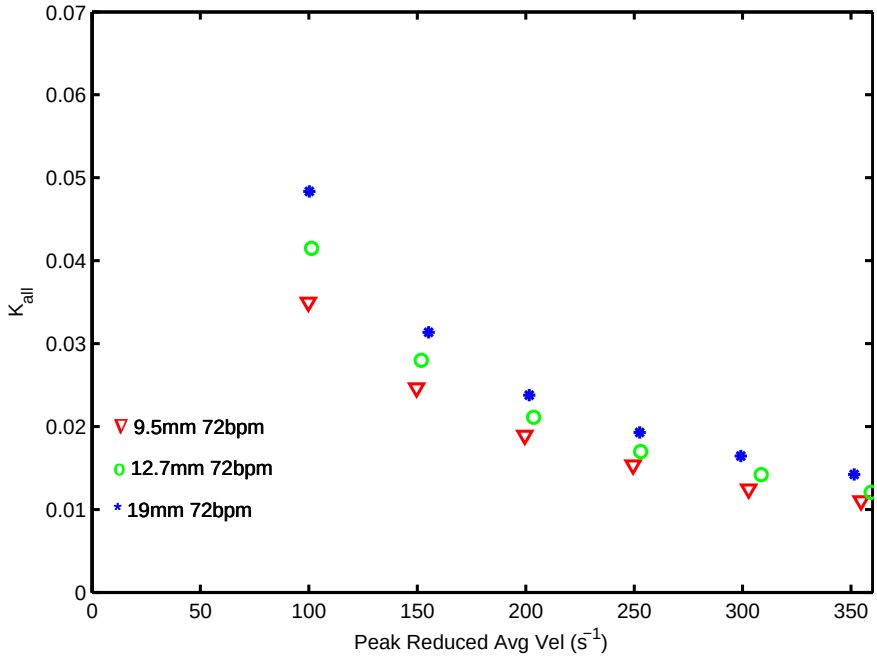

Figure 5.14: Theoretical variation in K with peak reduced average velocity during the entire pulse, h = 40%, T = 19^oC, SR = 35/65, f = 5 kHz

5.3 Variations in Temperature

Figure 5.15 shows the experimental impedance response for pulsatile blood flow for temperatures of 19 ^oC, 28 ^oC and 35 ^oC. Figure 5.16 shows the theoretical results for the same temperatures. An increase in the temperature of stationary blood produces an increase in the energy of the ions and cells within the blood. As a result, current is able to flow more easily through the blood and therefore the impedance will decrease at higher temperatures. The magnitude of the impedance measured at a temperature of 19 ^oC was the largest recorded in both Figure 5.15 (a) and 5.16 (a).

Figure 5.15 (b) shows the experimental percentage change in impedance from the minimum velocity during the pulse (i.e. the closest approximation to stationary blood). Although the absolute change in impedance (in Ohms) was larger for lower temperatures, the percentage change remained constant across the variation in temperature. This trend is not seen in the theoretical results of Figure 5.16 (b). The theoretical results are explained by a reduction in the viscosity of the blood due to an increase in temperature. As a result, the shearing forces that act on the cells to align them are reduced and the net orientation change over the cycle is reduced.

These conflicting results are difficult to explain and may be related to the assumption that the impedance at minimum velocity is equivalent to that of stationary blood. Figure 5.16 (c) shows the relative impedance change from the modelled stationary blood (%). This shows that the maximum relative impedance change from stationary blood is the same for all temperatures which is in agreement with the experimental results. However at low velocities, the relative impedance chance is different.

Published experimental studies have maintained the temperature of the blood at body temperature (de Vries et al., 1995; Liebman and Bagno, 1968;

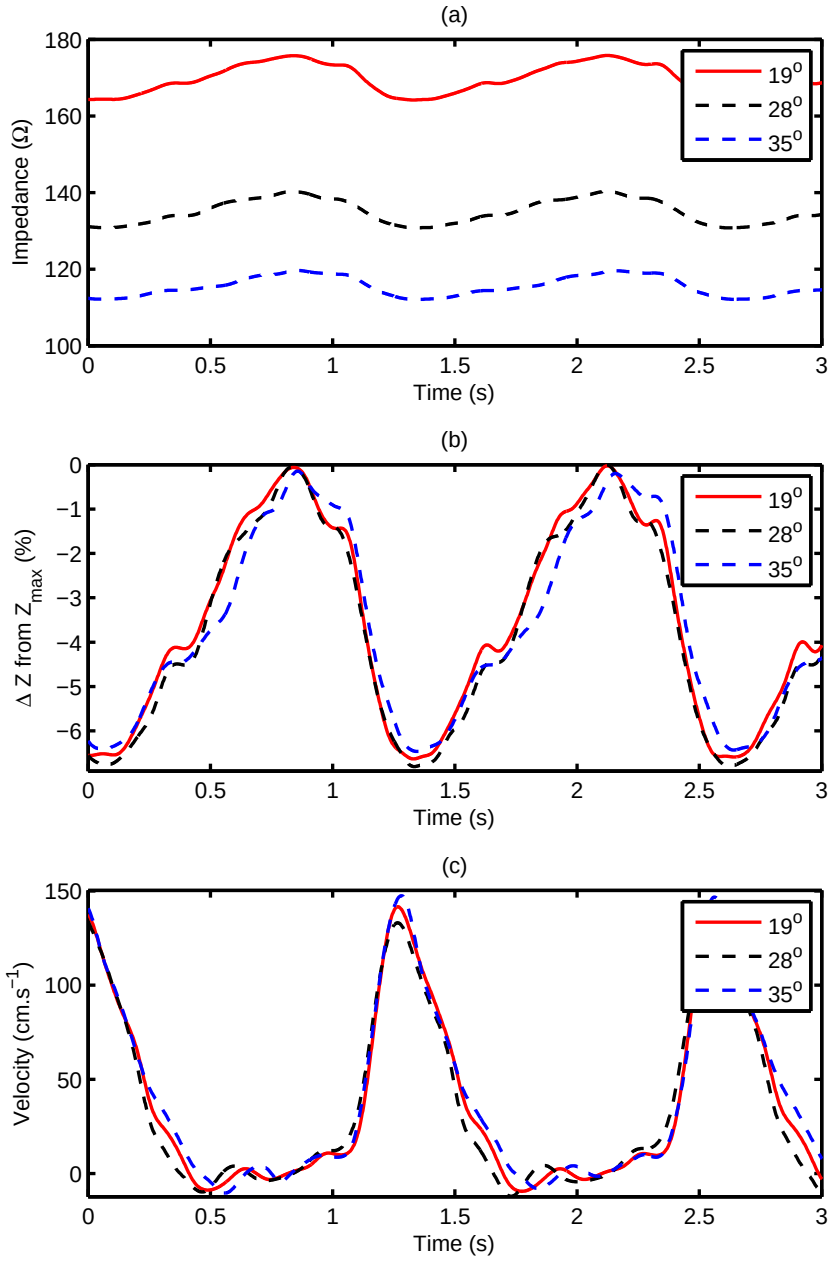

Figure 5.15: The experimental effect of variations in temperature on impedance measured for pulsatile blood, h = 46%, Pulse rate = 48 bpm, diameter = 12.7 mm, T = 19 ^oC, 28 ^oC, 35 ^oC. Compare Figure 5.16

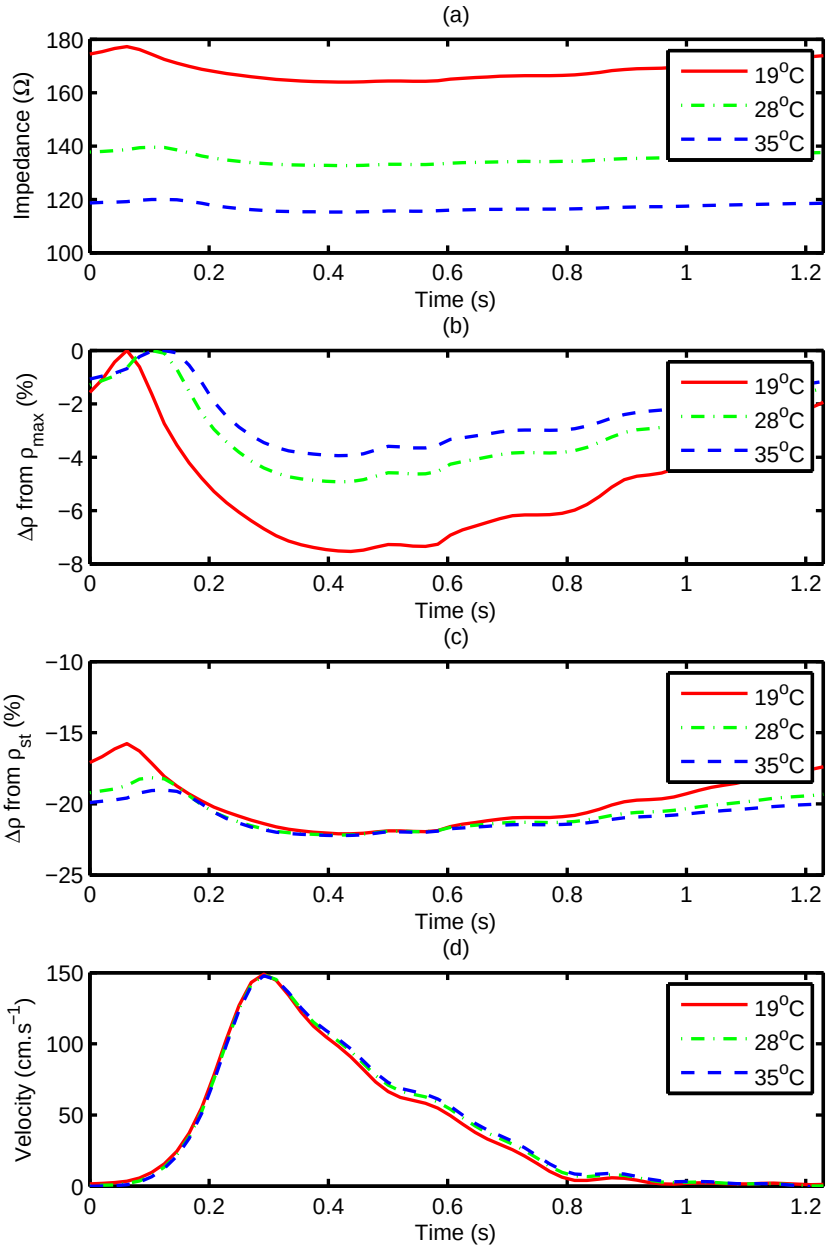

Figure 5.16: The theoretical effect of variations in temperature on impedance of pulsatile blood, h = 46%, Pulse rate = 48 bpm, diameter = 12.7 mm, T = 19 ^oC, 28 ^oC, 35 ^oC. Compare Figure 5.15

Visser, 1992) or room temperature (Sigman et al., 1937; Edgerton, 1974) during experimental measurements. Others do not explicitly state the experimental temperature. Although variations in temperature such as these are not physiologically relevant, studies such as this can help to explain some of the variations in published results.

5.4 Conclusions

Results of theoretical analysis and experimentation are in agreement for variations in haematocrit, radius and temperature. Where differences have been identified, they have been attributed to differences in the assumptions of the theoretical model.

An increase in the haematocrit of blood in both the experimental and theoretical results shows an increase in the flow induced orientation changes as more cells per cross section are present to rotate with the changes in flow. Both the deceleration time constant and the system gain have been shown to decrease as the haematocrit increases. These results show that variations in haematocrit affect the contribution of orientation changes to the impedance and therefore are important consideration in a clinical environment.

For the same spatial average velocity, the impedance change from minimum or stationary flow is largest in tubes with a smaller radius. This is due to the higher shear rates present and therefore larger orientation changes. For the same reduced average velocity however, the impedance change has been shown to be the same for two tubes of different sizes. This is because the reduced average velocity provides an indication of the average shear experienced by the cells. This allows conclusions drawn from previous studies using smaller tubes to be extrapolated to physiologically relevant sizes. To

fully confirm this statement, it would be pertinent to first explore the effect of tube radius under constant blood flow, in addition to investigating multiple radii. These results also suggest that changes in the radius of the blood vessel (such as a narrowing or blockage) will affect the impedance of the flowing blood.

Understanding the effect of temperature on the magnitude of the impedance change of flowing blood is vital in understanding the difference between published results. Experimental and theoretical results show that the relative impedance change due to the orientation of cells is consistent across the temperature range tested and should be comparable across studies performed at different temperatures. This again allows the results from in-vitro studies performed at various temperatures to be relevant to in-vivo studies.

Chapter 6

Theoretical Impedance of Blood Modelled in Stenosed Tubes

6.1 Background

The previous theoretical investigations described in Chapter 4 were limited to rigid straight tubes. However, blood vessels in the body are of varying size, shape and geometry. A specific example of a physiological variation from the straight rigid assumption is vessel and valve stenosis.

Aortic valve stenosis is an abnormal narrowing of the aortic valve which restricts the flow of blood from the heart into the aorta. This can be due to age related calcification of the normal tri-leaflet valve between the left ventricle and the aorta or congenital fusion of the cusps into a bicuspid valve. The heart must generate a larger pressure to accelerate the blood through the smaller area. The result is to alter the velocity pattern of the blood flowing through the aorta. The effects of a stenosis are not confined to the region

of physical constriction. Downstream, the blood is decelerated by frictional forces associated with turbulence (Brown & Smith 2002). The downstream distance from the aortic valve that the flow is disturbed is dependent on the stenosis severity (Otto 2004).

The correlation between increased turbulence and the severity of stenosis was explored for both normal and stenosed valves (Bluestein & Einav 1995). Turbulence was shown to peak during the deceleration phase, though at elevated levels for stenosed valves. The morphology of the velocity time signals also reflected the reduced flow rates through the stenoses. While the acceleration is gradual for the normal aortic valve, it was found to be delayed for the stenosed valve and then increase at a faster rate (Bluestein & Einav 1995).

To understand impedance changes in the presence of aortic valve stenosis, the theoretical impedance of blood flowing through a stenosis has been investigated in this project. The theoretical model presented in Chapter 4 is not adequate in modelling complex geometries such as those found in structures with stenoses. Instead, the Lattice Boltzmann Method (LBM) was used to model the flow of blood through a stenosis.

The LBM is a numerical method which uses a simplification of the molecular dynamics of the motion of individual fluid molecules. Rather than reviewing a large number of individual fluid molecules which can be computationally intensive, the LBM considers a smaller number of fluid particles which represent the average behaviour of a large group of molecules (Buick, Cosgrove, Tonge, Mulholland, Steves & Collins 2003). These particles are restricted to movement between discrete locations within a pre-defined lattice structure. Simple bounce back boundary conditions in which particle motion is reversed when a boundary is reached, can also be implemented locally

which makes the LBM highly suited to problems with complex boundaries such as the presence of stenosis.

Physiological applications of the LBM have included 2D and 3D blood flow, and oscillatory and steady blood flow (Boyd & Buick 2007, Boyd & Buick 2008*a*, Boyd & Buick 2008*b*), blood flow through bifurcations (Artoli, Kandhai, Hoefsloot, Hoekstra & Sloot 2004), flow through stenosis, (Boyd, Buick, Cosgrove & Stansell 2005, Boyd, Buick, Cosgrove & Stansell 2004), flow through elastic vessels (Leitner, Wassertheurer & Breitenecker 2006), turbulence (Peacock, Jones, Tock & Lutz 1998), multiphase flow of blood cells (Dupin, Halliday & Care 2006, Sun & Munn 2005) and blood clotting (Ouared & Chopard 2005).

6.2 Theory and Methods

A summary of the LBM is now presented. A detailed review of the method can be found in reference materials Chen & Doolen (1998), Wolf-Gladrow (2000), Succi (2001) and Sukop & Thorne Jr (2006).

Blood flow has been modelled in the lattice domain in two dimensions (using the D2Q9 framework shown in Figure 6.1) through rigid tubes. Space is divided into discrete nodes on a square lattice on which particles exist at discrete time steps. Motion of particles from each node is restricted to neighbouring nodes in a single time step. In the D2Q9 framework there exists 9 particle velocities (e_i, where $i = 0 - 8$) which are shown in Figure 6.1.

The direction of each velocity can be simply defined as Cartesian coordinates using only 1s and 0s. The lattice unit (lu) is the fundamental measure of length and the time step (ts) is the fundamental measure of time. Therefore the basic speed on the lattice is 1 $lu.ts^{-1}$. The velocity of particles in

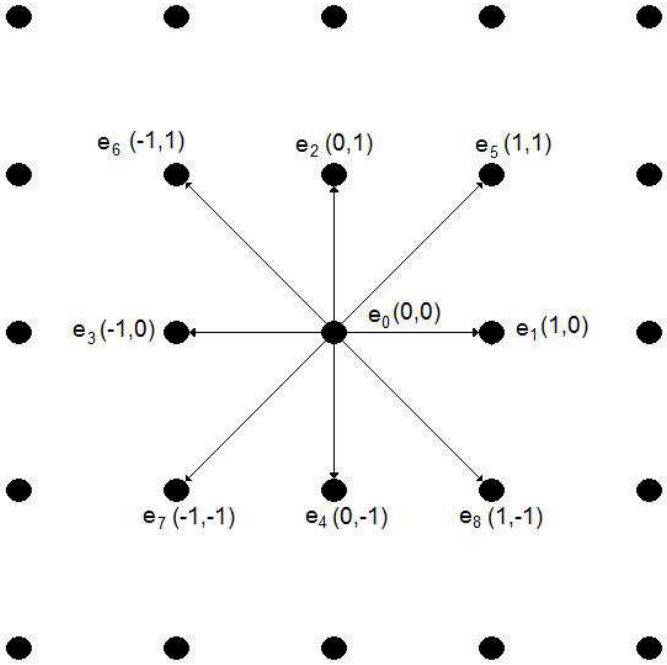

Figure 6.1: D2Q9 lattice and velocities

the directions 1 to 4 is 1 $lu.ts^{-1}$, while the velocity in the directions 5 to 8 is $\sqrt{2}\ lu.ts^{-1}$.

Each node on the lattice has nine particle distribution functions (f_i) which describes the statistically expected number of molecules travelling at each velocity. Assuming the mass of each particle is 1, the macroscopic fluid density and velocity can be calculated directly from the distribution function at each node using Equations 6.1 and 6.2.

$$\rho = \sum_{i=0}^{8} f_i \tag{6.1}$$

$$\mathbf{u} = \frac{1}{\rho} \sum_{i=0}^{1} f_i \mathbf{e}_i \tag{6.2}$$

During each time step, particles propagate to the neighbouring lattice

site along their direction of motion. Particle collision then occurs in which particles scatter towards equilibrium according to simple kinetic rules that conserve mass and momentum. The propagated distribution function is calculated at each time step using Equation 6.3 and Equation 6.4 where Ω_i is the collision operator. The BGK (Bhatnagar-Gross-Krook) approximation is the simplest method of collision.

$$f_i(\mathbf{x} + \mathbf{e}_i\Delta t, t + \Delta t) = f_i(\mathbf{x}, t) - \Omega_i(\mathbf{x}, t) \tag{6.3}$$

$$\Omega_i = \frac{-1}{\tau}\left[f_i(\mathbf{x}, t) - f_i^{eq}(\mathbf{x}, t)\right] \tag{6.4}$$

The equilibrium distribution (f_i^{eq}) can be calculated using Equation 6.5, where w_i are the weights of the particles: 4/9 for i = 0, 1/9 for i = 1 to 4 and 1/36 for i = 5 to 8.

$$f_i^{eq}(\mathbf{x}) = w_i\rho(\mathbf{x})\left[1 + 3\mathbf{e}_i \cdot \mathbf{u} + \frac{9}{2}(\mathbf{e}_i \cdot \mathbf{u})^2 - \frac{3}{2}\mathbf{u}^2\right] \tag{6.5}$$

The relaxation time of the particles, τ, is derived from the kinematic lattice viscosity using Equation 6.6.

$$\nu = \frac{2\tau - 1}{6} \tag{6.6}$$

To determine the lattice viscosity, two dimensionless numbers were required. These are the Reynolds number (in terms of boundary layer thickness, ς) and the Womersley number shown in Equations 6.7 and 6.8. This version of the Reynolds number is used for the oscillatory cs

$$Re_\varsigma = \frac{U_0}{\eta}\sqrt{\frac{T\eta}{\pi}} \tag{6.7}$$

$$\alpha_w = \frac{L}{2}\sqrt{\frac{2\pi}{T\nu}} \tag{6.8}$$

Where U_0 is the average velocity, T is the period of the pulse, ν is the absolute viscosity, η is the kinematics viscosity and L the width of the tube. The instantaneous spatial average velocity of a periodic cardiac blood flow pulse (u_{in}) was used to drive the flow. Given the input velocity in physical units, Re_ς and α_w can be calculated from the physical velocity, period, viscosity and diameter of the tube. The equivalent lattice parameters can then be calculated in lattice units. To do this, the average lattice velocity and resolution of the lattice nodes are chosen and ν_{lat} and T_{lat} are calculated.

In order to ensure that no slip boundary conditions exist (velocity must equal zero at the walls), simple half-way bounce back conditions are implemented. Each node is classified as a fluid node or a boundary node and any particle propagating to boundary nodes simply reverse the velocity ready to re-enter the fluid on the next time step. This is shown in Figure 6.2

To drive the flow through the tube, velocity boundaries were implemented at the entry and exit of the tube. At each time step, the particle distributions (f_i) along the entry and exit nodes were assigned the equilibrium distributions (f_i^{eq}) corresponding to the desired values of input density and velocity. In the case of oscillatory flow, this will change with each time step. The length of the tube was required to be long to avoid entry length effects, and the velocity was sampled at half the tube length.

To convert physical units to lattice units and vice-versa, the conversion factors for length (L_0), time (T_0) and mass (M_0) can be calculated from the known relationship between physical and lattice parameters. These are shown in Equation 6.9. Given the physical input velocity time signal, the driving lattice velocity can be calculated by multiplying by L_0 and dividing

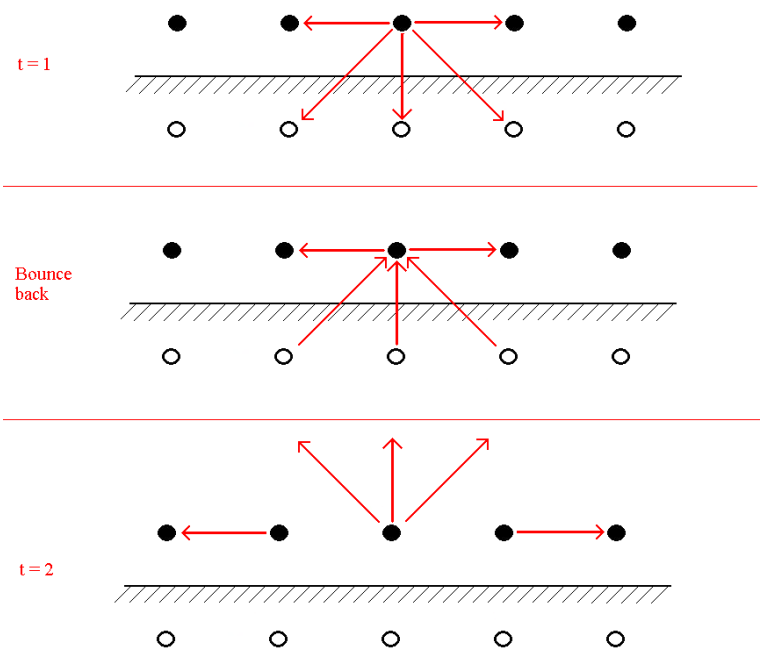

Figure 6.2: Half way bounce back technique

by T_0.

$$
\begin{aligned}
L_0 &= \frac{L_{lat}}{L_{phys}} \\
M_0 &= L_0^3 \frac{\rho_{lat}}{\rho_{phys}} \\
T_0 &= L_0^2 \frac{\nu_{phys}}{\nu_{lat}}
\end{aligned}
\tag{6.9}
$$

This is a numerical method and must be iterated for a number of time steps until the desired accuracy is reached. A flow chart of the algorithm implemented is shown in Figure 6.3.

The impedance of the blood is then calculated from the shear rate profiles of the LBM flow model by intergrating over the cross sectional area of the tube, to convert to meaningful 3D results.

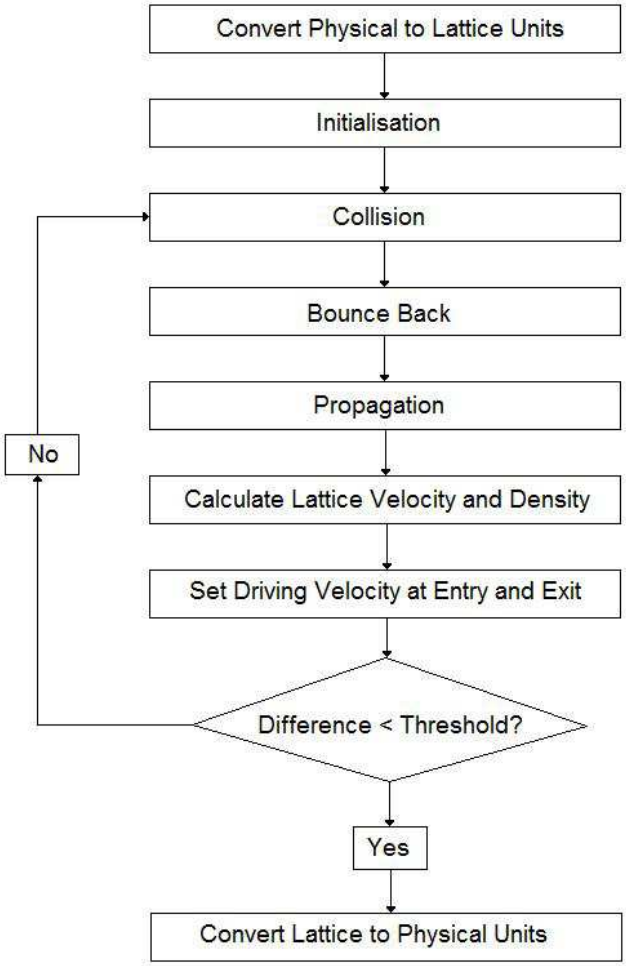

Figure 6.3: Flow chart of LBM algorithm

6.3 Accuracy of the LBM Model

The global error of the model is calculated by Equation 6.10 where the subscript a refers to the analytical solution and the subscript b refers to the simulated value and L is the number of nodes across the width of the tube.

$$\varepsilon = \frac{1}{L}\sqrt{\sum_{x=1}^{L} u_a(x)^2 - u_b(x)^2} \tag{6.10}$$

The accuracy of the model is verified during steady flow conditions. The LBM is a second order accurate model. That is, if the number of nodes across the lattice width was to double, the global error should reduce by a factor of four. When the error is plotted against the lattice width on a log-log scale, for second order accuracy, the slope of the line should be close to -2. The global error is plotted against the lattice width in Figure 6.4. The slope of this line is -1.7 which shows that the model implemented here achieves close to second order accuracy. the deviation from -2 is expected to be due to compression and the simplicity of the model.

Given the accuracy of the LBM flow model, the impedance of pulsatile blood through rigid straight tubes was calculated. These results were com-

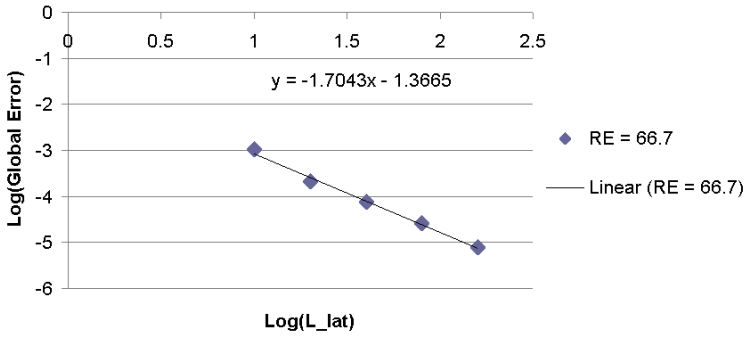

Figure 6.4: Second order accuracy of the LBM for steady flow

Parameter	Description	Physical Units	Lattice Units
LX	Length of Tube	0.5 m	5000 lu
LY	Width of Tube	0.01 m	100 lu
T	Period of Pulse	0.77 s	456274 ts
ν	Kinetic Viscosity	$4.01e^{-6}$ P	$6.76e^{-4}$ $mu.lu^{-1}.ts^{-1}$
ρ	Density of Fluid	1055 $kg.m^{-3}$	1 $mu.lu^{-3}$
u_{max}	Maximum Velocity	1.18 $m.s^{-1}$	0.03 $lu.ts^{-1}$

Table 6.1: Modelled parameters in physical and lattice units

Parameter	Description	Value
ϵ	Threshold	$1e^{-6}$
Re_{ς}	Reynold Number	293
α_w	Womersley Number	7.14
τ	Relaxation Parameter	0.502

Table 6.2: Dimensionless parameters used for modelling

pared to impedance results from the analytical theoretical model described in Chapter 4. The parameters used in both models are summarised in Tables 6.1 and 6.2.

The spatial average velocity calculated from the analytical model (of Chapter 4) was used to drive the flow at each node across the entrance and exit of the tube. The analytical and LBM shear rate profiles (measured at half the length of the tube) at a number of time steps during the pulse period are shown in Figure 6.5. This figure shows that the shear profile determined using the LBM agrees well with the analytically calculated shear profile.

The impedance of the flowing blood is then calculated using the shear profile of the LBM and the results are shown in Figure 6.6. The analytical shear profile is also shown. The velocity modelled using the LBM and analytical methods are shown in the lower graph and the impedance calculated using both models is shown in the upper graph. These results show that the two theoretical models provide very similar results, despite that the analytical model uses a 3D approach while the LBM model uses a 2D approach. The

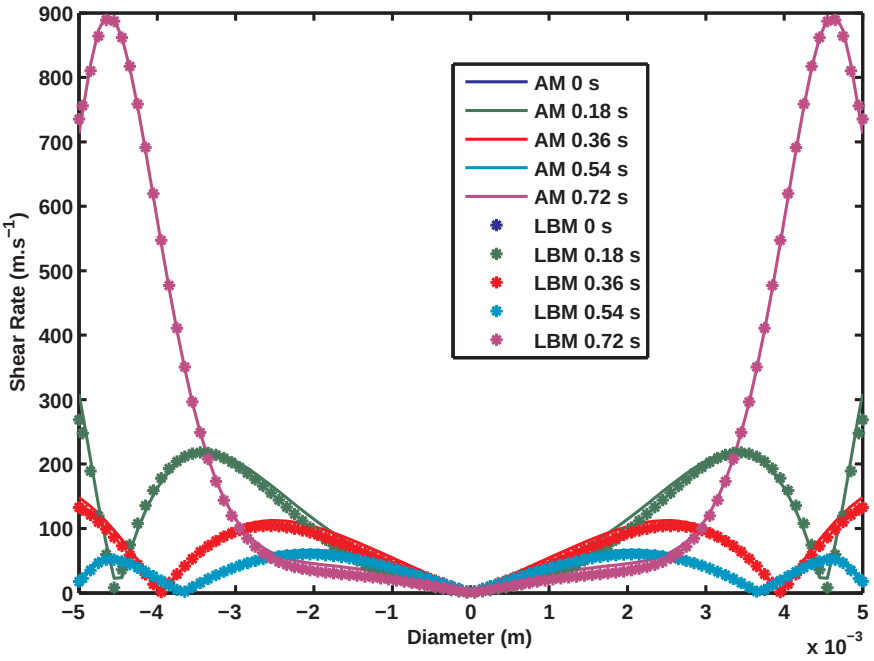

Figure 6.5: Shear rate profile at a number of time stamps calculated using analytical and LBM techniques

correlation at zero time delay between the two impedance signals is 0.973. Thus the 2D LBM model provides an adequate balance between simplicity and accuracy for impedance modelling.

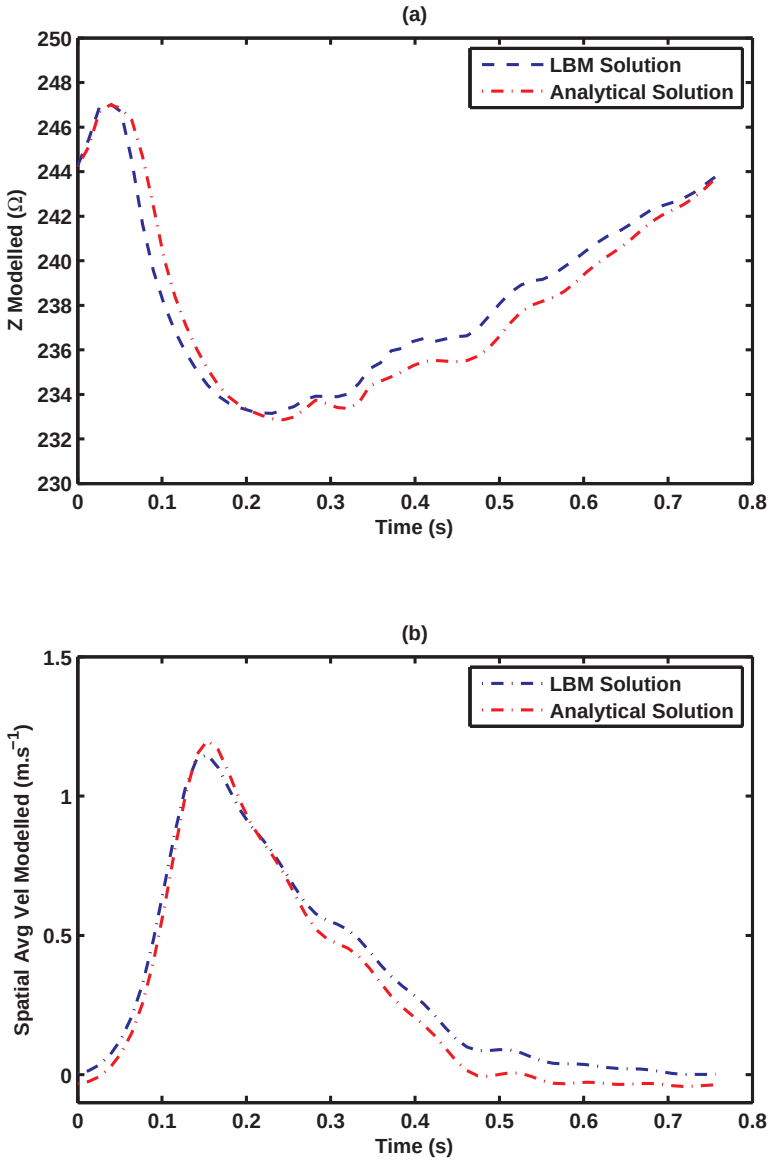

Figure 6.6: Impedance of pulsatile blood shown in (b) modelled from the velocity shown in (a) using LBM (described in this chapter) and Analytical techniques (described in Chapter 4)

6.4 Results and Analysis

The impedance of blood flowing through a stenosis was modelled using the 2D LBM method. The stenosis geometry is shown in Figure 6.7 where S is the degree of the stenosis, i.e. 20% means that 20% of the diameter will be blocked by the stenosis. In this initial study, very basic stenosis geometry was used which consisted of half way bounce back boundaries and a rectangular stenosis. More physiologically relevant geometries in addition to a 3D model should be investigated in the future.

The degree of stenosis was increased from 20% to 80% and the blood velocity profiles through each stenosis was calculated. The modelled flow parameters can be seen in Table 6.3. Due to computational limitations and the presence of instability at high velocities, the blood flow was modelled through a 5 mm tube with a maximum pulse velocity of $20cm.s^{-1}$. Previous results (Section 5.2.1) suggest that results from a smaller diameter tube can be considered indicative of those in a tube with larger diameter.

The flow through the stenosis was driven by the velocity time signal shown in Figure 6.8.

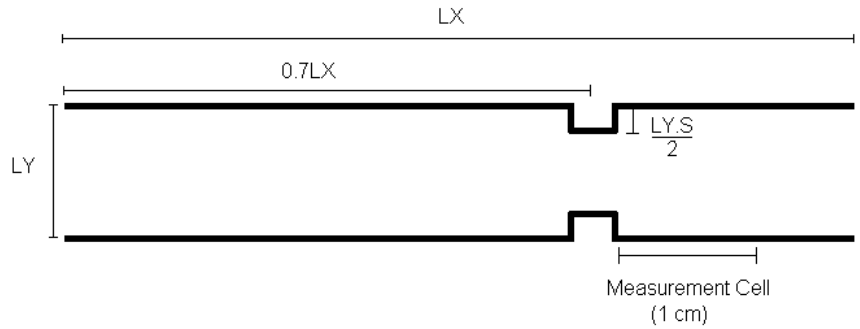

Figure 6.7: Stenosis Geometry

Parameter	Description	Value
H	Haematocrit of blood	0.45
ρ	Density of blood	1.055 $g.ml^{-1}$
ν_{bl}	Viscosity of blood	$4.00e^{-6}$ Poise
	Membrane shear modulus of cell	0.000015 $N.m^{-1}$
$2b_0$	Major axis length of RBC	8 μm
$\frac{a_0}{b_0}$	Axis ratio (minor/major) of RBC	0.38
N	Number of harmonics	10
f	Frequency of heartbeat	1.4 Hz (84 bpm)
R	Radius of tube	2.5 mm

Table 6.3: LBM Modelling Parameters

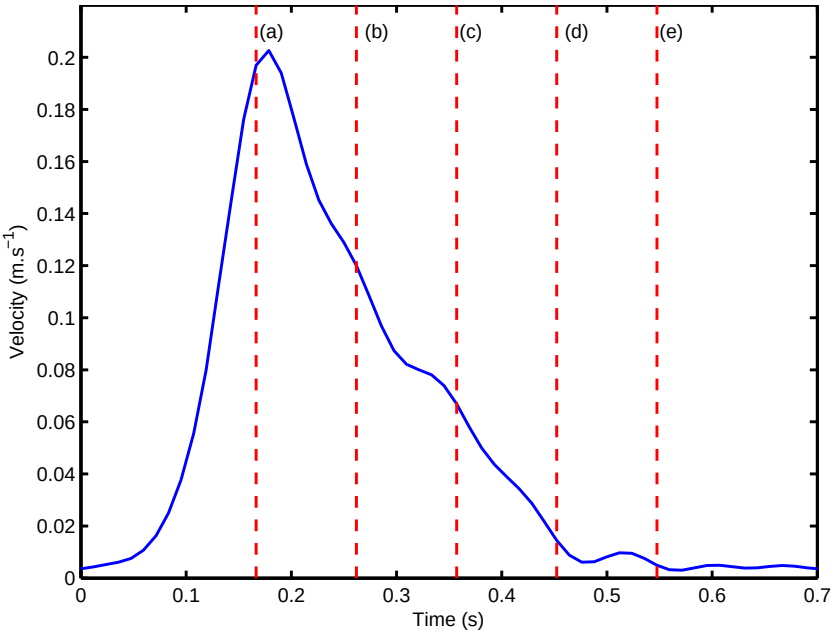

Figure 6.8: Driving velocity time signal (a) t = 0.17 s, (b) t = 0.27 s, (c) t = 0.36 s, (d) t = 0.46 s, (e) t = 0.55 s

The resulting LBM velocity profile at the exit of the stenosis is shown in Figure 6.9 by the open circles. The velocity profile through an equivalent straight tube calculated using the analytical model is also shown by the solid lines in this Figure. The velocity profile is shown for the time points during the cardiac cycle indicated by the dashed lines in Figure 6.8. The degree of stenosis was varied from 20% to 80%.

The effect of the stenosis is to disturb the laminar flow. As the degree of stenosis increases, the peak velocity over the profile also increases. Due to the conservation of mass, the volume flow remains constant and therefore as the cross sectional area decreases, the maximum velocity through the stenosis will increase. The peak velocity will remain high for a distance downstream of the stenosis dependent on the degree of the stenosis. This results in an increase in the shear rate experienced by the cells and therefore larger shear forces on the cells inducing alignment.

A simplified representation of the resulting jet of blood flow downstream of a stenosis is shown in Figure 6.10 to aid in explanation. The flow jet will reach a maximum velocity at a distance down stream of the stenosis (called the vena contracta) which coincides with the minimal cross sectional area of the jet (Brown & Smith 2002). In the post stenotic region, near the walls of the tube, slow moving recirculation of the blood will occur. Turbulence will result in severe cases as separation of flow occurs. As the degree of stenosis increases, the length of this region also increases. In this region, the cells will be oriented randomly.

The impedance response over one cardiac cycle for the varying degrees of stenosis is shown in Figure 6.11. To calculate the impedance, the velocity and shear rate profile were calculated at 1 mm intervals from the exit of the stenosis for a total of 10 mm. The impedance of the blood was calculated

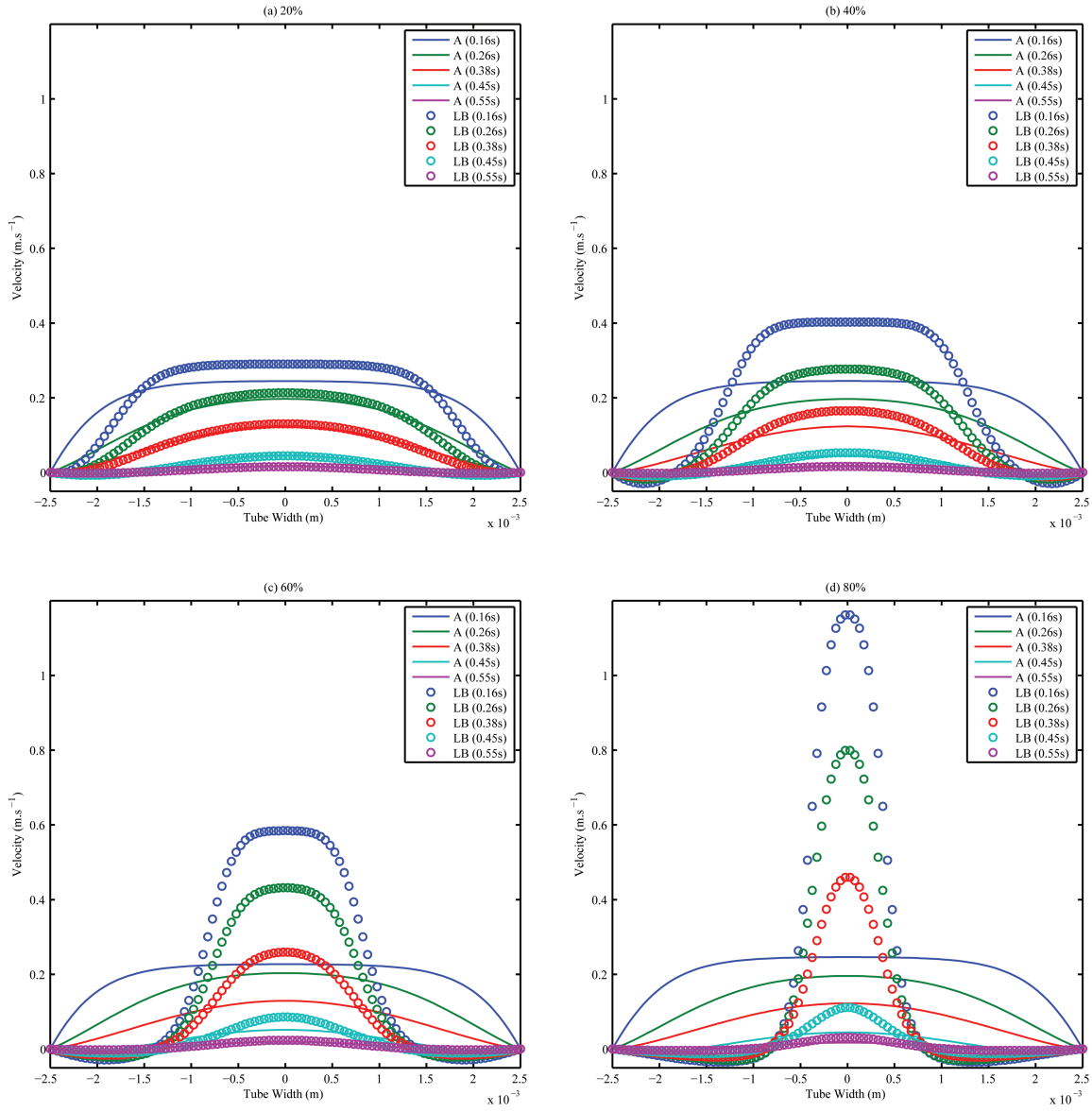

Figure 6.9: Velocity profiles at the exit of a stenosis at the times shown in 6.8: (a) t = 0.17 s, (b) t = 0.27 s, (c) t = 0.36 s, (d) t = 0.46 s, (e) t = 0.55 s

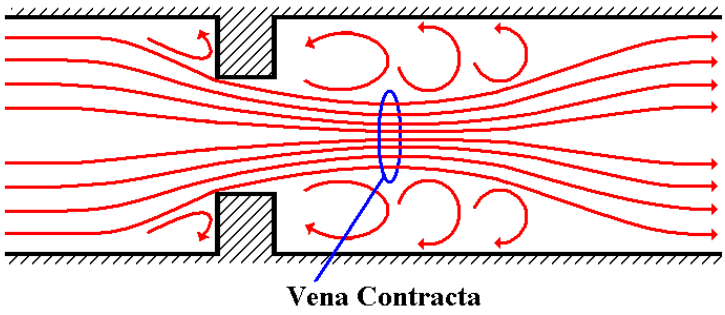

Figure 6.10: Simplified blood flow exiting a stenosis

for each 1 mm cylinder from the shear rate profile and summed to determine the impedance of a 10 mm cylinder directly downstream of the stenosis.

The impedance calculated for all levels of stenosis responds to inflections in the input velocity during deceleration. These inflections are larger in the 20% stenosis and decrease as the degree of stenosis increases. This agrees with the experimental results in Chapter 3 which show that fluctuations in impedance occur primarily at low velocities. As the degree of stenosis increases, the peak velocity through the orifice also increases and the number of fluctuations present in the measured impedance becomes minimal. The magnitude of the peak to peak impedance is not affected by the degree of stenosis.

During acceleration the relationship between the blood velocity and impedance was found to be linear during acceleration (r = -0.97 to -0.99). A linear relationship during acceleration was also found experimentally and theoretically for flow through straight rigid tubes in Chapters 3 and 4. Thus the theoretically modelled results for flow through a stenosis is consistent with the results for flow through straight tubes. During deceleration however, the relationship was not linear in straight tubes, and this is also confirmed in the case of flow through a stenosis.

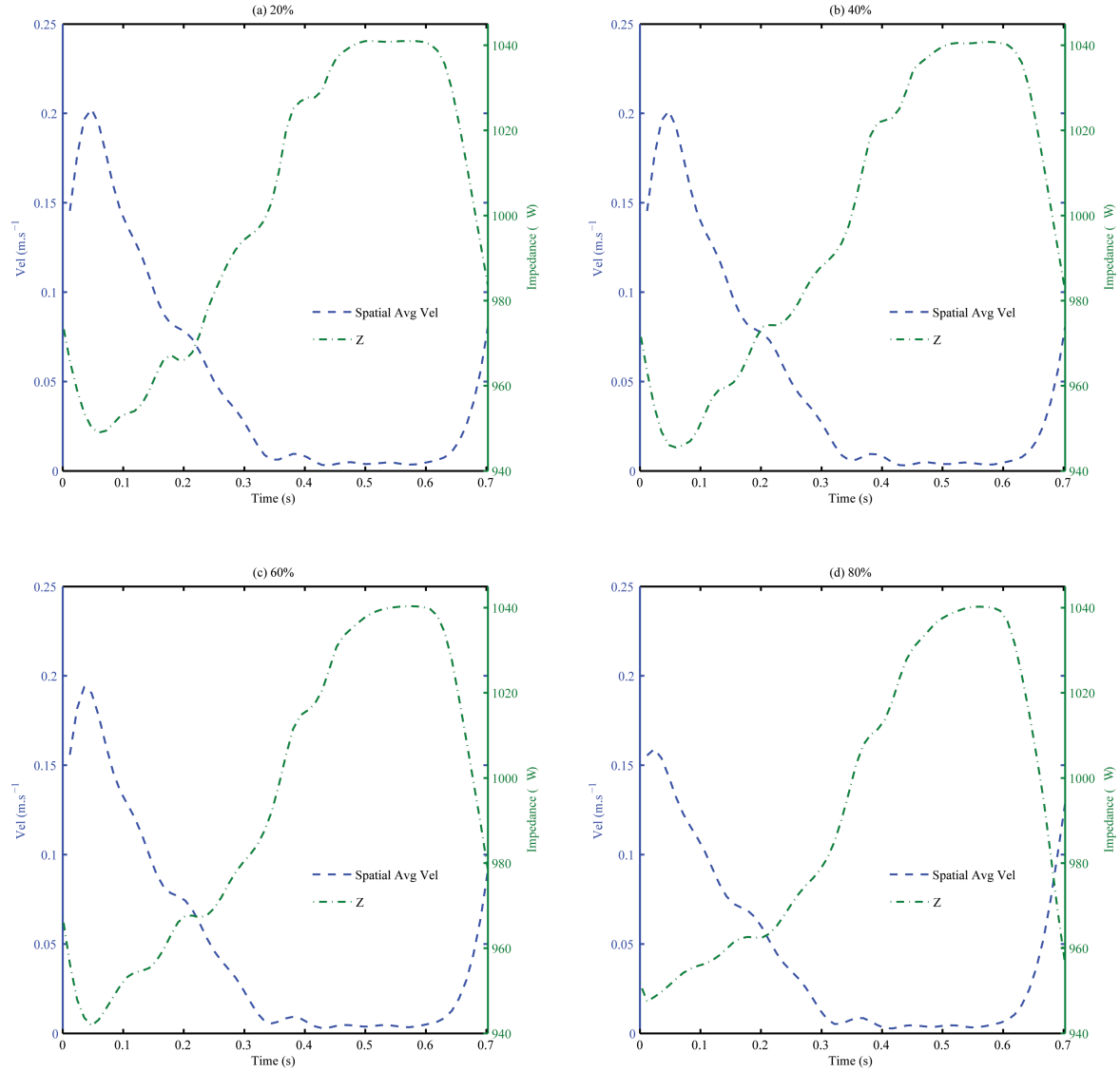

Figure 6.11: Impedance calculated in a 10 mm cylinder directly downstream of a stenosis (a) 20%, (b) 40%, (c) 60%, (d) 80%

As the degree of stenosis increases, the impedance response shows a delay in returning to the maximum value despite the return of the blood flow to zero during deceleration. This suggests a change in the deceleration time constant with the degree of stenosis. The characteristic time delay during the deceleration phase (calculated according to methods presented in Section 3.3.4) was calculated for each degree of stenosis. The time decay constant is plotted against the degree of stenosis in Figure 6.12. As the degree of stenosis increases, the time constant also increases. This agrees with the shape of the results shown in Figure 6.11 in which the time for the impedance to return to the peak value increases with an increase in the severity of the stenosis. This is thought to be due to the decreasing velocity jet area and increasing recirculation area as the level of stenosis increases. The central laminae have a high velocity and therefore a larger percentage of the cross sectional area is in the recirculation state. This means that the transfer of high velocity from the central lamina to the lamina at the wall of the tube will take longer due to the larger distance. Therefore, red blood cells will stay in alignment longer and the time of decay for impedance will increase.

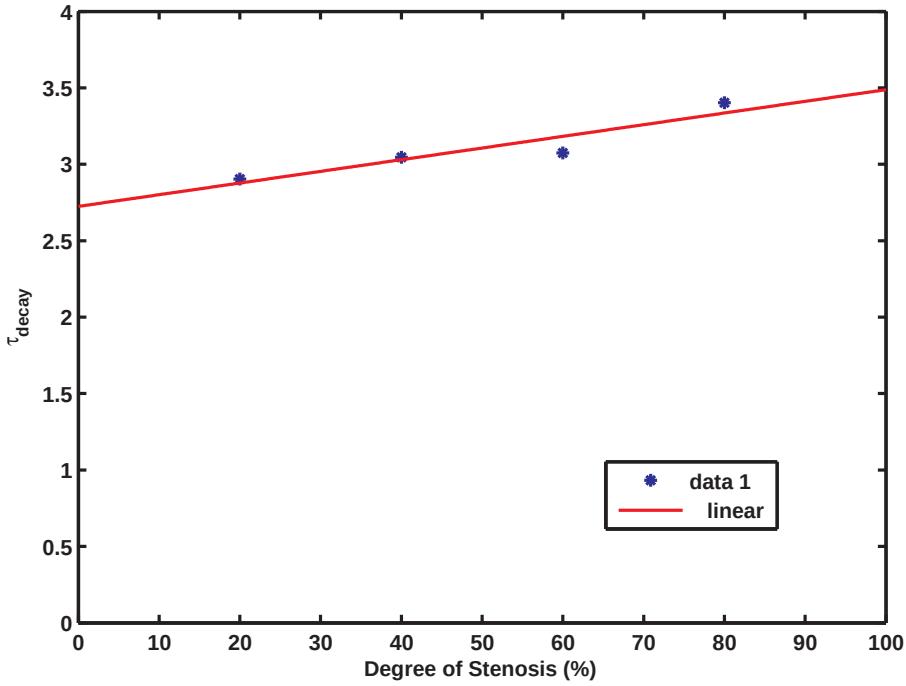

Figure 6.12: Decay time constant for varying degrees of stenosis

6.5 Conclusions

A theoretical model of the impedance of blood flowing through a rigid stenosis has been developed. This has not previously been investigated in published literature. The pulsatile flow of the blood was calculated using the 2D LBM. The LBM of blood flow was based on simplified kinetic equations and discrete particle interactions contained within a lattice structure. Using the D2Q9 framework and half way bounce back techniques, the LBM flow model was verified in straight tubes by comparison to the analytical 3D model and applied to flow through a stenosis. The shear stress profile was then used to determine the impedance of the blood using techniques discussed in Chapter 4. The impedance response of blood over one cardiac cycle exiting a stenosis was theoretically calculated for 1cm downstream of the stenosis for degrees of stenosis from 20% to 80%.

The velocity and shear profile exiting a stenosis was shown to be directly influenced by the degree of the stenosis and this in turn influenced the calculated impedance. The inflections in the calculated impedance were larger in the smaller degrees of stenosis and this agrees with experimental results recorded in Chapter 3.

As the degree of the stenosis was increased, the theoretically calculated impedance showed a delay in the return to the initial value. This was characterised by a decay time constant for the impedance to return to the maximum value. The decay time constant increased with the degree of stenosis. This was thought to be due to the theoretically modelled increase in the volume of blood undergoing downstream recirculation that occurred with an increase in the degree of stenosis. The variation of the decay time constant with the degree of stenosis was considered important and investigated clinically in the next chapter.

Chapter 7

Clinical Investigation using Impedance Cardiography

7.1 Background

Applications of impedance cardiography for heart failure assessment include diagnosis of haemodynamics and systolic function as well as patient monitoring during treatment and recovery (Yancy & Abraham 2003). Variations in the morphology of the impedance cardiography waveform have been suggested as a possible diagnostic tool in the assessment of abnormal cardiac function (Bour & Kellett 2008), such as aortic stenosis described in Chapter 6.

An example of an ICG waveform is shown in Figure 7.1. The A wave follows atrial contraction and can be abnormal in atrial and ventricular arrhythmias and abnormally increases when there is diastolic dysfunction. The S wave reflects ventricular contractility. The magnitude is indicative of the magnitude of cardiac output. In the presence of regurgitation in which the blood flows back towards the heart in the case of faulty valves, notching can

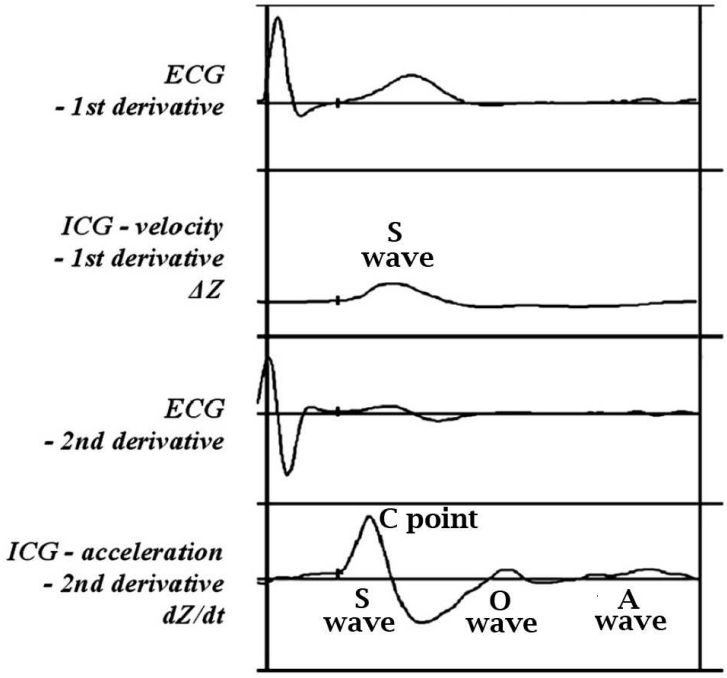

Figure 7.1: Example ICG and ECG waveform showing the S and O wave (Bour & Kellett 2008)

occur on the upstroke to the C point and ventricular dyssynchrony (between right and left ventricle) gives rise to an m shaped S wave. The O wave is associated with mitral valve opening and is abnormally enlarged in heart failure due to increased venous return (Bour & Kellett 2008).

By observing changes in the shape of the $\frac{dZ}{dt}$ waveform during postural change from sitting to supine, impedance cardiography has been reported to assess the response of left ventricular systolic function to increased end diastolic volume (DeMarzo et al. 2005, DeMarzo & Calvin 2007). The surge of blood during systole results in the peak impedance wave. The shape (height and area) of this wave has been shown to have diagnostic properties. Heart disorders that can cause a non-triangular wave include mitral valve regurgitation, aortic valve stenosis and ventricular regional wall motion abnormalities

(DeMarzo et al. 2007).

These pilot studies addressed the potential for impedance cardiography techniques to be used for the assessment of cardiac disease such as aortic stenosis. Aortic valve stenosis (AS) accounts for 5% of diagnosed congenital heart disease. The prevalence of AS in an aging poulation increases. Calcific aortic stenosis affects approximately 3% of the population over 75 years of age (Lindroos, Kupari, Heikkila & Tilvis 1993). It can cause progressive damage to the heart and leads to heart failure.

Presently, echocardiography is the primary diagnostic method used to detect and quantify aortic valve stenosis. The valve area and mean pressure gradient are used in the assessment of the disease as a smaller orifice area gives rise to a higher mean pressure gradient. Echocardiography techniques are expensive and require qualified technicians to perform the assessment. Impedance cardiography however, is relatively inexpensive and measurement procedures are simple, requiring minimal training and hence offers the potential to provide an alternative objective diagnostic technique.

The implications of velocity induced resistivity changes of blood for impedance cardiography are unknown. The erythrocytes are oriented randomly in response to reduced shear rates at the end of diastole. This is the condition of highest resistivity. During the rapid ejection phase of early systole, erythrocytes will align parallel to the direction of flow. This is the condition of lowest resistivity (Bernstein & Lemmens 2007). This suggests that the effect of red blood cell orientation changes during flow will influence an ICG.

The modelling of the impedance of blood flowing through a stenosis provided information on the likely effect of a narrowing of the aortic valve. A pilot clinical trial has been conducted to determine the applicability of these findings to in-vivo studies. The ethics approval for this study can be found

in the Appendix A.1.

7.2 Protocol

The pilot clinical trial was conducted at Queensland Cardiovascular Group (QCG), St Andrew's Place Cardiology in Spring Hill. The aim of this study was to investigate the hypothesis that non invasive bioimpedance measurements of the thorax may be used to monitor and detect aortic stenosis. This hypothesis was explored through a small observational clinical trial (simply to provide evidence for proof of concept) in which two sample populations were examined. Both study groups were recruited from the outpatient population at QCG. All participants had been scheduled for a routine echocardiogram. Clinical assessment of the presence of aortic stenosis using current clinical practice (echocardiography) was performed and the thoracic impedance of each subject was measured.

The first population group had structurally normal hearts. The data collected on this group provided a reference of normal heart operation and blood flow for both the Doppler echocardiography and impedance measurement. This allowed the normal relationship between thoracic impedance and blood flow to be assessed.

The second population group consisted of volunteers clinically diagnosed with moderate to severe aortic stenosis. The primary characteristic of this population group is a narrowing of the aorta opening which results in abnormal aortic flow through a constricted aorta. This provided data for both Doppler echocardiography and thoracic impedance characteristic of this disease state. Thus a relationship that varies from normal was assessed using this information.

All subjects included in this study adhered to the selection criteria summarised below.

Inclusion Criteria

All subjects were required to:

- Be aged between 18-85 years
- Understand the proposed study and be willing and fully able to comply with the study procedures
- Be a willing participant and be capable of giving informed written consent for entry into the study

Subjects in Group 1 must have a clinically diagnosed structurally normal heart. Subjects in Group 2 must have been clinically diagnosed with aortic stenosis.

Exclusion Criteria

All subjects must NOT:

- Have an implantable device such as a pacemaker or ICD
- Have a metallic surgical implant (e.g. total hip replacement) not including small implants such as sternal wires or surgical staples
- Be pregnant or currently breastfeeding

The electrical impedance of the thorax was recorded using the Imp SFB7. Cardiac parameters including aortic blood velocity was recorde using Doppler echocardiography. This data was then processed in order to correlate changes in aortic blood velocity with thoracic impedance changes in subjects with

both normal and abnormal blood flow due to the presence of aortic stenosis. This preliminary investigation aimed to demonstrate the potential for diagnosis of aortic stenosis using bioimpedance techniques. The study was deemed low risk as participants were scheduled for an echo regardless of the study in which case, only the ICG was an additional commitment.

The age, gender, weight, height, medical/surgery history and medications were recorded prior to measurement. A qualified sonographer performed an echocardiogram on each subject prior to the impedance cardiography measurement. The impedance of the chest was measured for 20 seconds using the modified Imp SFB7 attached via alligator clips to four ECG electrodes placed at standard placement sites on the chest shown in Figure 7.2.

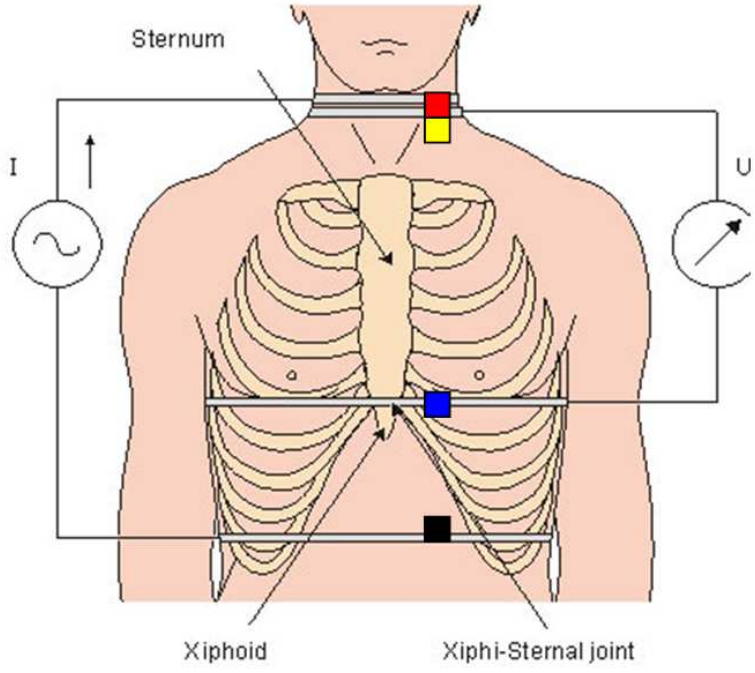

Figure 7.2: Electrode configuration for impedance cardiography measurements (Malmivuo & Plonsey 1995)

7.3 Results and Discussion

A total of 12 subjects were recruited for this pilot trial. Of those, four recorded data with an inadequate signal to noise ratio due to bad electrode connection. The facility to conduct a quick analysis of data and repeat if needed was not available in the clinical setting and so only the data from eight remaining subjects were analysed. The test (AS) population consisted of three females and one male ranging in age from 62 to 84 years. The control population consisted of one female and three males ranging from 25 to 41 years. Although not age nor gender matched, this was not considered essential for this proof of concept trial. The echo results are shown in Table 7.1 where a C prefix indicates a control subject and a T prefix indicates a test subject. V_{max} is the maximum blood velocity through the aortic valve, D_{LVOT} is the diameter of the left ventricular outflow tract and AVA is the opening area of the aortic valve.

The mean pressure gradient (Mean Grad) is the standard parameter used to assess the degree of stenosis. When the aortic valve is stenosed, the pressure in the left ventricle must increase in order to eject blood through the narrowing. The mean gradient reflects the pressure difference between the left ventricle and the aorta and is increased in AS patients. In order for the volume flow through the reduced AVA to remain constant, the velocity must increase. A higher V_{max} indicates a smaller AVA. The (D_{LVOT}) is also recorded using echocardiography techniques. This gives an indication of the size of the area of the outflow tract from the ventricle immediately prior to passing through the aortic valve. It can be considered similar to the diameter of the tube prior to the stenosis in the modelled case in Chapter 6.

An example of an ICG measured for both a control and test subject during the trial is shown in Figures 7.3 and 7.4 respectively. The raw impedance,

Subject	Gender	AS Grade	Mean Grad	V_{max} $m.s^{-1}$	D_{LVOT} cm	AVA cm^2
C02	Male	Not Present	4	1.3	2.1	2.36
C03	Male	Not Present	3	1.2	2.2	3.2
C04	Male	Not Present	2	0.9	2.1	3
C05	Female	Not Present	3	1.2	1.9	2.43
T01	Female	Moderate	45	4.3	2	0.92
T02	Female	Mild	29	3.4	2.2	0.97
T03	Female	Moderate	48	4.6	2	0.85
T05	Male	Moderate	45	4.3	2.1	0.86

Table 7.1: Echocardiography Results

Z, the ICG signal, $\frac{dZ}{dt}$, and the ECG are shown. These figures show typical variations in thoracic impedance. These signals have been band pass filtered to remove low frequency breathing effects and high frequency noise.

Visual inspection of the example ICG results for a control and test subject suggest small differences in the shape of the waveforms. The data recorded from the test subject shows more inflections during the cycle than the control data. The impedance, Z, of the test subject also appears to remain at a high impedance for a longer duration of the cycle (during what is assumed to be the period of decelerating flow). This is a similar characteristic to that modelled theoretically in Figure 6.11 in Chapter 6 in which the time to return to the peak impedance increased with an increase in the degree of stenosis.

The time decay constant modelled theoretically as a function of the degree of stenosis in Chapter 6, shows that as the degree of stenosis increases, the time decay constant also increases. The delay in the return to the initial impedance of the test subject in Figure 7.4 as compared to the control subject in 7.3 suggests a possible variation in the time decay constant of impedance (note Z, not $\frac{dZ}{dt}$ as used for stroke volume) between healthy and aortic valve stenosis subjects. The decay time constant of deceleration was calculated from the impedance signal measured on each subject. The time constant for

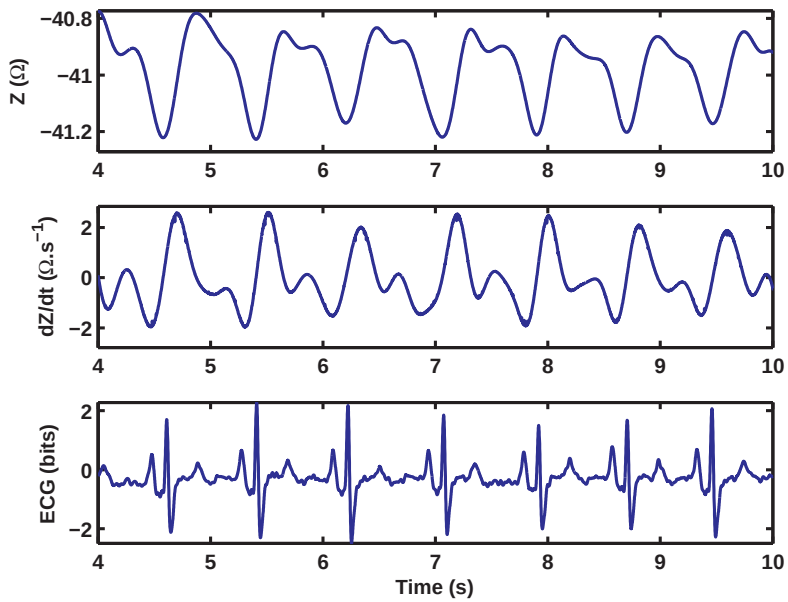

Figure 7.3: Example impedance cardiogram of control subject C02

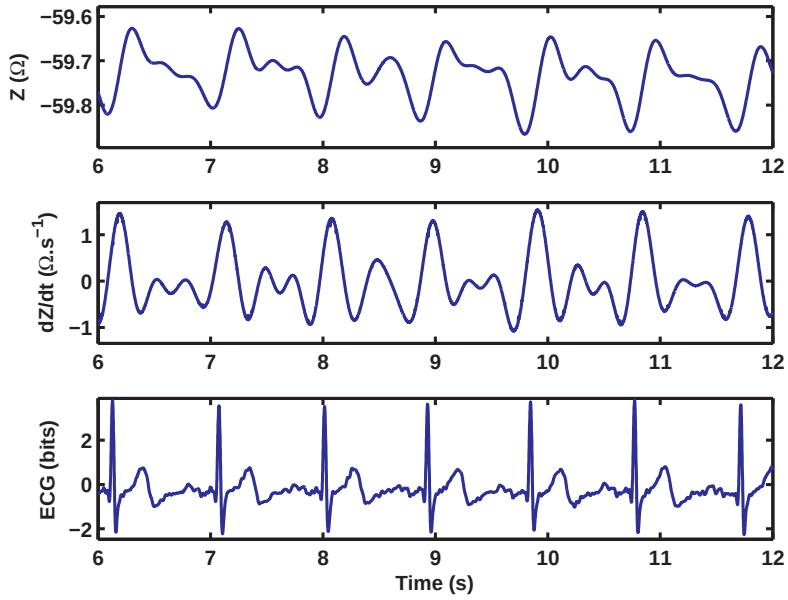

Figure 7.4: Example impedance cardiogram of test subject T04

each heartbeat was calculated. The average time constant for each subject and the standard deviation is shown in Figure 7.5. The time constant calculated for the clinical results is of a considerably larger magnitude than that calculated theoretically for flow through rigid tubes (50-250 clinically and 3 theoretically), however a number of influencing factors is different in each case such as the presence of volume changes in the clinical data which may account for this increase in magnitude.

This figure shows that for test subjects diagnosed with aortic valve stenosis (T01, T02, T03, T05), the decay time constant is consistently higher than for the control subjects (C02, C03, C04, C05). This is in agreement with the theoretical results which showed that an increase in the degree of stenosis led to an increase in the decay time constant (see Chapter 6). To determine if there exists a significant difference between the subject groups, a Mann-Whitney Rank Sum Test for independant samples was performed on the data. The P-value of $P = 0.03$ shows a statistically significant difference between the two samples.

It has been shown both theoretically (see Chapter 4) and experimentally (see Chapter 3) that the relationship between velocity and impedance is non-linear during the deceleration phase of blood. The statistically confirmed difference between the time constant for control and test subjects, suggests that the impedance measured during impedance cardiography is able to capture this changing relationship in the presence of a stenosis.

To compare the theoretical trends of Chapter 6 with the clinical results, a new parameter akin to the 'degree of stenosis as a percentage of the diameter' parameter of Figure 6.12 was calculated using Equation 7.1. First the approximate diameter of the aortic valve was calculated by assuming the valve opening is circular in nature. This was divided by the diameter of

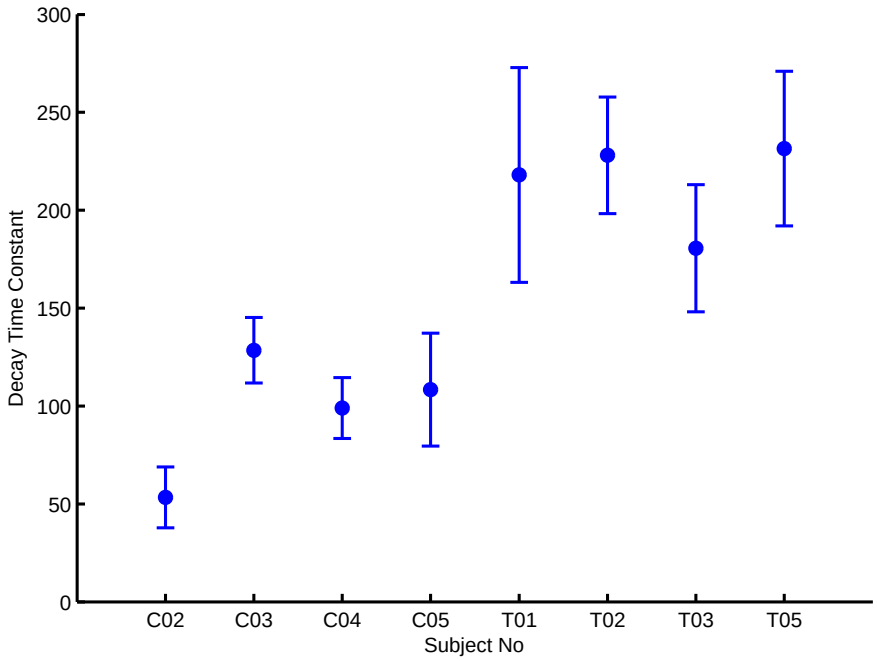

Figure 7.5: Average decay time constant, τ_{decel}, for each clinical trial subject

the inflow tract and subtracted from 1 to determine the percentage of the diameter that was blocked due to the stenosis.

$$StenosisDegree = 1 - \frac{D_{AV}}{D_{LVOT}} \tag{7.1}$$

$$= 1 - \frac{2\sqrt{\frac{AVA}{\pi}}}{D_{LVOT}} \tag{7.2}$$

The decay time constant is plotted with the degree of stenosis in Figure 7.6. Despite the absence of a range of stenosis degree, these results agree with that in Figure 6.12. As the degree of stenosis increases, so too does the decay time constant. The correlation co-efficient between the decay time constant and the degree of stenosis is 0.874, however this should be considered as an

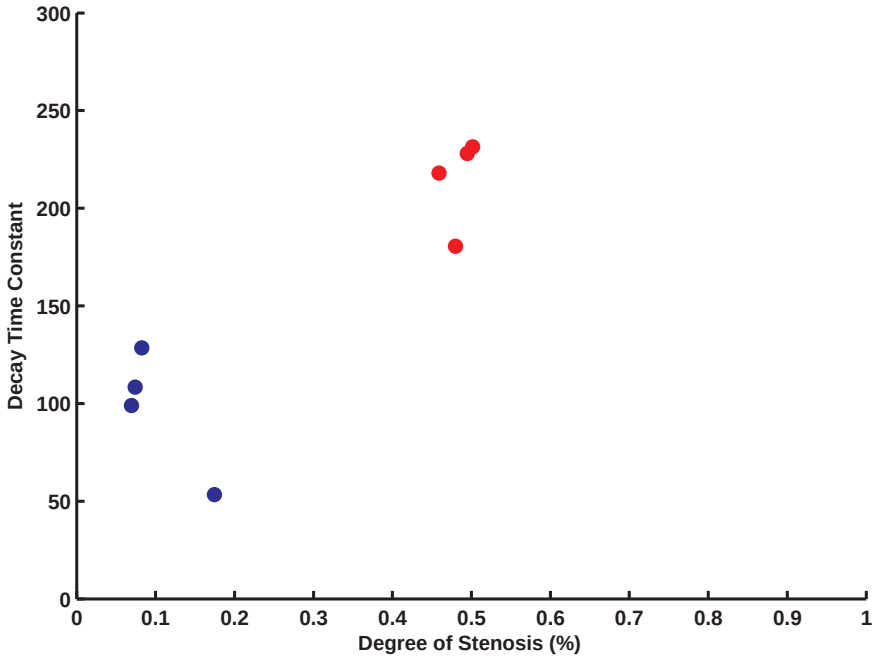

Figure 7.6: Decay time constant as a function of the degree of stenosis as calculated from the aortic valve area (AVA) and outflow tract diameter (D_{LVOT}). Blue data indicates control subjects and red data indicates test subjects.

approximation. A more reliable correlation co-efficient would be found if a wider spread of stenosis degree had been used.

7.4 Conclusions

The primary objective of the clinical pilot study was to determine if electrical bioimpedance techniques may be suitable for the assessment of aortic stenosis. Experimental and theoretical investigations of the impedance of pulsatile blood flow in Chapters 3 and 4 have explored the relationship between aortic blood flow through rigid tubes and the measured impedance. Perhaps the most important finding was the linear relationship between velocity and impedance during accelerating blood flow and non-linear relationship between velocity and impedance during decelerating blood flow.

Chapter 6 has extended the theoretical model to complex geometries and results also confirm that similar relationships exist between velocity and impedance during acceleration and deceleration in the presence of a stenosis in a rigid tube. However, the characteristic time decay during deceleration has shown to theoretically vary with the degree of stenosis. Given this, the diastolic period of an impedance cardiogram should hold additional information related to blood flow.

Thus this preliminary clinical investigation explored the clinical relationship between abnormal physiological aortic blood flow induced by flow through aortic stenosis and the entire thoracic electrical impedance. Clinical impedance cardiography waveforms were collected for both aortic valvular stenosis patients and control subjects. The decay time constant of the measured impedance was determined for each subject during deceleration. The decay time constant for the four aortic stenosis subjects was higher than the four control subjects in all cases.

The clinical time constants were shown to be statistically different between control and test subjects ($P = 0.03$). The correlation between the clinical time constant and the degree of stenosis calculated from the LVOT diameter and the AVA for all subjects was -0.874 which suggest that this may be a parameter worth investigating for the assesesment of aortic stenosis. The linear trend of the clinical data with stenosis degree also confirms the theoretical results derived in Chapter 6. It would be interesting to also collect experimental imepdance data of blood flow through a stenosis for comparison to the clinical results.

The decay time constant was shown to vary both theoretically and clinically in the presence of a stenosis and may be a useful parameter for the diagnosis of the presence of aortic valve stenosis. The knowledge gained from

this pilot study should lead to further research that will enable the routine monitoring and detection of aortic stenosis by a general practitioner. This would be potenitally very important as it means that diagnosis of this valvular heart disease could be performed as part of a regular check-up, by a practitioner who does not require skills in echocardiography techniques.

Chapter 8

Conclusion

Impedance cardiography has not been widely accepted as a clinical tool for determining cardiac output despite the many advantages over more invasive techniques such as the Fick method which uses intracardiac catheters. A lack of agreement on the origin of the impedance change in the thorax has resulted in a loss of confidence in the accuracy of the method. Traditionally, impedance changes were assumed to be a result of changes in blood volume as blood was pumped through the heart. However, further research has highlighted the existence of other physiological effects that contribute to the thoracic impedance. Of these, a significant proportion of the impedance change can be attributed to blood flow rate dependent changes in the resistivity of blood.

Variations in the impedance of flowing blood has been identified from as early as 1937 (Sigman et al. 1937). Due to their biconcave shape, changes in orientation of erythrocytes will cause changes in blood resistivity. As blood increases in velocity, the red blood cells experience increasing shear forces which act to align the cells with the minimal cross sectional area in the direction of flow in order to reduce these shear forces. As a result, the cross

sectional area of plasma increases and the resistivity of the blood decreases. This effect is assumed to be the primary cause of the impedance change of blood flowing through rigid tubes.

Despite many publications investigating the velocity dependent changes of flowing blood, the implications of this effect on impedance cardiography waveforms is not understood. This is because previous research has been limited to constant flow velocities. Understanding this effect during pulsatile velocity changes is important in better understanding an impedance cardiography waveform.

This research investigated the electrical characteristics of blood caused by flow induced changes in cell orientation and the potential implications for impedance cardiography waveforms. To do this, physiological human aortic blood flow was simulated experimentally using rigid tubes in a mock circulatory system. The variations of impedance and velocity were measured for a range of physical and flow parameters and the relationship between impedance and velocity was investigated. Human blood flow through the aorta was also modelled theoretically in rigid tubes both with and without stenosis. The modelled and experimental results for straight tubes were compared. A clinical trial was also conducted to compare the impedance cardiography waveforms for control and aortic stenosis subjects.

The impedance of bovine blood was experimentally measured in rigid tubes under pulsatile flow. It was shown that the acceleration is an important factor in determining the impedance of pulsatile blood flow. The relationship between the velocity and the impedance of blood was shown to be different for accelerating and decelerating blood. The peak impedance derivative of pulsatile blood flowing through rigid tubes occurs simultaneously in time with the peak acceleration of the blood. Therefore, the maximum aortic

blood flow acceleration will contribute to the $\frac{dZ}{dt}_{max}$ signal in an ICG (in addition to the peak blood volume change).

During acceleration the relationship between impedance and velocity was shown to be linear both experimentally and theoretically. As a result, it was concluded that the accuracy of stroke volume determined from impedance cardiography is not compromised by orientation effects. This is because $\frac{dZ}{dt}_{max}$ (which is used to calculate stroke volume) occurs during the acceleration phase of the heart beat. During deceleration however, the relationship is non linear and much more difficult to define. It is this phase that contains information related to blood flow. The time constant during deceleration characterises this relationship. The impedance does not respond instantaneously to changes in velocity and the time constant of decay increases with pulse rate and peak velocity due to changes in the orientation response of cells. Given the theoretical and experimental results, the diastolic portion of the impedance cardiogram will contain additional information related to the velocity of the blood flow.

Analysis of the time-frequency decomposition of the impedance and velocity of pulsatile blood show good correlation between the frequency components of both signals during a large proportion of the period of the signal. In particular during acceleration and deceleration of flow. The correlation reduces when the flow acceleration changes direction. The close correlation ($r > 0.85$) provides further evidence that the changes in impedance can be contributed to velocity dependent orientation states of the red blood cells during the different flow phases.

Experimental orthogonal measurements across the radius of the tube of flowing blood verify that the orientation of red blood cells varies only along the radius of the tube and not with the angle around the central axis i.e.

they are aligned tangentially. In impedance cardiography, the measurement of the thorax primarily captures longitudinal blood flow in the ascending and descending aorta. Blood flow through the aortic arch is essentially measured in an orthogonal manner, which will induce an impedance change in the opposite direction to the longitudinal measurements. However, the length of the aortic arch is short in comparison to the ascending and descending aorta which suggests that this effect will be negligible.

It has been shown that steady flow models presented in previous literature do not adequately describe the impedance response of pulsatile blood flow. The theoretical model developed here is the first for the determination of the impedance of pulsatile blood flow. The cell orientation and deformation dynamics were modelled as a function of the shear rate across the width of the tube and used to determine the impedance of the flowing blood. The model has been verified through comparisons to the experimentally measured impedance for the same parameters. The close agreement between the experimental and theoretical time signals demonstrates the validity of the theoretical model. These results demonstrate that the shear rate profile contains the information required to theoretically simulate the impedance of flowing blood. This explains why constant flow models do not successfully simulate the impedance of pulsatile flow as the shear rate profile is different for the same spatial average velocity during acceleration and deceleration.

Variations in the haematocrit and temperature of blood, and the radius of the rigid tube have all been shown to affect the experimental and theoretical impedance of flowing blood. Comparisons of the results determined experimentally and theoretically correlate well. An increase in haematocrit induces a large change in impedance due to an increase in the number of cells contributing to the orientation change. The time constant of decay decreases

as the haematocrit increases. The reduced average velocity has been shown to be a better indicator of similar impedance changes in tubes with different diameters. This is because the reduced average velocity can be thought of as the average shear force experienced by the cells across the diameter. Experimental and theoretical results show that the relative impedance change due to the orientation of cells is consistent regardless of the temperature of the blood.

A pilot study was performed in order to investigate the suitability of the measurement of thoracic impedance as a diagnostic tool in the assessment of aortic valve stenosis. In this investigation, the flow of blood exiting a stenosis was theoretically modelled using the Lattice Boltzmann Method. Clincial impedance cardiography measurements were also recorded for both aortic valvular stenosis patients and control subjects.

Results from the theoretical model have demonstrated that the decay time constant of impedance varies with the degree of stenosis. The results from the clinical trial also support these modelling conclusions. In the case of aortic valve stenosis subjects, the calculated decay time constant was consistently higher than the decay time constant of the control subjects and a statistically significant difference between the subject groups was found ($P = 0.03$). Thus the presence of a stenosis has been shown to affect the impedance response in both a theoretical and clinical environment. The decay time constant shows potential as a useful parameter in the assessment of aortic valve stenosis. This needs to be confirmed in a full clinical study involving larger numbers in each cohort.

Using theses results to increase understanding of the effect of orientation changes on IC waveforms may encourage the development of commercially viable applications. Further research should enable an inexpensive and non-

invasive cardiac screening tool using bioimpedance techniques to be used in the routine monitoring of aortic valve stenosis. Ensuring such a device is simple to use, will reduce the financial burden on the health care system. This will be achieved by allowing earlier detection and treatment of cardiac disease and reducing long term health management cost as well as reducing equipment and training costs to practitioners.

Appendix A

Appendix

A.1 Ethics Approval

University Human Research Ethics Committee

HUMAN ETHICS APPROVAL CERTIFICATE

NHMRC Registered Committee Number EC00171

Dear Ms Richelle Gaw

A UHREC should clearly communicate its decisions about a research proposal to the researcher and the final decision to approve or reject a proposal should be communicated to the researcher in writing. This Approval Certificate serves as your written notice that the proposal has met the requirements of the *National Statement on Research involving Human Participation* and has been approved on that basis. You are therefore authorized to commence activities as outlined in your proposal application, subject to any specific and standard conditions detailed in this document.

Within this Approval Certificate are:

* Project Details
* Participant Details
* Conditions of Approval (Specific and Standard)

Researchers should report to the UHREC, via the Research Ethics Officer, events that might affect continued ethical acceptability of the project, including, but not limited to:

(a) serious or unexpected adverse effects on participants; and
(b) proposed significant changes in the conduct, the participant profile or the risks of the proposed research.

Further information regarding your ongoing obligations regarding human based research can be found via the Research Ethics website http://www.research.qut.edu.au/ethics/ or by contacting the Research Ethics Coordinator on 07 3138 2340 or ethicscontact@qut.edu.au

If any details within this Approval Certificate are incorrect please advise Research Ethics within 10 days of receipt of this certificate.

Research Ethics Officer _____ Date 10/7/08
(on behalf of the Chairperson, UHREC)

Project Details

Category of Approval: Full Application

Approved Until: 8/07/2011

Approval Number: 0800000369

Project Title: The evaluation of bioimpedance techniques in the assessment of aortic blood flow

Project Chief Investigator: Ms Richelle Gaw

Other Project Staff/Students:
A/Prof Bruce Cornish , Adjunct Associate Professor Brian Thomas , Dr Wayne J Stafford

Experiment Summary:
Investigate the hypothesis that non invasive bioimpedance measurements of the chest may be used to monitor and detect aortic stenosis.

Participant Details

Participants:
Approximately 30

Location/s of the Work:
Queensland Cardiovascular Group Spring Hill

RM Report No. E801 Version 2

University Human Research Ethics Committee

HUMAN ETHICS APPROVAL CERTIFICATE

NHMRC Registered Committee Number EC00171

Conditions of Approval

Specific Conditions of Approval:
No special conditions placed on approval by the UHREC. Standard conditions apply.

Standard Conditions of Approval:

The University's standard conditions of approval require the research team to:

1. Conduct the project in accordance with University policy, NHMRC / AVCC guidelines and regulations, and the provisions of any relevant State / Territory or Commonwealth regulations or legislation;

2. Respond to the requests and instructions of the University Human Research Ethics Committee (UHREC);

3. Advise the Research Ethics Officer immediately if any complaints are made, or expressions of concern are raised, in relation to the project;

4. Suspend or modify the project if the risks to participants are found to be disproportionate to the benefits, and immediately advise the Research Ethics Officer of this action;

5. Stop any involvement of any participant if continuation of the research may be harmful to that person, and immediately advise the Research Ethics Officer of this action;

6. Advise the Research Ethics Officer of any unforeseen development or events that might affect the continued ethical acceptability of the project;

7. Report on the progress of the approved project at least annually, or at intervals determined by the Committee;

8. (Where the research is publicly or privately funded) publish the results of the project is such a way to permit scrutiny and contribute to public knowledge; and

9. Ensure that the results of the research are made available to the participants.

Modifying your Ethical Clearance:

The University has an expedited mechanism for the approval of minor modifications to an ethical clearance (this includes changes to the research team, subject pool, testing instruments, etc). In practice this mechanism enables researchers to conduct a number of projects under the same ethical clearance.

Any proposed modification to the project or variation to the ethical clearance must be reported immediately to the Committee (via the Research Ethics Officer), and cannot be implemented until the Chief Investigator has been notified of the Committee's approval for the change / variation.

Requests for changes / variations should be made in writing to the Research Ethics Officer. Minor changes (changes to the subject pool, the use of an additional instrument, etc) will be assessed on a case by case basis and interim approval may be granted subject to ratification at the subsequent meeting of the Committee.

It generally takes 7 -14 days to process and notify the Chief Investigator of the outcome of a request for a minor change / variation.

Major changes to your project must also be made in writing and will be considered by the UHREC. Depending upon the nature of your request, you may be asked to submit a new application form for your project.

Audits:

All active ethical clearances are subject to random audit by the UHREC, which will include the review of the signed consent forms for participants, whether any modifications / variations to the project have been approved, and the data storage arrangements.

End of Document

RM Report No. E801 Version 2

Bibliography

Artoli, A. M., Kandhai, D., Hoefsloot, H. C. J., Hoekstra, A. G. & Sloot, P. M. A. (2004), 'Lattice bgk simulations of flow in a symmetric bifurcation', *Future Gener Comp Sy* **20**(6), 909–16.

Bayram, M. & Yancy, C. (2009), 'Transthoracic impedance cardiography: A non invasive method of haemodynamic assessment', *Heart Failure Clin* **5**, 161–8.

Bernstein, D. & Lemmens, H. (2005), 'Stroke volume equation for impedance cardiography', *Med Biol Eng Comput* .

Bernstein, D. P. (1986), 'A new stroke volume equation for thoracic electrical bioimpedance: theory and rationale', *Crit Care Med* **14**(10), 904–9.

Bernstein, D. P. & Lemmens, H. J. M. (2007), Impedance cardiography: Development of the stroke volume equations and their electrodynmaic and biophysical foundations, *in* C. T. Leondes, ed., 'Biomechanical Systems Technology', World Scientific Publishing, Singapore, pp. 49–87.

Bishop, J. J., Nance, P. R., Popel, A. S., Intaglietta, M. & Johnson, P. C. (2001), 'Effect of erythrocyte aggregation on velocity profiles in venules', *Am J Physiol Heart Circ Physiol* **280**(1), H222–236.

Bitbol, M. (1986), 'Red blood cell orientation in orbit "c=0"', *Biophys J* **49**(5), 1055–68.

Bitbol, M. & Leterrier, F. (1982), 'Measurement of erythrocyte orientation in flow by spin labelling: I comparison between experimental and numerically simulated epr spectra', *Biorheology* **19**, 669–680.

Bitbol, M. & Quemada, D. (1985), 'Measurement of erythrocyte orientation in flow by spin labeling: Ii phenomenological models for erythrocyte orientation rate', *Biorheology* **22**(1), 31–42.

Bluestein, D. & Einav, S. (1995), 'The effect of varying degrees of stenosis on the characteristics of turbulent pulsatile flow through heart valves', *J Biomech* **28**(8), 915–924.

Bour, J. & Kellett, J. (2008), 'Impedance cardiography - a rapid and cost effective screening tool for cardiac disease', *Eur J Intern Med* **19**, 399–405.

Boyd, J., Buick, J., Cosgrove, J. A. & Stansell, P. (2005), 'Application of the lattice boltzmann model to simulated stenosis growth in a two-dimensional carotid artery', *Phys Med Biol* **50**(20), 4783–96.

Boyd, J. & Buick, J. M. (2007), Comparison of newtonian and non-newtonian flows in a two-dimensional carotid artery model using the lattice boltzmann method, p. 6215.

Boyd, J. & Buick, J. M. (2008*a*), 'Three-dimensional modelling of the human carotid artery using the lattice boltzmann method: I model and velocity analysis', *Physics in Medicine and Biology* **53**(20), 5767–5779.

Boyd, J. & Buick, J. M. (2008*b*), 'Three-dimensional modelling of the human carotid artery using the lattice boltzmann method: Ii shear analysis', *Physics in Medicine and Biology* **53**(20), 5781–5795.

Boyd, J., Buick, J. M., Cosgrove, J. A. & Stansell, P. (2004), 'Application of the lattice boltzmann method to arterial flow simulation: Investigation of boundary conditions for complex arterial geometries', *Australas Phys Eng Sci Med* **27**(4), 207–212.

Brown, D. J. & Smith, F. W. K. (2002), 'Stenosis hemodynamics: From physical principles to clinical indices', *J Vet Intern Med* **16**(6), 650–657.

Buick, J., Cosgrove, J. A., Tonge, S. J., Mulholland, B. A., Steves, B. A. & Collins, M. W. (2003), 'The lattice boltzmann equation for modelling arterial flows: review and application', *Intern Medi Clin Lab* **11**, 24–29.

Caro, C. G., Pedley, T. J., Schroter, R. C. & Seed, W. A. (1978), *The mechanics of circulation*, Oxford University Press, Oxford.

Chen, S. & Doolen, G. D. (1998), 'Lattice boltzmann method for fluid flows', *Annu Rev Fluid Mech* **30**, 329–64.

Chetham, S. M. (2003), Measurement of Cardiac Output by Multifrequency Bioimpedance, Research, Queensland University of Technology.

Cole, K. S. (1940), 'Permeability and impermeability of cell membranes for ions', *Cold Spring Harbor Sympos Quant Biol* **8**, 110–22.

Cole, K. S. (1968), *Membranes, ions, and impulses: a chapter of classical biophysics*, University of California Press, Berkeley.

Cotter, G., Schachner, A., Sasson, L., Dekel, H. & Moshkovitz, Y. (2006), 'Impedance cardiography revisited', *Physiol Meas* **27**(9), 817–27.

Critchley, L. A. (1998), 'Impedance cardiography. the impact of new technology', *Anaesthesia* **53**(7), 677–684.

de Vries, P. M., Langendijk, J. W. & Kouw, P. M. (1995), 'The influence of alternating current frequency on flow related admittance changes of blood: a concept for improvement of impedance cardiography', *Physiol Meas* **16**(1), 63–69.

Debnath, L. (2002), *Wavelet Transforms and Their Applications*, Birkhauser, Boston.

Dellimore, J. W. & Gosling, R. G. (1975), 'Change in blood conductivity with flow rate', *Med Biol Eng* **13**(6), 904–913.

DeMarzo, A. P. & Calvin, J. E. (2007), 'A new approach for low-cost non-invasive detection of asymptomatic heart disease at rest', *Prev Cardiol* **10**(1), 9–14.

DeMarzo, A. P., Calvin, J. E., Kelly, R. F. & Stamos, T. D. (2005), 'Using impedance cardiography to assess left ventricular systolic function via postural change in patients with heart failure', *Prog Cardiovasc Nurs* **20**(4), 163–167.

DeMarzo, A. P., Kelly, R. F. & Calvin, J. E. (2007), 'Impedance cardiography: a comparison of cardiac output vs waveform analysis for assessing left ventricular systolic dysfunction', *Prog Cardiovasc Nurs* **22**(3), 145–151.

Dupin, M. M., Halliday, I. & Care, C. M. (2006), 'A multi-component lattice boltzmann scheme: Towards the mesoscale simulation of blood flow', *Med Eng Phys* **28**(1 SPEC ISS), 13–18.

Edgerton, R. H. (1974), 'Conductivity of shear suspensions of ellipsoidal particles with application to blood flow', *IEEE Trans Biomed Eng* **BME-21**(1), 33–43.

Faes, T. J., Raaijmakers, E., Meijer, J. H., Goovaerts, H. G. & Heethaar, R. M. (1999), 'Towards a theoretical understanding of stroke volume estimation with impedance cardiography', *Ann NY Acad Sci* **873**, 128–134.

Fricke, H. (1924), 'A mathematical treatment of the electric conductivity and capacity of disperse systems i', *Phys Rev* **24**, 575587.

Fujii, M., Nakajima, K., Sakamoto, K. & Kanai, H. (1999), 'Orientation and deformation of erythrocytes in flowing blood', *Ann NY Acan Sci* **873**, 245–261.

Gaw, R., Cornish, B. & Thomas, B. (2007), Comparison of a theoretical impedance model with experimental measurements of pulsatile blood flow, *in* 'Proceedings of 13th International Conference on Electrical Bioimpedance', pp. 32–5.

Gaw, R., Cornish, B. & Thomas, B. (2008), 'The electrical impedance of pulsatile blood flowing through rigid tubes: a theoretical investigation', *IEEE Trans Biomed Eng* **55**, 721–7.

Gaw, R., Cornish, B. & Thomas, B. (2009*a*), Decay properties of the experimental electrical impedance of pulsatile blood flowing through rigid tubes, *in* 'Proceedings of 11th Medical Physics and Biomedical Engineering World Congress', Vol. 25/VII, pp. 259–62.

Gaw, R., Cornish, B. & Thomas, B. (2009*b*), Time frequency analysis of the experimental electrical impedance of pulsatile blood flowing through

rigid tubes, *in* 'Proceedings of 11th Medical Physics and Biomedical Engineering World Congress', Vol. 25/VII, pp. 255–8.

Geddes, L. A. & Baker, L. E. (1989), *Principles of Applied Biomedical Instrumentation*, John Wiley and Sons, Inc.

Geddes, L. A. & Sadler, C. (1973), 'The specific resistance of blood at body temperature', *Med Biol Eng* **11**(3), 336–339.

Goovaerts, H. G., Faes, T. J., Raaijmakers, E. & Heethaar, R. M. (1998), 'A wideband high common mode rejection ratio amplifier and phase-locked loop demodulator for multifrequency impedance measurement', *Med Biol Eng Comput* **36**(6), 761–767.

Grimnes, S. & Martinsen, O. (2000), *Bioimpedance and Bioelectricity Basics*, Academic Press, San Diego.

He, X. & Ku, D. N. (1994), 'Unsteady entrance flow development in a straight tube', *J Biomech Eng - T ASME* **116**(3), 355–360.

Hein, I. A. & O'Brien, W. D. (1992), 'A flexible blood flow phantom capable of independently producing constant and pulsatile flow with a predictable spatial flow profile for ultrasound flow measurement validations', *IEEE Trans Biomed Eng* **39**(11), 1111–22.

Hoetink, A. E., Faes, T. J. C., Visser, K. R. & Heethaar, R. M. (2004), 'On the flow dependency of the electrical conductivity of blood', *IEEE Trans Biomed Eng* **51**(7), 1251–1261.

Hoskins, P. R., Anderson, T. & McDicken, W. N. (1989), 'A computer controlled flow phantom for generation of physiological doppler waveforms', *Phys Med Biol* **34**, 1709–17.

Hu, W., Sun, H. H. & Wang, X. (1997), Study on methods for impedance cardiography, *in* 'Annual International Conference of the IEEE Engineering in Medicine and Biology - Proceedings', Vol. 5, pp. 2074–2077.

Jaspard, F. & Nadi, M. (2002), 'Dielectric properties of blood: an investigation of temperature dependence', *Physiol Meas* **23**(3), 547–554.

Katz, A. M. (1977), *Physiology of the heart*, New York Raven Press.

Kauppinen, P. K., Hyttinen, J. A. & Malmivuo, J. A. (1998), 'Sensitivity distributions of impedance cardiography using band and spot electrodes analysed by a three-dimensional computer model', *Ann Biomed Eng* **26**, 694–702.

Keller, S. R. & Skalak, R. (1982), 'Motion of a tank-treading ellipsoidal particle in a shear flow', *J Fluid Mech* **120**, 27–47.

Kim, D. W., Kim, D. W., Baker, L. E., Pearce, J. A. & Won Ky Kim, A. W. K. K. (1988), 'Origins of the impedance change in impedance cardiography by a three-dimensional finite element model', *IEEE Trans Biomed Eng* **35**(12), 993–1000.

Kosicki, J., Chen, L. H., Hobbie, R., Patterson, R. & Ackerman, E. (1986), 'Contributions to the impedance cardiogram waveform', *Ann Biomed Eng* **14**(1), 67–80.

Kubicek, W. G., Karnegis, J. N., Patterson, R. P., Witsoe, D. A. & Mattson, R. H. (1966), 'Development and evaluation of an impedance cardiac output system', *Aerospace Med* **37**(12), 1208–1212.

Leitner, D., Wassertheurer, S. & Breitenecker, F. (2006), A lattice boltzmann model for pulsative blood flow in elastic vessels, Proceedings. 5th

Vienna Symposium on Mathematical Modelling, Vienna University of Technology, Vienna, Austria, p. 83.

Liebman, F. & Bagno, S. (1968), 'The behaiviour of red blood cells in flowing blood which accounts for conductivity changes', *Biomed Sci Instrum* **4**, 25–35.

Liebman, F., Pearl, J. & Bagno, S. (1962), 'The electrical conductance properties of blood in motion', *Phys Med Biol* **7**, 177–194.

Lindroos, M., Kupari, M., Heikkila, J. & Tilvis, R. (1993), 'Prevalence of aortic valve abnormalities in the elderly: an echocardiographic study of a random population sample', *J Am Coll Cardiol* **21**(5), 1220–1225.

Malmivuo, J. & Plonsey, R. (1995), *Bioelectromagnetism: Principles and applications of bioelectric and biomagnetic fields*, Oxford University Press.

McDonald, D. A. (1974), *Blood Flow in Arteries*, second edition edn, Edward Arnold (Publishers) Ltd, London.

Meijer, J. H., Boesveldt, S., Elbertse, E. & Berendse, H. W. (2007), Using time interval parameters from impedance cardiography to evaluate autonomic nervous function in parkinson's disease, *in* H. Scharfetter & R. Merwa, eds, '13th International Conference on Electrical Bioimpedance and the 8th Conference on Electrical Impedance Tomography', Springer, Graz, Austria.

Mohapatra, S. N. (1981), *Non-invasive cardiovascular monitoring by electrical impedance technique*, Pitman Medical, London.

Mohapatra, S. N. & Hill, D. W. (1975), 'The changes in blood resistivity with haematocrit and temperature', *Eur J Inten Care Med* **1**, 153–162.

Moshkovitz, Y., Kaluski, E., Milo, O., Vered, Z. & Cotter, G. (2004), 'Recent developments in cardiac output determination by bioimpedance: comparison with invasive cardiac output and potential cardiovascular applications', *Curr Opin Cardiol* **19**(3), 229–237.

Nakayama, Y. & Boucher, R. (2000), 'Introduction to fluid mechanics'.

Newman, D. G. & Callister, R. (1999), 'The non-invasive assessment of stroke volume and cardiac output by impedance cardiography: a review', *Aviat Space Environ Med* **70**(8), 780–789.

Ninomiya, M., Fujii, M., Niwa, M., Sakamoto, K. & Kanai, H. (1988), 'Physical properties of flowing blood', *Biorheology* **25**(1-2), 319–28.

Nowakowski, A., Palko, T. & Wtorek, J. (2005), 'Advances in electrical impedance methods in medical diagnostics', *Bull Pol Acad Sci-TE* **53**(3), 231–43.

Otto, C. M. (2004), *Textbook of clincial echocardiography*, Saunders, Philadelphia.

Ouared, R. & Chopard, B. (2005), 'Lattice boltzmann simulations of blood flow: non-newtonian rheology and clotting processes', *J Stat Phys* **121**(1-2), 209–21.

Palko, T., Bialokoz, F. & Weglarz, J. (1995), Multifrequency device for measurement of the complex electrical bio-impedance-design and application, *in* 'Engineering in Medicine and Biology Society, 1995 and 14th Conference of the Biomedical Engineering Society of India. An International Meeting, Proceedings of the First Regional Conference., IEEE', pp. 1/45–1/46.

Patterson, R. (1989), 'Fundamentals of impedance cardiography', *IEEE Eng Med Biol Mag* **8**(1), 35–38.

Patterson, R. P. (1985), 'Sources of the thoracic cardiogenic electrical impedance signal as determined by a model', *Med Biol Eng Comput* **23**(5), 411–7.

Peacock, J., Jones, T., Tock, C. & Lutz, R. (1998), 'The onset of turbulence in physiological pulsatile flow in a straight tube', *Exp Fluids* **24**(1), 1–9.

Pedley, T. J. (2003), "arterial and venous fluid dynamic", *in* G. Pedrizzetti & K. Perktold, eds, 'Cardiovascular Fluid Mechanics', Vol. 446 of *CISM Courses and Lectures*, Springer Wein New York, Italy, p. 271.

Peura, R. A., Penney, B. C., Arcuri, J., Anderson, F. A., J. & Wheeler, H. B. (1978), 'Influence of erythrocyte velocity on impedance plethysmographic measurements', *Med Biol Eng Comut* **16**(2), 147–54.

Raaijmakers, E., Marcus, J., Goovaerts, H., De Vries, P., Faes, T. & Heethaar, R. (1996), The influence of pulsatile flow on blood resistivity in impedance cardiography, *in* 'Engineering in Medicine and Biology Society, 1996. Bridging Disciplines for Biomedicine. Proceedings of the 18th Annual International Conference of the IEEE', Vol. 5, pp. 1957–1958 vol.5.

Sakamoto, K. & Kanai, H. (1979), 'Electrical characteristics of flowing blood', *IEEE Trans Biomed Eng* **BME-26**(12), 686–695.

Sakamoto, K., Muto, K., Kanai, H. & Iizuka, M. (1979), 'Problems of impedance cardiography', *Med Biol Eng Comput* **17**(6), 697–709.

Schuster, C. J. & Schuster, H. P. (1984), 'Application of impedance cardiography in critical care medicine', *Resuscitation* **11**(3-4), 255–274.

Shankar, T. M. R., Webster, J. G. & Shao, S.-Y. (1985), 'The contribution of vessel volume change and blood resistivity change to the electrical impedance pulse', *IEEE Trans Biomed Eng* **BME-32**(3), 192–198.

Shul'man, Z. P. & Makhanek, A. A. (2005), 'Influence of the temperature and oversouring of blood on its hemorheological properties', *J Eng Phys Thermophys* **78**(5), 1022–28.

Shyu, L.-Y., Lin, Y.-S., Liu, C.-P. & Hu, W.-C. (2004), 'The detection of impedance cardiogram characteristic points using wavelet transform', *Comput Biol Med* **34**(2), 165–175.

Siconolfi, S. F., Gretebeck, R. J., Wong, W. W., Pietrzyk, R. A. & Suire, S. S. (1997), 'Assessing total body and extracellular water from bioelectrical response spectroscopy', *J Appl Physiol* **82**(2), 704–710.

Sigman, E., Kolin, A., Katz, L. N. & Jochim, K. (1937), 'Effect of motion on the electrical conductivity of the blood'.

Sramek, B. B. (1982), 'Cardiac output by electrical impedance', *Med Electron* **13**(2), 93–7.

Stout, C. L., Van De Water, J. M., Thompson, W. M., Bowers, E. W., Sheppard, S. W., Tewari, A. M. & Dalton, M. L. (2006), 'Impedance cardiography: can it replace thermodilution and the pulmonary artery catheter?', *Am Surgeon* **72**(8), 728–734.

Succi, S. (2001), *The Lattice Boltzmann Equation for Fluid Dynamics and Beyond*, Clarendon Press, Oxford.

Sukop, M. C. & Thorne Jr, D. T. (2006), *Lattice Boltzmann Modeling: An introduction for Geoscientists and Engineers*, Springer, Berlin.

Sun, C. & Munn, L. L. (2005), 'Particulate nature of blood determines macroscopic rheology: a 2d lattice boltzmann analysis', *Biophys J* **88**, 1635–1645.

Taylor, B. C., Timmons, W. D. & Hines, A. S. (1999), A modelling solution to the origin of the electrical impedance cardiogram, *in* '1st Joint BMES/EMBS Conference', The Institute of Electrical and Electronics Engineers, Atlanta, p. 233.

Tjin, S. C., Xie, T. & Lam, Y. Z. (1998), 'Investigation into the effects of haematocrit and temperature on the resistivity of mammalian blood using a four-electrode probe', *Med Biol Eng Comput* **36**(4), 467–70.

Trautman, E. D. & Newbower, R. S. (1983), 'A practical analysis of the electrical conductivity of blood', *IEEE Trans Biomed Eng* **BME-30**(3), 141–54.

Ulgen, Y. & Sezdi, M. (1998), Hematocrit dependence of the cole-cole parameters of human blood, Proceedings of the International Conference on Biomedical Engineering Days, IEEE, Piscataway, NJ, USA, Istanbul, Turkey, pp. 71–74.

Van De Water, J. M., Miller, T. W., Vogel, R. L., Mount, B. E. & Dalton, M. L. (2003), 'Impedance cardiography: The next vital sign technology?', *Chest* **123**(6), 2028–2033.

Visser, K., Lamberts, R. & Zijlstra, W. (1988), Origin of the impedance cardiogram, *in* 'Engineering in Medicine and Biology Society, 1988. Pro-

ceedings of the Annual International Conference of the IEEE', Vol. 2, pp. 763–765.

Visser, K. R. (1989), 'Electric properties of flowing blood and impdance cardiography', *Ann Biomed Eng* **17**, 463 – 473.

Visser, K. R. (1992), 'Electric conductivity of stationary and flowing human blood at low frequencies', *Med Biol Eng Comput* **30**(6), 636–640.

Visser, K. R., Lamberts, R., Korsten, H. H. & Zijlstra, W. G. (1976), 'Observations on blood flow related electrical impedance changes in rigid tubes', *Pflugers Arch* **366**(2-3), 289–91.

Visser, K. R., Mook, G. A., van der Wall, E. & Zijlstra, W. G. (1993), 'Theory of the determination of systolic time intervals by impedance cardiography', *Biol Psychol* **36**(1-2), 43–50.

Wang, L. & Patterson, R. (1992), The effect of blood resistivity changes on impedance cardiography determined by 3d finite difference models of human thorax, *in* 'Engineering in Medicine and Biology Society, 1992. Vol.14. Proceedings of the Annual International Conference of the IEEE', Vol. 5, pp. 1736–1737.

Wang, L. & Patterson, R. (1995), 'Multiple sources of the impedance cardiogram based on 3-d finite difference human thorax models', *IEEE Trans Biomed Eng* **42**(2), 141–148.

Wang, X., Sun, H. & Van De Water, J. (1995), 'An advanced signal processing technique for impedance cardiography', *IEEE Trans Biomed Eng* **42**(2), 224–230.

Wang, Y., Haynor, D. R. & Kim, Y. (2001), 'A finite-element study of the effects of electrode position on the measured impedance change in impedance cardiography', *IEEE Trans Biomed Eng* **48**(12), 1390–401.

Windberger, U., Bartholovitsch, A., Plasenzotti, R., Korak, K. J. & Hienze, G. (2003), 'Whole blood viscosity, plasma viscosity and erythrocyte aggregation in nine mammalian species: reference values and comparison of data', *Exp Physiol* **88**(3), 431–440.

Wolf-Gladrow, D. A. (2000), Lattice boltzmann models, *in* 'Lattice Gas Cellular Automata and Lattice Boltzmann Models: An Introduction', Springer, pp. 159–246.

Wtorek, J. & Polinski, A. (1996), Multifrequency impedance plethysmograph, Vol. 2 of *Conference Record - IEEE Instrumentation and Measurement Technology Conference*, IEEE, Piscataway, NJ, USA, Brussels, Belgium, pp. 1452–1455.

Wtorek, J. & Polinski, A. (2005), 'The contribution of blood-flow-induced conductivity changes to measured impedance', *IEEE Trans Biomed Eng* **52**(1), 41–9.

Yancy, C. & Abraham, W. T. (2003), 'Noninvasive hemodynamic monitoring in heart failure: utilization of impedance cardiography', *Congest Heart Fail* **9**(5), 241–250.

Zamir, M. (2000), *The physics of pulsatile flow*, Biological physics series., AIP Press ; Springer, New York.

Zhang, M. I. N. & Willison, J. H. M. (1991), 'Electrical impedance analysis in plant tissue: a double shell model', *J Exp Bot* **42**(244), 1465–1475.

Zhao Shuguang, Fang Yanhong, Z. H. & Min, T. (2005), Detection of impedance cardioaraphys characteristic points based on wavelet transform, *in* 'Proceedings of the 2005 IEEE Engineering in Medicine and Biology 27th Annual Conference', pp. 2730–2.